Nonlinear Synchrosqueezing for Dispersive Signal Analysis

by

Javaid Ikram

A Dissertation Presented in Partial Fulfillment
of the Requirements for the Degree
Doctor of Philosophy

Approved October 2023 by the
Graduate Supervisory Committee:

Antonia Papandreou-Suppappola, Co-Chair
Aditi Chattopadhyay, Co-Chair
Mariana Bertoni
Kanu Sinha

ARIZONA STATE UNIVERSITY

December 2023

ABSTRACT

The propagation of waves in solids, especially when characterized by dispersion, remains a topic of profound interest in the field of signal processing. Dispersion represents a phenomenon where wave speed becomes a function of frequency and results in multiple oscillatory modes. Such signals find application in structural health monitoring for identifying potential damage sensitive features in complex materials. Consequently, it becomes important to find matched time-frequency representations for characterizing the properties of the multiple frequency-dependent modes of propagation in dispersive material. Various time-frequency representations have been used for dispersive signal analysis. However, some of them suffered from poor time-frequency localization or were designed to match only specific dispersion modes with known characteristics, or could not reconstruct individual dispersive modes. This thesis proposes a new time-frequency representation, the nonlinear synchrosqueezing transform (NSST) that is designed to offer high localization to signals with nonlinear time-frequency group delay signatures. The NSST follows the technique used by reassignment and synchrosqueezing methods to reassign time-frequency points of the short-time Fourier transform and wavelet transform to specific localized regions in the time-frequency plane. As the NSST is designed to match signals with third order polynomial phase functions in the frequency domain, we derive matched group delay estimators for the time-frequency point reassignment. This leads to a highly localized representation for nonlinear time-frequency characteristics that also allow for the reconstruction of individual dispersive modes from multicomponent signals. For the reconstruction process, we propose a novel unsupervised learning approach that does not require prior information on the variation or number of modes in the signal. We also propose a Bayesian group delay mode merging approach for reconstructing modes that overlap in time and frequency. In addition to using simulated signals, we

demonstrate the performance of the new NSST, together with mode extraction, using real experimental data of ultrasonic guided waves propagating through a composite plate.

DEDICATION

To my beloved wife Laila, who anchored my journey through her love and support;

To my parents, for their support and beautiful patience;

And to Elias and Omar, who remind me every day of the joys of discovery.

ACKNOWLEDGMENTS

The completion of this dissertation is a milestone that I would not have reached without the efforts of many people to whom I owe much appreciation. I am forever indebted to my co-advisors, Professor Antonia Papandreou-Suppappola and Professor Aditi Chattopadhyay, for their guidance, encouragement, and the challenge they provided me throughout the doctoral program. I am especially grateful for all their advice and supervision that has helped me mature into someone deserving of the doctoral title. I would also like to thank the members of my Supervisory Committee, Professor Mariana Bertoni and Professor Kanu Sinha for all their valuable insight and feedback that helped me improve the quality of the research presented in this work. Gratitude is also due to my colleagues in Professor Antonia Papandreou-Suppappola's research group. I would also like to thank my supportive colleagues at Intel Corporation who encouraged and motivated me throughout this journey. Special mention in this regard is due to my valued mentor and friend Dr. Osborne Martin, whose advice and support I greatly value.

TABLE OF CONTENTS

Page

LIST OF TABLES viii

LIST OF FIGURES ix

CHAPTER

1 INTRODUCTION 1

1.1 Motivation: Time Frequency Analysis of Dispersive Propagation ... 1

1.2 Historical Development of TFRs for SHM 2

1.3 Localized TFRs 6

1.4 Contributions 7

1.5 Research Organization 10

2 DISPERSION IN ULTRASONIC GUIDED WAVES 12

2.1 Ultrasonic Guided Waves 12

2.2 Lamb Wave Dispersion 15

2.3 Anisotropic Dispersion 19

2.4 UGW for Damage Detection 19

2.4.1 Numerical Modeling of UGW 20

2.4.2 Dispersion Compensation 21

3 SIGNAL PROCESSING IN SHM 23

3.1 Overview of Signal Analysis 23

3.1.1 Time of Flight Based Defect Detection 26

3.1.2 Wavelet Transform for SHM 27

3.1.3 Wigner Distribution 29

3.1.4 Matching Pursuit Decomposition 30

3.1.5 Orthogonal Matching Pursuit 32

3.1.6 Reassignment 33

CHAPTER Page

3.2 Highly Localized Time Frequency Transforms 33
3.2.1 UGW Inspection of Integrated Circuits Using MPD 34
3.2.2 UGW Inspection of Integrated Circuits Using the Synchrosqueezing Transform 38
3.2.3 Group Velocity Estimation for UGW Propagating in Dispersive Material 39
3.3 Conclusion 44
4 NEW TIME FREQUENCY TRANSFORM MATCHED TO GROUP DELAY 48
4.1 Problem Formulation 48
4.2 Proposed Group Delay Estimation Approach 54
4.3 Analysis of Parabolic Frequency Modulated Signal 57
4.4 Quantitative Comparison 59
4.4.1 Normalized Energy 59
4.4.2 Signal Reconstruction 60
4.4.3 Reconstruction Quality Factor 61
4.5 Hyperbolic Frequency Modulated Signals 63
5 UNSUPERVISED MODE EXTRACTION 65
5.1 Previous Methods of Mode Extraction 65
5.2 Unsupervised Mode Extraction 66
5.3 Simulations 71
5.3.1 Parabolic Frequency Modulation 71
5.3.2 Multiple PFM Signals with No Overlap 71
5.4 Isotropic UGW Analysis 72

CHAPTER Page

5.5 Defect Detection in Isotropic Media 75
5.6 Analysis of Real Data 75
6 BAYESIAN GROUP DELAY MODE MERGING 81
6.1 Extracting Signals Overlapping in Time-frequency 81
6.2 Summary on Bayesian Inference Methods 84
6.2.1 Bayesian Filtering 84
6.2.2 Monte Carlo Methods 85
6.2.3 Particle Filter Algorithm 86
6.3 Bayesian Mode Merging 87
6.4 Bayesian Mode Merging Simulations 89
6.4.1 Merging of Two Overlapping Parabolic Frequency-Modulated Signals 89
6.4.2 Merging of UGW Modes 90
7 CONCLUSIONS AND FUTURE WORK 96
7.1 Conclusions 96
7.2 Future Work 97
REFERENCES 99
APPENDIX
7.3 QUADRATIC GD FUNCTION ESTIMATION 110

LIST OF TABLES

Table Page

4.1 Summary of Synchrosqueezed STFT TFRs Providing High TF Localization for Signals with Time Domain Phase Function $\phi(t)$ and Signals with Frequency Domain Phase Function $\Phi(f)$. 52

4.2 Notation of STFTs Based on Choice of Window. Operators $\mathcal{D}$ and $\mathcal{M}$ Denote Differentiation and Multiplication, Respectively. The Operator Precedence Follows, for Example, $(\mathcal{M}^2\mathcal{D}H)(f) = (\mathcal{M}(\mathcal{M}(\mathcal{D}H)))(f)$. 55

LIST OF FIGURES

Figure		Page
2.1	Time Frequency Techniques and Select Applications.	13
2.2	Theoretical Dispersion Curves For Aluminium-6061.	14
2.3	Schematic Description of Lamb Wave Generation in Aluminum Plate. Image Source: [1]	16
2.4	Challenges in Dispersion Modelling	20
3.1	Signal Processing in SHM.	26
3.2	Flowchart Summarizing the Matching Pursuit Decomposition Algorithm [2]	32
3.3	Cross Section View of a Typical IC Package	34
3.4	Actuator and Sensors Bonded to an IC Package	35
3.5	Matching Pursuit Decomposition to Detect Damage in IC Packages	37
3.6	Signal Reconstruction for Healthy and Damaged States	39
3.7	(a) Time Domain and (b) MDST of an UGW Signal.	46
3.8	Dispersion Analysis of UGW in Isotropic Medium.	47
4.1	Time Frequency Representations: STFT, FR-SST [3], FR-SST2 [4, 5], TR-SST2[6] and NSST[7]	58
4.2	Normalized Energy as a Function of the Number of Coefficients. Faster Growth of Energy Towards 1 Represents Sharper Representation.	60
4.3	Signal Reconstructed from TF Domain to Time Domain	61
4.4	Analysis of Performance in Noise Using Reconstruction Quality Factor. Higher Value of RQF Represents Better Reconstruction Performance	62
4.5	Perfect Localization in TF Plane for Nonlinear HFM Signal	64

Figure Page

5.1 UMS Algorithm Example, Nine Time Frequency Vertices with Edge Weights 67

5.2 Step by Step Implementation of UMS Algorithm Starting with Lowest Edge Weight to Largest for Component 1 68

5.3 Step by Step Implementation of UMS Algorithm Starting with Lowest Edge Weight to Largest for Component 2 69

5.4 Two PFM Matched to Dual Hyperbolas 72

5.5 NSST GD Estimation in Isotropic Material. 73

5.6 Group Velocity Estimation and Comparison of Dispersion curves 74

5.7 Time Domain Signal of Healthy and Damage CFRP 75

5.8 NSST Isotropic UGW Simulated Signal with Damage 76

5.9 DSST of UGW Propagating in Quasi-Isotropic Media 79

5.10 Damage Detection in CFRP Using DSST with Unsupervised Mode Separation 80

6.1 NSST of Two Overlapping PFM Signals in the TF Domain. 82

6.2 Cluster Components After Unsupervised Mode Extraction of the NSST in Figure 6.1. 83

6.3 Mode Merging Framework 84

6.4 Steps of Particle Filter Algorithm (Taken From [8]). 87

6.5 Segments of 200 Sample Length for 4 Out of the 6 Clusters $c_1, c_2, c_3,$ And c_4 of the Sum of Two PFM Signals in Figure 6.2. 90

6.6 Particle Filter Estimation of the Slopes of the Indicated Segments in Figure 6.5. 91

6.7 Particle Filter Estimation of Slopes 92

Figure Page

6.8 Bayesian Mode Merging for Mode 1 92
6.9 Time Domain Signal Reconstruction of Mode 1. Note That the Large Error Around $t=2$ s is Due to the Missing Data at Intersection points. 93
6.10 Region of Interest for Bayesian Mode Merging. 93
6.11 Particle Filter Estimation of Slopes of the Indicated Segments of UGW 94
6.12 RMSE of Segments in UGW 95

Chapter 1

INTRODUCTION

1.1 Motivation: Time Frequency Analysis of Dispersive Propagation

Ultrasonic guided wave (UGW) testing is commonly used for structural health monitoring, based on processing waves propagating through structures. The method exploits resonances between structure boundaries in order to detect changes that can be used to evaluate the degree of damage and localize defects in the structure [9]. As UGWs propagate through a structure, they undergo frequency-dependent attenuation and dispersion due to changes in their velocity as a result of multiple reflection modes and material and geometry of the structure.

Due to their highly dispersive characteristics, UGWs are time-varying signals, that is signals whose frequency content changes with time. Such signals can be successfully analyzed using time-frequency representations (TFRs), which are two-dimensional (2-D) signal transformations that provide joint time and frequency information [10]. Various TFRs used for dispersive signal analysis include linear TFRs such as the short-time Fourier transform (STFT) and wavelet transform (WT).

However, these transforms result in trade off between time and frequency localization [11, 12]. The Wigner Distribution (WD) quadratic TFR preserves many desirable signal properties. However, the presence of oscillatory cross terms when analyzing multicomponent signals can lead to misinterpretation of signal information [10]. Smoothed versions of the WD were also used to analyze guided wave modes [13]. Note, however, that smoothing can remove some of the cross terms, it also causes

some loss of time-frequency (TF) resolution. The Matching Pursuit Decomposition (MPD) TF method is useful in extracting highly localized features in composites [14]. But, as the MPD is an iterative approach, it can be very computationally intensive for analyzing highly nonlinear signal modes. Data-driven approaches to signal decomposition such as the the Empirical Mode Decomposition (EMD) [15] have been proposed. Although the methodology is attractive for various applications, it lacks a mathematical formulation and relies on heuristics to select the appropriate Intrinsic Mode Function (IMF) from a filter bank.

1.2 Historical Development of TFRs for SHM

The squared magnitude of the STFT, referred to as the spectrogram, is one of the most widely used TFRs to analyze a time domain signal jointly in time and frequency. However the STFT technique suffers from poor localization. One way to overcome the poor localization issue is to utilize the phase information which is discarded in the spectrogram. Kodera [16] first introduced a modification to the STFT by taking into account the phase information of the signal. The group delay and instantaneous frequency of the signal are calculated and is distributed at the corresponding TF points resulting in a highly localized TFR. Auger and Flandrin [17] presented the reassignment method which is a nonlinear technique that utilizes the phase and magnitude signal characteristics to improve the time frequency localization of the spectrogram. They developed a mathematically rigorous formulation by concentrating the signal energy around the local instantaneous frequency and group delay. Daubechies [18] introduced the Synchrosqueezed Transform (SST) to overcome the limitations of Empirical Mode Decomposition (EMD). The SST provides the same high TF resolution properties as the reassignment method, but with the additional advantage of reconstructing the signal components under assumptions on

the time-varying phase function.

Signal processing is a critical component of structural health monitoring (SHM) systems when distinguishing between damaged and undamaged states of a material. The objective of signal processing in ultrasonic guided wave (UGW) based SHM is to extract information from sensors to analyze the structural state of the system. A damaged structure causes modification of structural characteristics such as stiffness, resulting in subtle differences in the measured signal. Hence, robust signal processing techniques are required to extract features that quantify presence of damage and severity as seen in figure. The signal processing technique should be exhibit robust sensitivity to noise as the sensors are generally susceptible to noise from the environment. Various denoising algorithms have been shown to be effective such as the statistical global averaging [19] and the time reversal method [20]. After signal denoising is achieved, the most critical task is feature extraction which is the selection of damage sensitive parameters from the sensor signal. A significant amount of research has been conducted for efficient feature extraction using signal processing of UGWs.

In the early 1990s, Alleyne and Cawley [11, 21] experimentally generated frequency-wavenumber plots to characterize dispersion using the two dimensional Fourier Transform. The technique relies on collecting frequency domain information over equally spaced intervals on a structure and plotting amplitude versus frequency-wavenumber information. The primary drawback of the technique was the loss of time information essential for signal analysis. Dalton [22] demonstrated the potential for UGW based signal processing for large aircraft structures, however due to complex materials involved in aircrafts, multimodal dispersive propagation limited the successful analysis to localized regions on the aircraft. Similarly Wilcox [23, 24] also highlighted dispersion as a major challenge in signal processing of UGWs. Sohn et al. [25] used

to compensate for dispersion using the time reversal method. The method used a combination of narrow band and multiresolution signal processing to minimize dispersion in the experimental signal. However, the major drawback of this technique is the requirement of prior knowledge of propagation.

While time domain analysis can provide spatial information about the signal, Fourier analysis provides information about the frequency spectrum of a signal. However, it does not offer any visual representation of which frequency components appear at specific moments in the signal. TFRs are specifically engineered to accomplish this task by producing an image that maps onto the time-frequency plane, followed by extraction of time-frequency centers of individual modes. TFRs such as the reassigned spectrogram, were used to analyze UGWs. [26, 27]. TFRs were also used to identify and extract individual dispersive modes [28, 29, 30]. Warped TFRs have also been considered as they better match dispersive characteristics [28]; however, the resulting analysis suffers from time-frequency (TF) resolution. The Chirplet Transform (CT) [29] requires prior knowledge of the dispersion characteristic for mode identification. The Synchrosqueezing Transform (ST) TFR was recently developed that provides high localization along the signal's Instantaneous Frequency (IF) [30]. It can also reconstruct individual mode components provided they are sufficiently separable in TF and the IF is not highly dispersive [31, 32]. A second-order ST was introduced to improve the localization of strongly modulated signals [4, 5]; higher order estimators for IF were also proposed , for both biased and unbiased estimation [6]. These aforementioned ST-based methods concentrate on estimating the IF of a signal. For UGW propagation modeling, however, the TF signature of interest is group delay (GD), as it can be related to UGW group velocity. The potential of ST for inspection of UGW propagating in highly dispersive and inhomogeneous medium, such as integrated circuit package, was demonstrated by extracting TF features. [30].

The detection of structural defects has become increasingly important in the fields of aerospace engineering [33], civil infrastructure monitoring [34], as well as microelectronics packaging [30]. The process of interrogating the structure using actuators and sensors to extract damage sensitive features is formally defined as structural health monitoring. Historically, SHM applications have focused on improving condition monitoring, damage prognosis and non destructive evaluation. The four key issues in SHM are detection, localization, quantification, and prognosis. Detection of the defect determines if there is indeed a defect in the structure. Localization deals with identifying where the damage exists in the structure. Quantification dictates the severity of the damage. Finally, the advanced field of prognosis deals with forecasting the remaining useful life (RUL) of the material.

High fidelity detection of damage is the first critical task in SHM. Sensing technologies are used to obtain information about the condition of a structure or object. Two of the most useful SHM techniques are vibration based and ultrasonic guided waves structural interrogation.

Vibration-based approaches utilize mode shapes and natural frequencies of the structure to detect damage. When the damage occurs, the natural frequencies and mode shapes of the structure change, and by monitoring this change is possible to identify damage [35]. While vibration-based approaches are simple to implement, they have key limitations that the technique is not sensitive to small scale damage or precursors of damage and does not provide spatial data critical for defect localization. Moreover, because the vibration based techniques are influenced by the environmental factors such as temperature and humidity, it becomes a challenging task to detect damage in real world applications.

The use of UGWs is one of the most important techniques in SHM because it allows

for the detection of hidden damage over the entire structure. UGWs are elastic stress waves which propagate in bounded, thin-walled structures and allow for subsurface inspection and analysis of damage sensitive characteristics [36]. When damage occurs, the guided waves will be scattered or reflected. By monitoring the changes in the guided waves, it is possible to identify damage. Despite the advantages, UGW requires advanced signal processing techniques. Moreover UGW are challenging to use in SHM because they have frequency-dependent propagation velocity which leads to multiple dispersive modes. The modes behave differently based on the material and cannot be analytically derived for all material. When damage is present, scattering and mode conversions further complicate this problem. As a result, modeling the wave propagation and dispersion is important for SHM. The complexity of such modeling depends on the material and can be used to determine frequency-dependent group velocity, dispersion relation, and multi mode characteristics. Knowledge of these dispersive properties for different material can then be used to investigate structural failure modes. For anisotropic material, closed form solutions are not easily available and numerical methods are often used for modeling; however, the modeling complexity increases for composite material [37]. We thus require advanced signal processing techniques to analyze closely-spaced propagating dispersive modes.

1.3 Localized TFRs

Recently, localized TFR matched to signals with linear GD have been reported which offer high localization by reassigning the STFT time and frequency axis along the signal's IF and/or GD. The Reassignment method is one such method that improves the TF resolution, however does not allow for the transform of the signal back to the time domain [27]. The SST is another such TFR that provides high TF localization for signals with slow varying frequency modulation and can also recon-

struct signal components [31, 3, 5]. The frequency-reassigned (FR) SST is designed to reassign TF points of the short-time Fourier transform (STFT) along the signal's instantaneous frequency (IF) [31]. The original SST is based on frequency reassignment. The localization property depends on some signal constraints, including weak frequency modulation. Due to this weak localization condition, the TFR are not suitable for UGW applications.

1.4 Contributions

The proposed research focuses on developing methods for analyzing, separating and reconstructing multiple dispersive signal components or modes. In particular, we first propose a new TFR that provides a highly-localized representation for multi-component signals with nonlinear group delay characteristics. We then integrate the new TFR with a novel unsupervised learning approach to separate and reconstruct the individual dispersive modes. For the more challenging case of modes overlapping both in time and frequency, we propose a Bayesian mode merging algorithm that infers and merges clusters belonging to the same mode, before mode reconstruction.

Contribution 1: Ultrasonic guided wave based inspection of integrated circuit packages using the synchrosqueezing transform.

UGW signals can be used to inspect integrated circuit (IC) packages using wave based techniques due to their excellent sub surface penetration through metallic and dielectric material. Guided waves in a heterogeneous composite assembly such as an IC package have modes with complex dispersion characteristics due to multiple layers of material with intricate geometry. No analytical solution exists for predicting dispersion in highly anisotropic composites. Numerical methods, such as the finite element method, have been used to model dispersion in composites, however these

methods are computationally intensive and not feasible for predicting dispersion in IC packages. We study the time-frequency characteristics of guided waves propagating through a complex IC using the the highly localized synchrosqueezing transform. This transform has been shown to be robust to bounded signal perturbations, provide highly localized time and frequency information for highly nonlinear modes, and reconstruct the signal corresponding to each mode. Reference UGW signals were collected for the IC package in its healthy and damaged states using piezoelectric transducers to characterize the dispersion modes in the excitation region. Initial results demonstrate that the dispersive mode information from the extracted transform ridges provide an effective damage indicator for IC packaging [**?** 30, 38].

Contribution 2: Synchrosqueezing time-frequency processing matched to nonlinear group delay characteristics.

The UGW signal propagation of dispersion modes for isotropic materials is characterized by estimating the modes' dispersive group velocity [39]. We thus propose a new nonlinear synchrosqueezing transform (NSST) that can be used to provide accurate estimates of the dispersive group velocities. This is because we formulate the NSST such that it is matched to provide high localization to signals with nonlinear time-frequency signatures. We mathematically derive the NSST formulation using a third order Taylor series approximation of the nonlinear phase function of the signal spectrum.

Contribution 3: Unsupervised mode extraction for separation and reconstruction of NSST dispersive modes

In UGW signal analysis, it is important to be able to localize and separately analyze each of the multiple dispersive components. The proposed NSST can be used

to reconstruct individual modes, provided the time-frequency region of the mode is identified. This is a difficult problem, especially because the number of modes is unknown. With UGW propagation, new modes result when the wave encounters a different boundary and each different modes can provide different information, such as varying thickness of a structure or defect detection sensitivity. We consider a mode reconstruction method that is based on the unsupervised graph-based algorithm used for efficient image segmentation. The method does not require training or tuning parameters. Using this approach, multicomponent signals with nonlinear and high varying time-frequency characteristics can be decomposed and reconstructed into individual components, without prior knowledge on the number of modes.

Contribution 4: Bayesian-based merging approach for reconstructing modes overlapping in the time-frequency domain.

UGW signal propagation can result in modes that have overlapping time-frequency characteristics. For such casees, more clusters than the number of modes can be extracted. We propose a Bayesian mode merging method to address the problem of overlapping modes. The method uses Bayesian inference to identify cluster regions that are continuous over a span of time-frequency points. This allows for adaptively merging clusters belonging to the same mode.

We demonstrate the performance of our aforementioned contributions using both real and simulated signals. The simulations were carried out on hyperbolic frequency modulation (HFM) and parabolic frequency modulation (PFM) signals. Additionally propagation of UGW in isotropic Aluminum plate is demonstrated using the waveform revealer software [40]. Real data on propagation of UGW in composite material is obtained using the Open Guided Wave platform [41].

1.5 Research Organization

Chapter 2 lays the conceptual foundations of a specific case of dispersive propagation. Ultrasonic guided waves are introduced and the challenges posed by dispersive propagation in structural health monitoring are explained.

Chapter 3 introduces the signal processing techniques used in dispersive signal processing with special focus on the STFT, Wigner Distribution, and the reassignment technique. This chapter also discusses applications of time-frequency signal processing in structural health monitoring. The chapter concludes with a detailed discussion on the investigations in interactions of UGW with anisotropic and non-homogeneous materials such as an integrated circuit.

Chapter 4 develops the use of new synchrosqueezing transform for analysis of a special case of UGW, which is isotropic propagation in context of Lamb waves modelled by a simulation software. The framework establishes in detail the estimation of group velocity of dispersive lamb wave modes with the synchrosqueezing transform. The chapter also references proposals from Chapter 2 during the discussion of time frequency analysis of Lamb waves. Chapter 4 also establishes an in-depth mathematical framework of nonlinear synchrosqueezing. Quantitative assessment of the transform are demonstrated. These include the normalized energy method and reconstruction quality factor. All the factors show that the new transform is robust to noise and provides statistically better results than the state of the art techniques.

Chapter 5 introduces a new unsupervised mode extraction algorithm which does not rely on apriori information of heuristic parameters. Mode extraction of three hyperbolic frequency modulated signals is demonstrated as well as the statistical efficiency of the separated modes. Simulated isotropic dispersion as well as real CFRP

plate dispersion are shown. It is proven that the technique can effectively detect anamolies in a structural material.

Chapter 6 discusses the Bayesian mode merging algorithm to address the case of intersecting modes. The technique is applied to simulated signals to demonstrate effectiveness.

Finally important conclusions, discussions from the research as well as avenues for future work are presented in Chapter 7.

Chapter 2

DISPERSION IN ULTRASONIC GUIDED WAVES

2.1 Ultrasonic Guided Waves

An important step in analyzing the structural health of a system is processing the sensor signal for damage sensitive characteristics. Time frequency representations have been shown to be effective signal processing paradigm for sensitive damage sensing applications. Figure 2.1 depicts the various time frequency techniques and their application in damage detection. The Short Time Fourier Transform (STFT) using a time varying spectrum has been shown to be effective in identifying damage in cylindrical shells [42]. Dispersion adapted STFT has also been used to characterize the dispersion of simple structures for which elastic properties are known in advance [43]. The use of Wigner Distribution provides a sharp TF representation, albeit with the introduction of cross terms [13]. The Wavelet Transform (WT) has been shown to be effective for the analysis of beams [44]. Several adaptive TF techniques [2, 45, 46, 47] have been proposed which are tailored for specific applications.

Despite the implementation of signal analysis techniques, the phenomenon of dispersive propagation continues to be a challenging task. Wave propagation through material is considered dispersive if the wave velocity (phase velocity) changes with frequency [48]. This means that the signal experiences temporal spreading and magnitude attenuation as it propagates through the material [43]. The cause of dispersion is because of multiple factors such as geometry, boundaries, interfaces, material properties, scattering, and dissipation. The graphical relationship between frequency and phase velocity is referred to as the dispersion curve of the material and is obtained

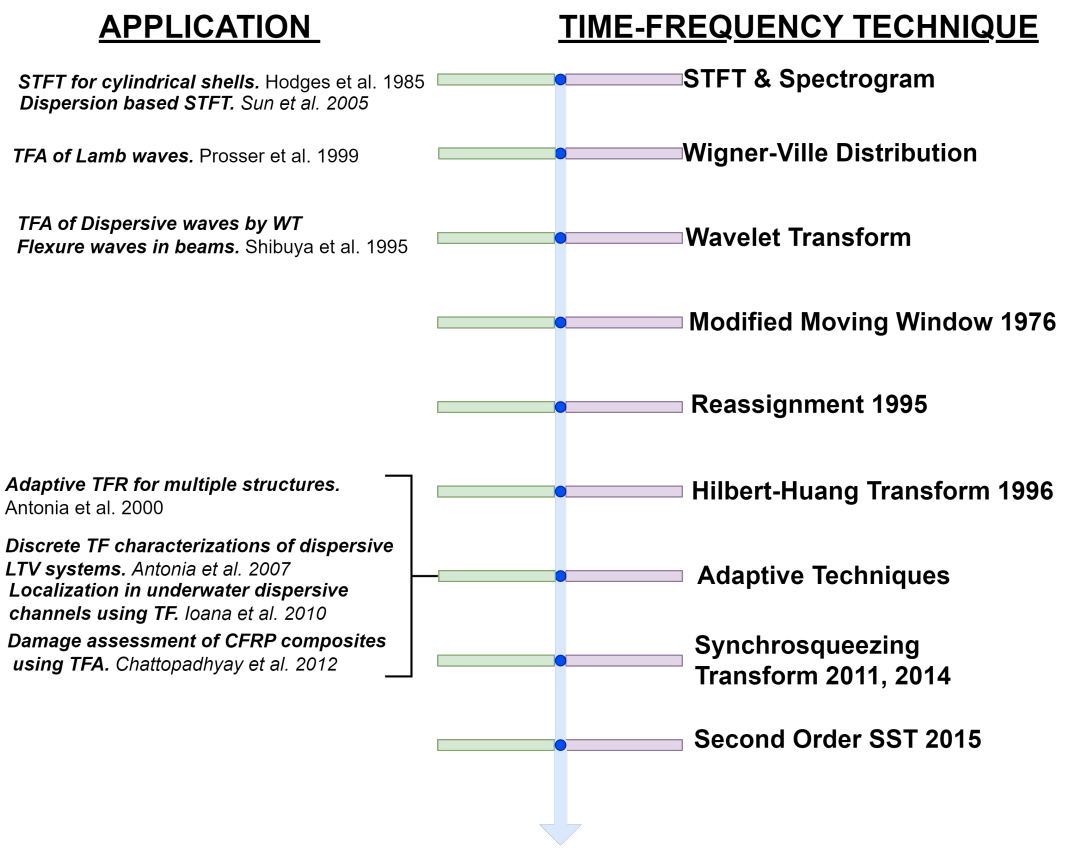

Figure 2.1: Time Frequency Techniques and Select Applications.

by solving a system of wave equations. In order to extract meaningful insights, signal processing techniques can be used account for the dispersive nature of the waveform. Figure 2.2 shows a dispersion curve of an Aluminum alloy. The product of frequency and material thickness is plotted on the x-axis and is referred to as the damage sensitive parameter. It can be seen that multiple propagation modes exist due to dispersion which results in complications for signal processing algorithms.

Wave propagation through material can be further subdivided into bulk wave and guided wave propagation. Bulk waves refer to wave propagation in infinite media such that the waves do not encounter material boundaries. In contrast, elastic waves that are guided by the path defined by the structural boundary are referred to as guided waves. Since the commonly used frequencies for guided wave testing is in

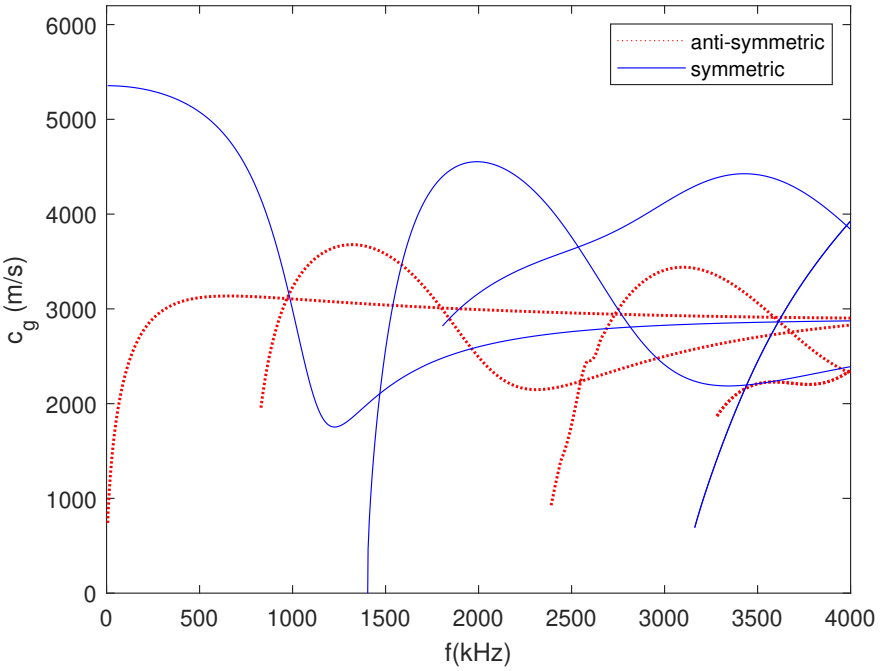

Figure 2.2: Theoretical Dispersion Curves For Aluminium-6061.

the ultrasonic range from 10 kilohertz (kHz) through several megahertz (MHz), these waves are more commonly referred to as ultrasonic guided waves (UGW).

The frequency of excitation as well as the presence of boundaries (such as in plates, rods and tubes) determine if the bulk waves or guided waves are generated. As postulated by [36], if the excitation wavelength is greater than the thickness of the structure, then guided waves will be generated. For example, we consider guided wave propagation through a 1 millimeter thick aluminum plate. The speed of sound in aluminum is 6320 m/s. For an excitation frequency of 100 kHz, the corresponding wavelength is calculated using the relationship, $\lambda = \frac{c}{f}$, where λ is the wavelength, c is the speed of sound in the material and f is the excitation frequency. Using this relation, we obtain the propagating wavelength of 63.2 mm. Because the excitation wavelength is greater than the material thickness of 1 mm, hence guided waves would be generated in this case.

UGW allow for subsurface inspection over long distances as compared to bulk waves, which have limited inspection capability, only directly below the area of inspection. Moreover, UGW allow for the extraction and analysis of damage sensitive material characteristics. These characteristics include time of flight, amplitude and frequency variations as a function of propagation distance. This is because when the UGW encounters a discontinuity in the material, the UGW is scattered in all directions. The discontinuity can either be a structural boundary or damage, such as crack or delamination. In order for scattering to occur, the size of the discontinuity should be comparable to the wavelength of the UGW. These characteristics make UGW inspection highly sensitive to subsurface damage. Sensor architecture and signal processing are used to extract the features of interest in the structure. Apriori information about the undamaged state can be compared to the existing state to assess the health of the structure.

2.2 Lamb Wave Dispersion

The classic problem of Lamb wave propagation in isotropic plate is reviewed, since the exact solution has been obtained using different approaches. Lamb waves are plane strain waves that occur in a free plate and the related traction forces vanish at upper and lower surfaces. Lamb waves propagate between two parallel traction free plate like structure. The free plate geometry in figure 2.3 is considered. Mode conversions occur as UGW reflect off the upper and lower boundaries of the plate. Superposition of the reflected waves results in the formation of wave packets known as guided wave modes.

Using the the tensor notation [9] in conjunction with equation, two uncoupled

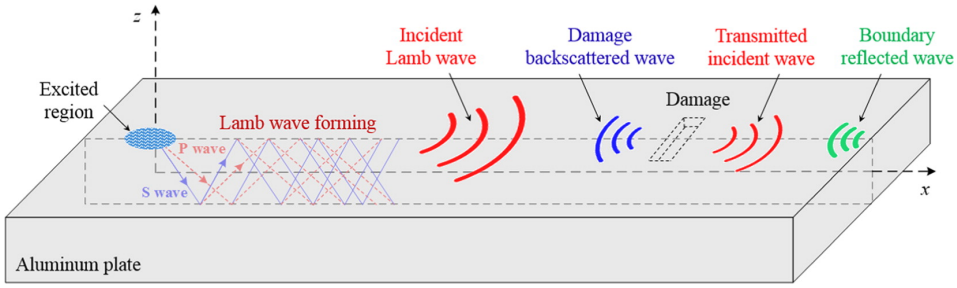

Figure 2.3: Schematic Description of Lamb Wave Generation in Aluminum Plate. Image Source: [1]

.

equations for plane strain are obtained for longitudinal and shear waves,

$$\frac{\delta^2\phi}{\delta x^2} + \frac{\delta^2\phi}{\delta z^2} = \frac{1}{c_L^2}\frac{\delta^2\phi}{\delta t^2} \tag{2.1}$$

$$\frac{\delta^2\psi}{\delta x^2} + \frac{\delta^2\psi}{\delta z^2} = \frac{1}{c_T^2}\frac{\delta^2\psi}{\delta t^2} \tag{2.2}$$

where c_L and c_T are the longitudinal and transverse waves respectively.

One of the most effective and widely used way to solve the Navier equations for elastic wave propagation is known as the wave potential approach. By defining the scalar potential ϕ and ψ, the wave potential based formulations can be formed. The analysis assumes the solution to the equations (2.2) and (2.1) in the form of

$$\phi = \Phi(z)exp[j(kx - \omega t)]$$

and

$$\psi = \Phi(z)exp[j(kx - \omega t)]$$

These solutions represent the travelling waves in the x direction and standing waves in the z direction. Substituting these equations in (2.2) and (2.1) leads to the solution

$$\phi = \Phi(z) = A_1 sin(pz) + A_2 cos(pz)$$

$$\psi = \Psi(z) = B_1 sin(qz) + B_2 cos(qz)$$

where $p^2 = \frac{\omega^2}{c_L^2} - k^2$ and $q^2 = \frac{\omega^2}{c_T^2} - k^2$

If plane stress condition is assumed, then the displacements and stresses can be simplified as the expression,

$$u_1 = \left[ik\Phi + \frac{d\Psi}{dz} \right]$$

$$u_3 = \left[\frac{d\Phi}{dz} + ik\Psi \right]$$

$$\sigma_{31} = \mu \left[2ik\frac{d\Phi}{dz} + +k^2\Psi + \frac{d^2\Psi}{dz^2} \right]$$

$$\sigma_{33} = \left[\lambda \left(-k^2\Phi + \frac{d^2\Phi}{dz^2} \right) + 2\mu \left(\frac{d^2\Phi}{dz^2} - ik\frac{d\Psi}{dz} \right) \right]$$

It is possible to split the solution of these equations into two sets of modes called symmetric and antisymmetric modes.

Symmetric modes are given by :

$$\Phi = A_2 cos(pz); \Psi = B_1 sin(qz),$$

$$u_1 = -ikA_2 cos(pz) + qB_1 cos(qz),$$

$$u_3 = -pA_2 sin(pz) - ikB_1 sin(qz),$$

$$\sigma_{31} = \mu[-2ikpA_2 sin(pz) + (k^2 - q^2)B_1 sin(qz)],$$

$$\sigma_{33} = -\lambda(k^2 + p^2)A_2 cos(pz) - 2\mu[p^2 A_2 cos(pz) + ikqB_1 cos(qz)],$$

Antisymmetric modes are given by:

$$\Phi = A_1 sin(pz); \Psi = B_2 cos(qz),$$

$$u_1 = ikA_1 sin(pz) - qB_2 cos(qz),$$

$$u_3 = -pA_1 cos(pz) - ikB_2 cos(qz),$$

$$\sigma_{31} = \mu[2ikpA_1 cos(pz) + (k^2 - q^2)B_2 sin(qz)],$$

$$\sigma_{33} = -\lambda(k^2 + p^2)A_1 sin(pz) - 2\mu[p^2 A_1 sin(pz) - ikqB_2 sin(qz)],$$

By applying traction free boundary conditions $\sigma_{31} = \sigma_{33} = 0$ at boundaries and simplifying for the plane strain, two equations known as the Rayleigh-Lamb wave frequency relationships are obtained.

$$\frac{\tan(q\,h)}{\tan(p\,h)} = -\frac{4\,k^2\,p\,q}{(q^2 - k^2)^2} \quad \text{and} \quad \frac{\tan(q\,h)}{\tan(p\,h)} = -\frac{(q^2 - k^2)^2}{4\,k^2\,p\,q}$$

The expressions can be expanded as $p^2 = (\frac{\omega}{c_L})^2 - k^2$ and $q^2 = (\frac{\omega}{c_T})^2 - k^2$. As wavenumber is given by the expression $k = \frac{\omega}{c_p}$ and the corresponding phase velocity is $c_p = \frac{\omega}{2\pi}\lambda$.

These equations can only be solved using numerical methods if boundary conditions and material properties are known.

The numerical solutions of equations (2.3) are represented by the wavenumber of the symmetric and antisymmetric modes. The group velocity is an important characteristic of lamb waves which can be obtained by the formula $c_g = \frac{d\omega}{dk}$, where $k = \frac{\omega}{c_p}$. After simplifications, an expression of group velocity in terms of phase velocity, c_p, and damage sensitive parameter which is the product of frequency and plate thickness, fd, is obtained.

$$c_g = c_p^2 \left[c_p - (fd)\frac{dc_p}{d(fd)} \right]^{-1}$$

2.3 Anisotropic Dispersion

UGW modes cannot be split up into symmetric and antisymmetric modes in anisotropic plates. This is due to the fact that phenomenon specific to anisotropic propagation has to be taken into account. In isotropic propagation, phase velocities of the propagating modes were direction independent. However, for the anisotropic case, there is a strong dependence of group velocity on propagation direction. As explained in [49], the incident and the reflected waves in an anisotropic media cannot be thought to be purely longitudinal or shear and the group velocity is not normal to the wave-front. In such a case, a sixth order polynomial has to be solved and complete elastic properties of the individual material must be known. In other words, the only way to predict the behavior of UGW in anisotropic media is if the stiffness matrix is known using material properties. The unique challenges for accurately modelling UGW propagation are discussed in [50] and [51]. In addition to multiples modes and dispersive behavior, the anisotropic propagation phenomenon have to be taken into account such as Steering effect, mode coupling, directional dependence on group velocity and higher attenuation than isotropic case. Due to these reasons, it is not possible to analytically model wave propagation behavior in anisotropic plates without a fully coupled physics-based model which constitutes the complete dynamics of the system.

2.4 UGW for Damage Detection

Unlike bulk waves, the solution to the equation must satisfy the physical boundary conditions. A physical actuator probe or Piezoelectric Transducer (PZT) is used to excite the UGW in the plate and a sensor is used to detect the material response. However, as described in the prior sections, challenges arise with real world appli-

cations due to dispersive nature of UGW, generation of multiple modes, reflections at structural boundaries, mode conversions, sensitivity to environmental factors and mode conversions

2.4.1 Numerical Modeling of UGW

One way to account for the complexity of UGW wave analysis is to numerically model the dispersive propagation through the material. Dispersion causes the UGW modes to be frequency dependent which leads to spreading of the wave packet in space and time as it propagates through the structure. The spreading of the wave packet in space and time results in reduced signal resolution.

To numerically predict dispersive propagation, it is essential to develop a model that describes the behavior of the UGW wave packet propagation in a dispersive medium. Such a model would be able to predict the shape of the UGW signal at any given distance from the source. Figure 2.4 summarizes the progressive increase in difficulty to obtain an analytical solution and to model the dispersion caused by material complexity.

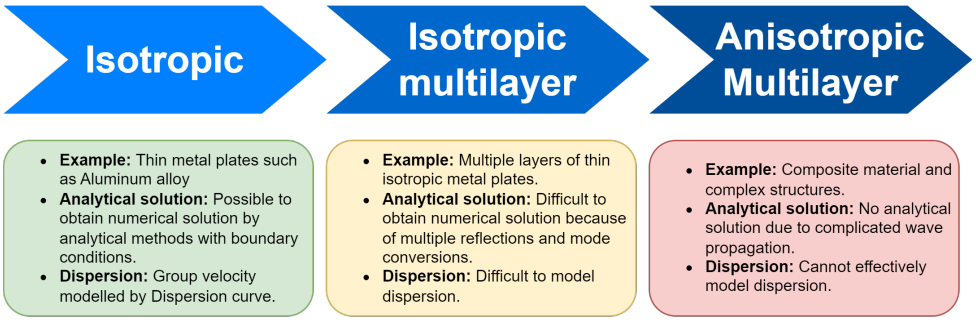

Figure 2.4: Challenges in Dispersion Modelling

2.4.2 Dispersion Compensation

Ultrasonic guided waves, exhibit a unique property known as dispersion, which fundamentally affects their propagation characteristics [9]. Dispersion occurs when the phase velocity of a wave mode is frequency-dependent, resulting in different frequency components of a wave packet traveling at different velocities. This can lead to the spreading or distortion of the wave packet as it propagates along a structure. The phenomenon arises due to the geometry and boundary conditions of the structure, combined with the elastic properties of the material from which it is made. For example, in cylindrical structures like pipes, different guided wave modes, such as the longitudinal L(0,1), torsional T(0,1), and flexural F(n,1) modes, each exhibit distinct dispersive behaviors [52]. Accurate understanding and modeling of dispersion is essential in the application of guided waves for structural health monitoring (SHM) and NDE, as it affects signal interpretation, defect detection, and localization.

Efforts to minimize the effects of dispersion have been attempted. Most importantly, the use of very limited bandwidth input signals would concentrate the energy over a specific frequency range of the dispersion curve such that the group velocity is stationary. However, due to the Heisenberg uncertainty principle, it is impossible to concentrate all the energy of a finite time duration signal at a single frequency.

Wilcox et al. [53] proposed a technique called Minimum Resolvable Distance (MRD) to compare dispersion along an Aluminum plate in order to predict th shape of the UGW. However, a major limitation of the technique is that the complete dispersion curve data for the group velocity and phase velocity must be known in advance. Since such information is only available for simple geometries and homogeneous material, the technique cannot be used for real world applications.

A similar dispersion compensation algorithm was also proposed [54] to minimize the effects of dispersion. In this technique, the time to distance mapping from the frequency-wavelength domain is used. While this technique provides the ability to map time domain signals to propagation distance, it suffers from the same limitation that the complete dispersion curve information must be known apriori.

In conclusion, it can be stated that due to the complexity of the material, it is not possible to completely and sufficiently model dispersion by numerical modeling. Moreover, it is not possible to completely eliminate dispersion due to the physics of the Heisenberg uncertainty principle as well not having prior knowledge of complete group velocity information of real world applications.

Chapter 3

SIGNAL PROCESSING IN SHM

3.1 Overview of Signal Analysis

A time domain signal $x(t)$ can be classified as stationary or time-varying. For a time varying signal $x(t) = Ae^{j2\pi f_0 t}$, the amplitude and/or frequency changes with time. Since the phase function is is linear f_0, the signal exhibits a single frequency f_0 over all time. In another case, $x(t) = e^{j2\pi\alpha t^2}$ [55], the phase function varies in a quadratic manner over the range of the signal. We can write the generalized form of a time varying signal as:

$$x(t) = a(t)e^{j2\pi c\zeta(\frac{t}{t_r})}$$

Where $a(t)$ is the time varying amplitude modulation (AM), $\zeta(\frac{t}{t_r})$ is the time varying phase modulation (PM), $t_r > 0$ is the normalization time constant and c is the rate of change of information also known as the FM rate. As an example a generalized frequency modulated signal (GFM) signal can be shown as:

$$x_c(t) = \sqrt{|\nu(t)|}e^{j2\pi c\zeta(\frac{t}{t_r})}$$

Which is a time varying signal whose amplitude modulation is fixed to $a(t) = \sqrt{|\nu(t)|}$, $\nu(t) = \frac{d}{dt}\zeta(\frac{t}{t_r})$ describes how the signal phase information changes over time and the range of $\zeta(\frac{t}{t_r})$ is the set of real numbers.

Historically, the mathematical formulation of the frequency representation of signals was invented by Fourier in 1807, whose main motivation was the solution of the heat equations which have discontinuities from hot to cold temperatures. His idea was that a discontinuous function may be represented as a sum of continuous functions.

The implementation and usefulness of this technique occurred with the advent of the spectroscope in 1865 [10]. The frequency representation of the signal primarily has several advantages. The physical understanding and knowledge about the material can be obtained. Additionally, since the wave propagation in the medium is dispersive, a simplified understanding of the waveform allows for mathematical modeling.

The GFM signal can be used to generalize the Fourier transform (FT) [55]:

$$X(f) = \int x(t)e^{-j2\pi ft}dt$$

The FT can be interpreted as decomposing the signal $x(t)$ into its complex sinusoids. When the FT is matched to complex sinusoids when, $x(t) = e^{j2\pi f_1 t}$:

$$X(f) = \int e^{j2\pi f_1 t}e^{-j2\pi ft}dt = \delta(f - f_1)$$

The Heisenberg uncertainty principle, originally formulated in the realm of quantum mechanics, posits an inherent limit to the precision with which pairs of physical properties of a particle, such as position and momentum, can simultaneously be known. This principle has found analogous applications in the field of signal processing, especially in the context of time-frequency analysis. In signal processing, the principle underscores an intrinsic trade-off between the localization of a function in the time domain and its localization in the frequency domain. More precisely, it can be described by the inequality $\Delta t \Delta f \geq \frac{1}{4\pi}$, where Δt and Δf represent the uncertainties (or spreads) in time and frequency, respectively. This implies that it's impossible to have a signal that is simultaneously arbitrarily localized in both time and frequency domains. The Gabor limit, named after Dennis Gabor, who first recognized the relevance of the uncertainty principle in signal analysis [56], quantifies this trade-off and forms the basis for many time-frequency representation techniques, such as the Short-Time Fourier Transform (STFT) and Wavelet Transform. The

principle also has implications in the design of window functions: a narrower window in the time domain results in a broader spectral width and vice versa. This inherent trade-off serves as a fundamental constraint in various signal processing tasks, such as filtering and signal decomposition.

The Heisenberg uncertainty principle, also known as the time-bandwidth product theorem was initially presented in the context of quantum mechanics which is inherently probabilistic in nature. The extension of the Heisenberg uncertainty principle in the signal analysis domain occurred in the context of join time-frequency domain analysis. The simplified definition of the principle is that it is not possible to construct a signal with time duration and frequency bandwidth arbitrarily small. In other words, the signal cannot have arbitrarily small concentration in both time and frequency domain. Mathematically the lower bound on the time-bandwidth product $T_x F_x$ of the signal can be represented as:

$$T_x F_x \geq \frac{1}{4\pi}$$

where T_x is the duration and F_x is the bandwidth of the signal. It can be shown that the only signal that achieves the lower bound is the Gaussian signal, hence it is the most concentrated signal in the TF plane.

$$s(t) = ce^{-\alpha t^2} \implies T_x F_x = \frac{1}{4\pi}$$

With these definitions established we discuss some of the signal processing methods used in practical analysis of UGW. There are several methodologies to investigate UGW in SHM. A non-exhaustive list of techniques is shown in figure 3.1.

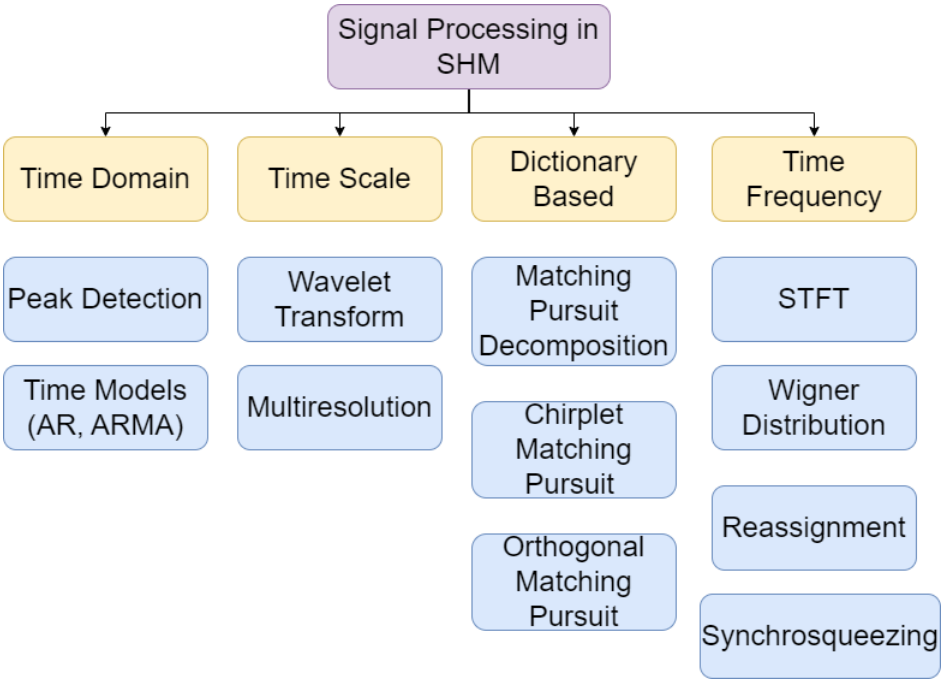

Figure 3.1: Signal Processing in SHM.

3.1.1 Time of Flight Based Defect Detection

Due to simplicity of use, time of flight (TOF) methods have been extensively used in signal processing for SHM to extract information from signals. The choice of input signals is a critical factor in determining which TOF algorithm to use. For most applications a narrow band pulse is preferred in order to minimize dispersion. However due to the Heisenberg uncertainty principle it is not possible to eliminate dispersion entirely. Moreover the frequency of the narrow band pulse has to be carefully chosen apriori. For instance, even though the fundamental antisymmetric mode A_0 becomes less susceptible to dispersion at higher frequencies, the use of the higher frequency itself results in excitation of more UGW modes. Moreover at higher frequencies the A_0 mode becomes highly attenuating resulting in a weaker response. Hence, the choice of narrow band signal frequency is a critical decision in TOF detection frameworks.

An implementation of the TOF signal processing method using narrow band signal

excitation for detaction and localization was conducted by Tua [57]. The techniques was used to localize damage in Aluminum plates using Lamb wave propagation. The localization algorithm relied on TOF extraction by the signal processing technique known as the Hilbert Huang Transform (HHT) [15]. The HHT decomposes the signal into intrinsic mode functions (IMF) and the TOF is extracted from the energy-time spectrum. The limitation of HHT is that it lacks a robust mathematical framework, and as a result relies on setting heuristic parameters. Moreover the experimental techniques requires tuning the input narrowband signal for best performance for the defect type known in advance. Similar TOF methods utilizing thresholds [58] and peak finding [41, 59] have been used demonstrating the same limitations as peak detection uncertainty and not accounting for dispersive propagation.

A modified peak detection algorithm was proposed by [60] using the normalized hilbert transform in the form of an envelop vector. The guided wave modes were tracked by correlating wave modes in the time-space domain. However due to the dispersive nature of the UGW, mode tracking is complicated due to the fact that the number of modes are not known in advance. To mitigate this limitation the number of modes have to be predetermined by analyzing the kernal density function of the initial peak vector. Another major limitation of the mode tracking approach is that if there exist overlapping modes as in the case of anisotropic propagation, the algorithm is unable to track the overlapping peaks effectively.

3.1.2 Wavelet Transform for SHM

The *Wavelet Transform* (WT) has emerged as a versatile tool in the domain of signal processing, providing a multi-resolution analysis of signals. Unlike the traditional Fourier Transform, which decomposes signals into sinusoidal bases, the WT employs wavelets - functions localized in both time and frequency. The fundamental advan-

tage of the WT is its ability to represent signals with varying temporal characteristics more effectively. This is particularly useful in scenarios where the signal has transient or non-stationary features. Mathematically, the continuous wavelet transform of a signal $f(t)$ with respect to a wavelet $\psi(t)$ is given by:

$$W_f(a,b) = \int_{-\infty}^{\infty} f(t) \cdot \psi^* \left(\frac{t-b}{a} \right) dt \tag{3.1}$$

where a and b are the scale and translation parameters, respectively, and ψ^* denotes the complex conjugate of the wavelet. The adaptability of wavelets to various applications in signal processing, ranging from compression to denoising, underscores the significance of the wavelet transform in contemporary research.

Sohn et al. [61] present a approach for detecting delamination in composite structures using wavelet-based active sensing. The technique involves using an active piezoelectric transducer to emit a wavelet signal, which is then analyzed using a wavelet transform to identify the presence of delamination in the structure. The authors conducted experiments on composite panels with artificially introduced delamination and demonstrated that the proposed approach is effective in detecting and localizing delamination in composite structures.

Dispersion curve analysis of Lamb waves using the chirplet transform was performed by Niethammer et al. [62]. The study utilizes the chirplet transform technique to analyze dispersive wave signals based on a dispersion model. The chirplet transform is a more advanced version of the wavelet and short-time Fourier transforms, which can extract specific components of a signal with a particular instantaneous frequency and group delay. To extract the proportional energy distribution of a single mode from a multimode dispersive wave signal, an adaptive algorithm identifies frequency regions and uses locally adapted chirplets based on a dispersion curve model, allowing quantitative statements to be made about an individual mode's energy. The

adaptive chirplet algorithm proposed in this study is based on a model that uses the Rayleigh-Lamb equations to describe the dispersion relationship. By fitting chirplets to the known modelines based on this model, the algorithm assigns wave energy to the individual propagation modes.

Multiresolution analysis provides a systematic way to decompose a signal into its constituent scales or frequencies, making it an essential tool in signal processing [63]. The fundamental idea behind multiresolution analysis is to represent a signal at various levels of resolution, ranging from coarse approximations to detailed information. Wavelet transform, which stems from multiresolution analysis, has gained immense popularity for its capability to represent non-stationary signals with both time and frequency localization [64]. This multiresolution approach facilitates efficient signal compression, denoising, and feature extraction, especially in scenarios where the signal exhibits diverse spectral characteristics over different time intervals. By allowing for a hierarchical representation of the signal, multiresolution techniques enable a more intuitive and compact representation of complex signals, making them indispensable in modern signal processing tasks.

3.1.3 Wigner Distribution

The Wigner distribution, also referred to as the Wigner-Ville distribution (WVD), is a well-established tool in the domain of time-frequency signal analysis, providing a representation of a signal in both time and frequency domains simultaneously [65, 66]. The WVD is defined for a continuous-time signal $x(t)$ as

$$W_x(t,f) = \int_{-\infty}^{\infty} x\left(t+\frac{\tau}{2}\right) x^*\left(t-\frac{\tau}{2}\right) e^{-j2\pi f\tau} d\tau,$$

where $x^*(t)$ is the complex conjugate of $x(t)$. One of the significant advantages of the WVD is its ability to provide a high-resolution view of the signal's time-frequency

characteristics. However, it may also introduce cross-terms that can obscure the signal's actual time-frequency content, especially in multi-component signals [67]. Despite this limitation, the Wigner distribution remains a cornerstone in various signal processing applications, from radar to speech processing.

3.1.4 Matching Pursuit Decomposition

The matching pursuit decomposition (MPD) algorithm [68] is an iterative processing method that expands a signal into a weighted linear combination of elementary basis functions or "atoms" chosen from a complete dictionary. A comprehensive dictionary is utilized to choose atoms through progressive estimations of the signal using orthogonal projections on dictionary components. This involves a dictionary comprising of Gaussian atoms that have all potential time-frequency shifts and scale changes, and a quadratic time-frequency representation (TFR) is created by adding up the Wigner distribution (WD) of every chosen atom in the expansion. The altered WD maintains the signal energy, time-frequency shifts, and scale changes, while being free from any cross terms [69]. Various MPD algorithms have been suggested to accommodate signals with different nonlinear time-frequency characteristics [2]

The MPD dictionary is formed using a basic Gaussian signal $g(t) = e^{-t^2/2}$ as it is the most concentrated signal in TF, according to the uncertainty principle [10]. The dictionary $\mathcal{D}$ consists of time-shifted, frequency-shifted and scaled versions of the basic Gaussian signal

$$g_{\gamma_k}(t) = \sqrt{a_k}\; g(a_k(t-\tau_k)\, e^{j2\pi\nu_k\, t} = \sqrt{a_k}\; \exp\!\big(-a_k^2\,(t-\tau_k)^2/2\big)\; e^{j2\pi\nu_k\, t}$$

The parameter set of the kth dictionary atom is $\gamma_k = \{\tau_k,\ \nu_k,\ a_k\},\ \gamma_k \in \Gamma$ where $\tau_k \in \mathbb{R}$ is time-shift, $\nu_k \in \mathbb{R}$ is frequency-shift and $a_k \in \mathbb{R}^+$ is scale parameter.

We use the MPD to iteratively decompose a finite energy signal $x(t)$ as

$$x(t) = \sum_{i=0}^{\infty} \beta_i \, g_{\gamma_i}(t)$$

where $g_{\gamma_i}(t)$ and β_i is the ith selected dictionary atom and expansion coefficient, respectively. At the ith iteration, and starting with $r_0(t) = x(t)$, we form the inner product of the residual signal $r_i(t)$ and each dictionary element. We then select the ith element $g_{\gamma_i}(t)$ that results in the maximum inner product. Specifically, we select $g_{\gamma_i}(t)$ such that

$$g_{\gamma_i}(t) = \arg \max_{g_\gamma \in \mathcal{D}} \left| \int_{-\infty}^{\infty} r_i(t) \, g_\gamma^*(t) \, \mathrm{d}t \right| = \arg \max_{g_\gamma \in \mathcal{D}} | \langle r_i, g_\gamma \rangle |$$

The residual signal is given by

$$r_{i+1}(t) = r_i(t) - \beta_i \, g_{\gamma_i}$$

where the ith expansion coefficient is given by

$$\beta_i = \int_{-\infty}^{\infty} r_i(t) \, g_{\gamma_i}^*(t) \, \mathrm{d}t$$

The signal representation up to the ith iteration is

$$x(t) = r_{i+1}(t) + \sum_{\ell=0}^{i} \beta_\ell \, g_{\gamma_\ell}(t)$$

The maximum number of iterations L is normally selected to ensure that $E\%$ of the signal energy has been extracted, where E is a pre-defined threshold. After L iterations, the signal can be represented as

$$x(t) = r_L(t) + \sum_{i=0}^{L-1} \beta_i \, g_{\gamma_i}(t)$$

A block diagram summarizing the MPD is given in Figure 3.2

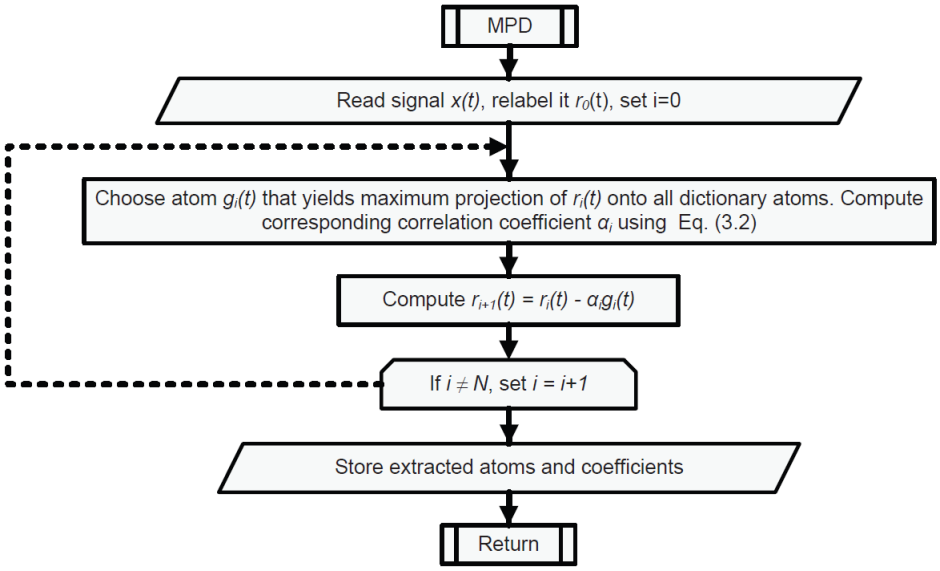

Figure 3.2: Flowchart Summarizing the Matching Pursuit Decomposition Algorithm [2]

3.1.5 Orthogonal Matching Pursuit

Orthogonal Matching Pursuit (OMP) is a greedy algorithm employed for sparse signal representation and has gained significant traction in the field of signal processing, especially in the domain of compressive sensing [70]. The fundamental principle behind OMP is to iteratively select the dictionary atom that is most correlated with the current residual, followed by the update of the signal approximation and the residual itself. Upon each iteration, OMP projects the original signal onto the subspace spanned by the selected dictionary atoms, ensuring an orthogonal projection, hence the name *orthogonal* matching pursuit [68]. The process is repeated until a predefined number of atoms are selected or the residual reaches a specified threshold. OMP's greedy nature ensures a computationally efficient approach to sparse decomposition, especially when compared to non-greedy methods that might involve convex optimization solutions, such as Basis Pursuit [71]. However, it is worth noting that while OMP can provide a near-optimal solution, there's no guarantee for a globally optimal

solution to the sparse representation problem, especially in the presence of highly coherent dictionaries. Nevertheless, the success of OMP in practical applications, such as image processing, audio signal reconstruction, and radar signal processing, highlights its robustness and efficiency in extracting sparse representations from redundant dictionaries.

3.1.6 Reassignment

Reassignment is a technique used in signal processing to refine the representation of energy in a time-frequency distribution, improving its readability and interpretability [17]. The core idea behind reassignment is to move energy from an original location in a spectrogram to a location that better represents the true center of energy of the nearby region. This technique often involves the use of the Short-Time Fourier Transform (STFT) along with its instantaneous frequency and group delay components. Reassignment effectively sharpens blurry regions in a spectrogram, enhancing the visualization of time-frequency characteristics of signals and facilitating a clearer distinction between closely spaced signal components [72]. Its application spans various fields, from music signal analysis to biomedical signal processing, where accurate time-frequency representation is crucial.

3.2 Highly Localized Time Frequency Transforms

A wide range of signal processing techniques are available to study UGW for SHM applications, however there are significant challenges in analyzing signals when complex material systems are involved. Firstly, while dispersive propagation is sufficiently understood for very simple material such as Aluminum plates, when dealing with anisotropic and heterogeneous material, no closed form solution exists to simulate dispersion characteristics. Experimental methods cannot simulate every possible

wave propagation scenario.

3.2.1 UGW Inspection of Integrated Circuits Using MPD

One such novel application of UGW is detection of defects in integrated circuit (IC) packages was investigated by Ikram et al [73]. Adhesive failure in an IC package occurs due to certain loading conditions or manufacturing induced defects such as the presence of residual moisture, foreign material or insufficient copper roughening, causing delamination between the layers and subsequent failure of the IC package. A key component of an integrated circuit (IC) package is the substrate, which consists of alternating layers of copper conductors on epoxy dielectric layers, laminated on to a fiberglass epoxy matrix core and is held together by mechanical adhesion as shown in figure 3.3. IC packages typically range from a few millimeters to tens of millimeters in length and width; the thickness of these packages is typically a few hundred microns. Heterogeneous integration of various components such as the silicon die, integrated heat spreader and printed circuit board lead to anisotropy in the assembled package. The presence of the geometric constraints, material anisotropy and sample fragility introduces enormous challenges in detection of subsurface defects in IC packages. Furthermore, the delamination defect size may be as small as a few hundred microns, further complicating the resolution requirements.

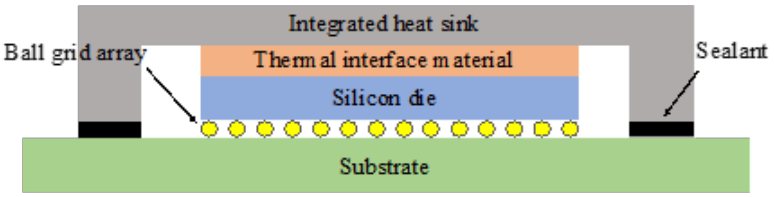

Figure 3.3: Cross Section View of a Typical IC Package

The use of NDE for detection of delamination in the IHS-Sealant interface requires penetration of few hundred millimeters and a sub millimeter spatial resolution. Due

to manufacturing design rules, the footprint of the interface is only a few millimeters wide, which poses an additional geometric constraint on sensor placement. Traditional X-Ray inspection techniques are expensive and pose a radiation hazard. Another state of the art in delamination inspection is the scanning acoustic microscopy (SAM) method, which is widely used in the semiconductor industry to conduct ultrasonic inspection in IC packages [2]. Research has been conducted using SAM with immersion based ultrasonic transducers to find sub surface defects in IC packages [74, 75]. In IC packaging, ultrasonic guided wave based techniques have potential to inspect bonded assemblies due to good sub surface penetration through metallic and dielectric material. However, the presence of a diverse range of material properties pose significant challenges in developing an ultrasonic wave based NDE methodology. The heterogeneity, anisotropy and nonlinear behavior of IC packages have a detrimental impact on transmission and detection of ultrasonic waves. A promising solution to these challenges is the use of guided ultrasonic waves to assess the condition of IC package. Guided waves allow instrumentation of the IC package over a large area and the IC package does not need to be submerged in liquid.

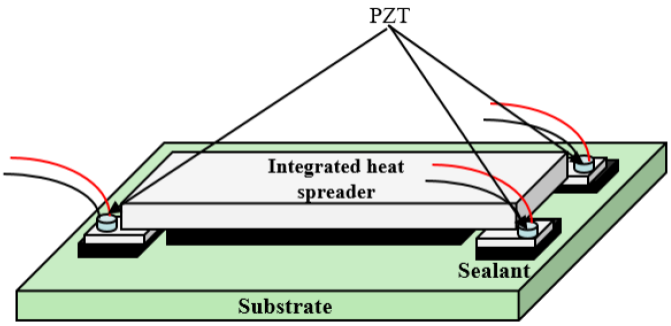

Figure 3.4: Actuator and Sensors Bonded to an IC Package

Sensor placement is critical for signal acquisition. A key considerations in sensor placement is wave reflections which occur every time a wave encounters an interface.

Hence it is essential to limit interfacial boundaries at the inspection region. Moreover, Scattering can occur at higher frequencies from coarse grain structures or inhomogeneous materials. Sensors should be placed in a region of highest homogeneity.

Piezoelectric (PZT) sensors are bonded to various locations on the IC package for evaluation. Various combinations of sensor placement were examined to determine the optimal sensor location paradigm, and the bonding locations are shown in figure 3.4. This results in a guided wave signal due to the variation between each unit leading to several mode conversions in the guided wave. Ten samples were examined with this configuration and the guided wave profile was not repeatable. An appropriate excitation frequency needs to be used for exciting guided waves in the test sample. Figure 3.5 shows the amplitude of the sensor place on the region of interest. The maximum amplitude is obtained when a frequency of 375 kHz is used. Hence a frequency of 375 kHz frequency will be used as the excitation frequency. The PZT sensors were excited using a digital acquisition card (National Instruments) and ultrasonic energy was transmitted through the test sample in the form of guided waves.

The MPD can be used to obtain highly localized and concentrated time-frequency representation. The MPD algorithm is capable of extracting MPD energy and their associated frequency components. The time-frequency representation is used to separate the modes in the time-frequency domain. The IHS-Sealant interface is now delaminated and instrumented under the same conditions. The results show a clear impact of delamination on the presence of guided wave modes as shown in figure 3.5.

Guided wave based NDE technique has been shown a promising application for detecting the delamination of the IC package at the IHS-Sealant interface that result in catastrophic failure of the part. In this study, results were presented on detection

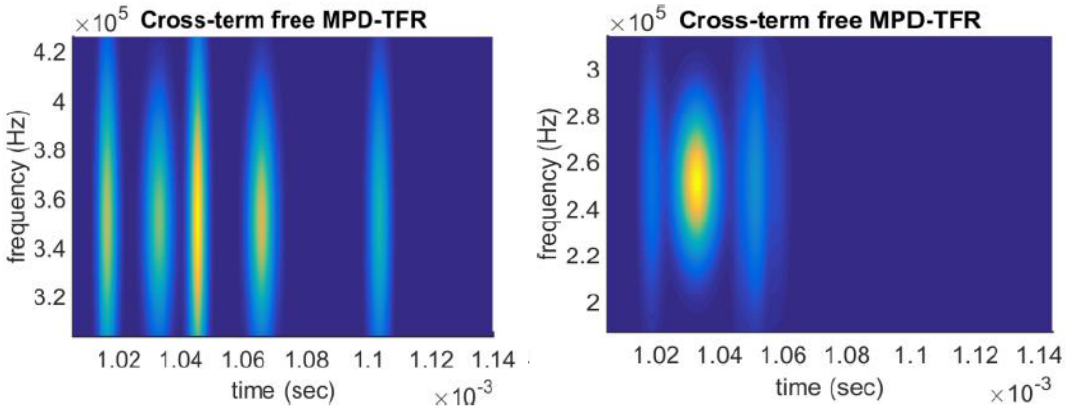

(a) MPD Results for Healthy IC (b) MPD Results for Damaged IC

Figure 3.5: Matching Pursuit Decomposition to Detect Damage in IC Packages

of delamination of the IHS-Sealant interface when instrumented with surface mount PZT actuator and Sensor at 375 kHz frequency. Optimal sensor placement paradigm was evaluated. Effects of damage on guided wave propagation through IHS-Sealant interface were studied. Due to material heterogeneity, it is not possible to obtain dispersion curves. Instead, a calibration methodology was incorporated to monitor the observable and repeatable changes in time-frequency domain. MPD algorithm is used to iteratively decompose and then represents the time-frequency components of the signal. The result of delamination is the elimination of higher order modes. This methodology can be used for structural health monitoring (SHM) of IC packages because active monitoring of health level is possible and has the potential to be extended to real time monitoring. The main limitation of this study is that the effects of dispersion are not considered in detail.

3.2.2 UGW Inspection of Integrated Circuits Using the Synchrosqueezing Transform

In order to incorporate the effects of dispersion while analyzing IC packages, Ikram et al [38] used first order SST. This is a transform that has been shown to be robust to bounded signal perturbations, to provide highly localized time and frequency information for highly nonlinear modes, and to reconstruct the signal corresponding to each mode. Reference ultrasonic guided wave signals are collected for the IC package in its healthy and damaged states using piezoelectric transducers to characterize the dispersion modes in the excitation region. Initial results demonstrate that the dispersive mode information from the extracted SST ridges provide an effective damage indicator for IC packaging.

The IC package used in this study is a large form factor (56 mm x 40 mm) IC package. The experimental setup uses the National Instruments PXI 14 bit 100 MS/s arbitrary wave generator (AWG) and 12 bits 60 MS/s digitizer are used to generate a 5-cycle cosine tone burst excitation signal and collect signals from each sensor with sampling frequency of 20 MHz. The adjacent actuator-sensor pairs are also placed at maximum distances from each other so that the signals have minimal superposition. This configuration also ensures that the boundary reflections arrive at the offset in the temporal domain, and hence can be filtered out of the data. Additionally, in order to optimize the signal-to-noise ratio, we select the frequency of maximum guided wave amplitude. This is experimentally achieved by scanning the frequency ranges from 100 kHz to 600 kHz in 25 kHz intervals. It is observed that at lower frequencies, the amplitude of the signal is lowest. The highest amplitude is around 400 kHz, after which the signal amplitude declines. The final signal was the average of ten measurements in order to maintain maximum signal integrity. The

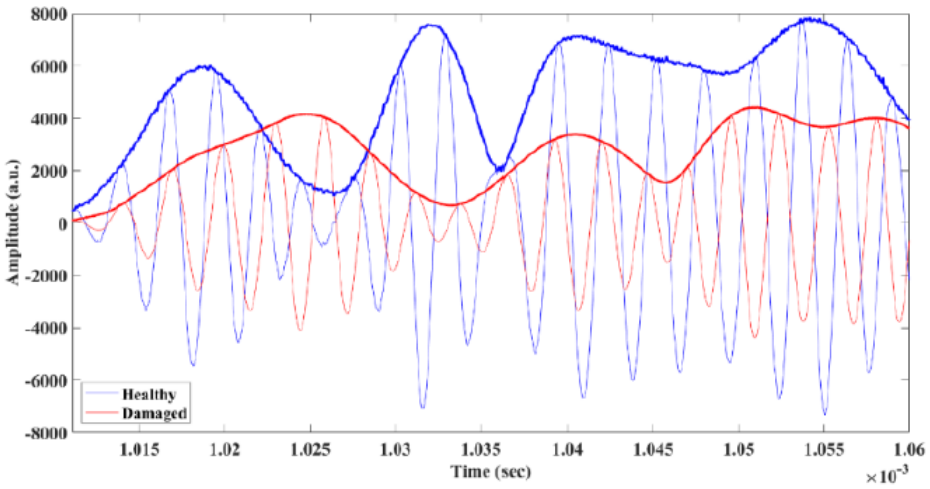

Figure 3.6: Signal Reconstruction for Healthy and Damaged States

framework consists of dispersion calibration, data collection and analysis.

The first order SST algorithm developed by Thakur et al [76] is used to analyze the signal. The time domain signals from healthy and damage IC packages are transformed to the TF domain. Ridge extraction and reconstruction is used to convert to the time domain without mode separation for comparison. Preliminary IC package health inspection results from experimental data shown in figure 3.6 demonstrate the effectiveness of the data driven approach. The methodology does not require numerical modeling as features can be directly estimated over the entire excitation range in the TF domain using experimental methods. The limitation of this approach is that while the algorithm utilizes the SST to account for dispersion, the algorithm is not matched to the signal characteristics and as a result does not account for non-linearities in the system.

3.2.3 Group Velocity Estimation for UGW Propagating in Dispersive Material

In order to account for nonlinear behavior of UGW and to account for dispersion, Ikram et al [39] developed an approach for characterizing frequency-dependent

mode properties of ultrasonic guided wave propagation in dispersive material. The approach exploits the relation between propagation group velocity and signal group delay changes to study a highly-localized time- frequency representation.

The short-time Fourier transform (STFT) of a signal $x(t)$ is

$$S_x(t, f; g) = \int x(\tau)\, g(\tau - t)\, e^{-j2\pi f \tau} d\tau\,, \tag{3.2}$$

where $g(t)$ is an analysis window. Although the STFT can resolve multicomponent signals, it suffers from loss of TF resolution caused by windowing. By reassigning the STFT along the signal's IF, $\zeta_x(t; f)$, result in the ST, given by

$$\mathrm{ST}_x(t, f; g) = \int S_x(t, \nu; g)\, \delta(f - \zeta_x(t; \nu))\, e^{j2\pi t f} d\nu\,, \tag{3.3}$$

where

$$\zeta_x(t; f) = f + \mathrm{Im}\left(\frac{S_x(t, f; g_d)}{S_x(t, f; g)}\right)\,, \tag{3.4}$$

$g_d(t) = \dot{g}(t) = \frac{d}{dt} g(t)$, and the operator $\mathrm{Im}(\cdot)$ takes the imaginary part of a complex value. Note that the IF $\zeta_x(t; f)$ in (3.4) assumes a differentiable window $g(t)$ and non-zero STFT values in the denominator. In addition to offering high TF localization along the signal's IF, it is possible to use the ST to reconstruct individual signal components and estimate their IFs; this is under the assumption that the signal satisfies some constraints, including weak frequency modulation [31, 4].

The assumed signal model

$$x(t) = a(t)\, e^{j2\pi(f_c t + 0.5\alpha\, t^2)}$$

is of a linear frequency-modulated (LFM) chirp signal with Gaussian amplitude modulation given by $a(t) = e^{-0.5\, t^2/T_x^2}$; the LFM IF is obtained as $f_c + \alpha\, t$. Following [5], $x(t)$ and its partial derivative $\dot{x}(t)$ with respect to time can be shown to be related

according to

$$\dot{x}(t) = (q_x\, t + p_x)x(t)$$

where $q_x = j2\pi\alpha - (1/T_x^2)$ and $p_x = j2\pi f_c + (1/T_x^2)$. Making use of this relation, and taking the partial derivative of the STFT with respect to time, an unbiased IF estimate can be obtained by solving for the LFM rate α. This estimate is given by

$$\zeta_{x,1}(t; f) = f + \frac{\mathrm{Im}\left(S_x(t, f; g_d)\, S_x(t, f; g_m)\right)}{\mathrm{Re}\left(S_x(t, f; g)\, S_x(t, f; g_t)\right)}$$

where $g_m(t) = t\, g(t)$ and the operator $\mathrm{Re}(\cdot)$ takes the real part of a complex value. A modified ST, that corresponds to a first-order synchrosqueezed STFT, leads to unbiased IF estimates; this TFR can be obtained by replacing $\zeta(t; f)$ in Equation (3.3) with $\zeta_{x,1}(t; f)$. As was shown in [5], new unbiased LFM IF estimates can be obtained by taking multiple partial derivatives of the STFT with respect to time; using higher order derivatives yields in unbiased estimators that offer better TF localization for strongly frequency modulated signals.

GD Based Dual Synchrosqueezing Transform

For UGW propagation modeling, we require a TFR that is highly localized along the signal's GD in addition to being able to reconstruct individual modes. Using Fourier transform (FT) duality, the time domain signal $x(t)$ and its IF are dual pairs to the signal's FT $X(f)$ and its GD. As a result, a dual ST can be obtained as in (3.5), but reassigning the STFT the signal GD $\tau_x(f; t)$. Specifically, re-formulating the STFT in the FT domain, we obtain

$$S_x(t, f; G) = e^{j2\pi tf} \int X(\nu)\, G(\nu - f)\, e^{-j2\pi t\nu} d\nu$$

where $G(f)$ is the FT of the window $g(t)$. Reassigning the STFT along the signal's GD results in the DST is given by

$$\mathrm{DST}_x(t,f;g) = \int S_x(\hat{t},\ f;g)\,\delta(t-\tau_x(f;\hat{t}))\,e^{j2\pi\hat{t}f}d\hat{t}\,, \tag{3.5}$$

where

$$\tau_x(f;t) = t - \mathrm{Re}\left(\frac{S_x(t,f;\mathcal{G}_d)}{S_x(t,f;G)}\right).$$

and $\mathcal{G}_d = \dot{G}(f) = \frac{d}{df}G(f)$. Note that other ST modifications that concentrate on estimating GD have been independently proposed by the authors in [6] and [77].

Modified DST for Group Velocity Estimation

We propose a modification to the DST (MDST) that replaces $\tau_x(f;t)$ in (3.5) with an unbiased GD estimate that is better matched to the stronger modulation resulting from UGW propagation. In order to match the MDST to dispersive group velocity modes, we assume that the transmit signal $x(t)$, with FT $X(f)$, is a windowed sinusoid with frequency f_c and Gaussian amplitude modulation. Specifically, $x(t) = a(t)\,e^{j2\pi f_c t} = e^{-0.5\,t^2/T_x^2}\,e^{j2\pi f_c t}$, with FT given by $X(f) = 2\pi\,T_x\,e^{-2\pi^2\,T_x(f-f_c)^2}$. Note that the parameter T_x is directly related to the signal duration in time. Thus, the spectral mode at distance r is thus given by

$$X_r(f) = 2\pi\,T_x\,e^{-2\pi^2\,T_x(f-f_c)^2}\,e^{j2\pi k(f)r}\,. \tag{3.6}$$

As the phase function of $X_r(f)$ is $k(f)$, the mode group velocity $c_g(f) = 1/\tau(f)$. Following similar steps as in [5] but in the frequency domain, we can show that $X_r(f)$ is related to its first order derivative with respect to frequency according to

$$\dot{X}_r(f) = \big(j2\pi r\,\tau(f) - 4\pi^2\,T_x(f-f_c)\big)\,X_r(f)\,. \tag{3.7}$$

When re-written as $\dot{X}_r(f) = (Q_x\,\tau(f) + P_x)X_r(f)$, this relation is dually similar to the one for the LFM case, $q_x\,f + p_x$. However, simply taking partial derivatives of the STFT with respect to frequency does not provide an estimate of the GD, $\tau(f)$. It is important to note from Equation (3.7) that transmit signals must have short durations as T_x cannot go to infinity.

Using a second-order Taylor series' expansion about the transmit frequency, we approximate the phase function in (3.6) as $k(f) \approx k(f_c) + k'(f_c)\,(f - f_c) + \frac{1}{2!}k''(f_c)\,(f - f_c)^2$. Here, $k'(f)$ and $k''(f)$ are the first and second order derivatives of $k(f)$ with respect to frequency. Using this approximation, and computing second order derivatives of the STFT with respect to frequency, we derive the new GD estimate as

$$\tau_{x,2}(f;t) = t - \mathrm{Re}\left(\frac{S_x(\mathcal{G}_{dd})\,S_x(G) - S_x^2(\mathcal{G}_d)}{S_x(\mathcal{G}_d)\,S_x(\mathcal{G}_m) - S_x(\mathcal{G}_{md})\,S_x(G)}\right) \tag{3.8}$$

where, for ease of notation, $S_x(G) \equiv S_x(t, f; G)$; also, the STFT windows are given by $\mathcal{G}_{dd} = \frac{d^2}{df^2}\mathcal{G}_d(f)$, $\mathcal{G}_m(f) = f\mathcal{G}_d(f)$, and $\mathcal{G}_{md}(f) = f\dfrac{d}{df}\mathcal{G}(f)$. A modified DST (MDST), that corresponds to a second-order synchrosqueezed STFT, leads to unbiased GD estimates; this TFR can be obtained by replacing $\tau(f;t)$ in Equation (3.5) with $\tau_{x,2}(f;t)$. Note that the MDST is different from the TFR obtained when taking partial derivatives of the STFT with respect to frequency, with the STFT defined as in (4.1) (see Equation (17) in [5]).

Simulation Results

The proposed MDST TFR can be used to extract individual GD signal components. The performance of this new approach for extracting individual group velocity modes using wave propagation through an isotropic Aluminium plate. We used the Waveform Revealer software tool [40] to simulate UGWs propagating in isotropic Aluminum 6061 with 2 mm thickness and 2700 kg/m^3 material density. The input signal

is a tone burst with center frequency ranging from 100 to 1500 kHz, in 1 kHz intervals; this results in exciting both symmetric and anti-symmetric Lamb waves through the plate. Measurements are provided using two sensors placed in a pitch-catch configuration. The first sensor is collocated with the actuator to measure the excitation wave; the second sensor is placed at a distance of 500 mm away from the source. Dispersion leads to Lamb wave modes traveling with varying group velocities through the plate. Figure 3.7a shows the time-domain UGW received at the sensor. By implementing the GD estimator defined in equation (3.8), the highly-localized MDST of the same signal is shown in Figure 3.7b.

Dispersion Evaluation

The dispersive model accuracy is improved by the use of the unbiased GD estimator in the MDST formulation. The multimodal energy distribution from the MDST can be visualized in the slowness-frequency domain, where slowness is inversely proportional to the group velocity, as shown in figure 3.8. Moreover, the group velocity can be accurately extracted and represented as shown in 3.8 (a). Figures 3.8 (b) and 3.8 (c) show that the extracted group velocity modes are in agreement with the theoretical calculations.

3.3 Conclusion

A novel approach to analyze UGW is developed by extracting and characterizing dispersive ultrasonic guided wave modes in isotropic media. The approach first derives an unbiased group delay estimator that is matched to strongly modulated signals; the estimator is then incorporated into a synchrosqueezed short-time Fourier transform. The resulting time-frequency representation (TFR) is well matched to guided wave dispersive propagation. Individual dispersive modes are extracted using this TFR

and an unsupervised clustering algorithm followed by curve fitting.

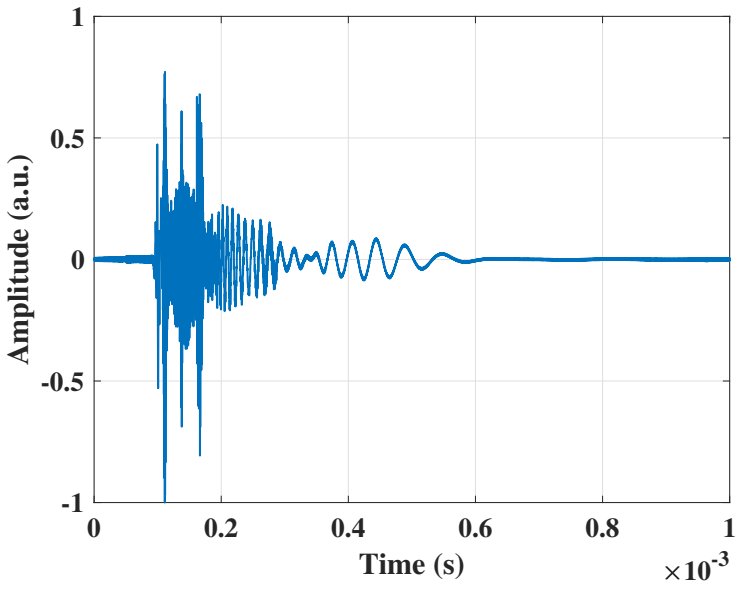

(a)

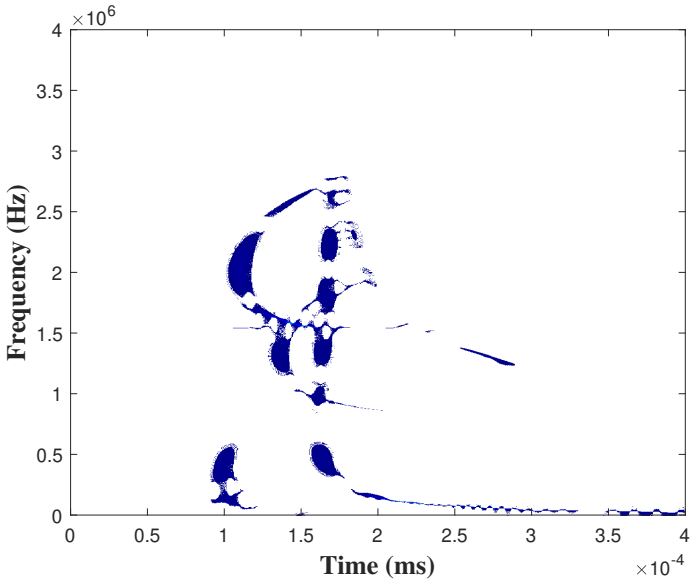

(b)

Figure 3.7: (a) Time Domain and (b) MDST of an UGW Signal.

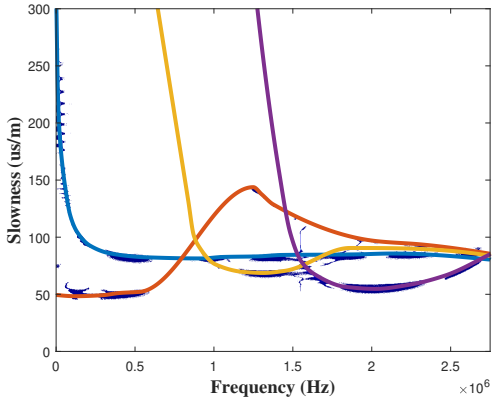

(a) Dispersion in Slowness-frequency Domain

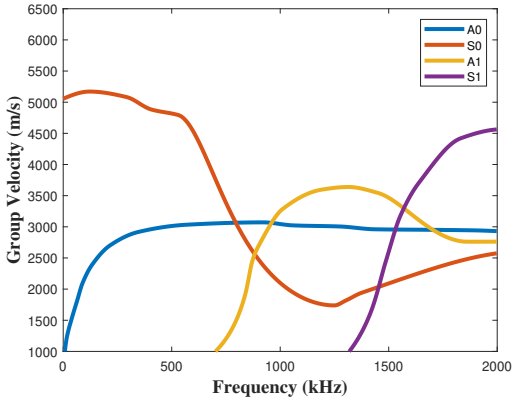

(b) MDST Estimated Group Velocity

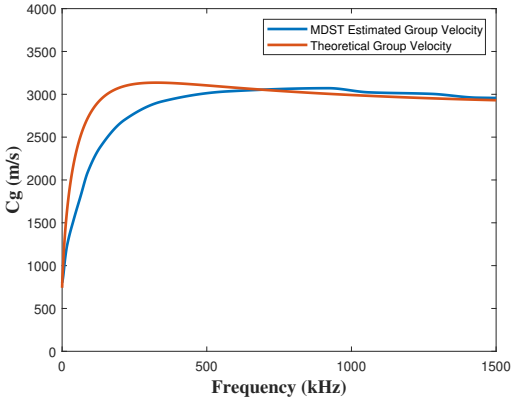

(c) A0 Mode Group Velocity

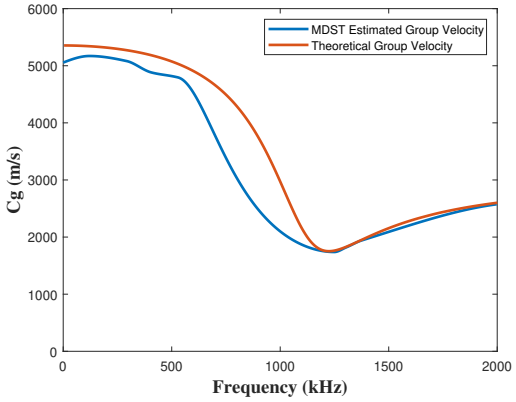

(d) S0 Mode Group Velocity

Figure 3.8: Dispersion Analysis of UGW in Isotropic Medium.

Chapter 4

NEW TIME FREQUENCY TRANSFORM MATCHED TO GROUP DELAY

4.1 Problem Formulation

Interpretation of UGW propagation by numerical modelling and analytical simulation can potentially allow for robust damage detection. However, analytical solutions for UGW propagation are extremely challenging for complex structures due to the dispersive nature of these waves. Despite the challenges of modelling highly dispersive UGW, significant efforts have been made in developing analytical solutions for dispersion curves. In his classical work on elastic wave propagation in 1885, Lord Rayleigh was the first to investigate the behavior of waves in free surface of an infinite, homogeneous and isotropic solids [78]. He determined that such a case was analogous to that of deep water waves and that such waves are confined to the surface of the elastic solid. Hence such waves came to be known as surface waves. In 1911, Love generalized the surface wave solution by incorporating an additional finite thickness layer [79]. The study developed the horizontally polarized shear-horizontal (SH) wave. Soon afterwards Lamb published his groundbreaking study of wave propagation in a layer of finite thickness and identified the two possible wave modes that can propagate in such a situation. These wave modes are called the symmetric and antisymmetric wave modes [80].

Until this point in time, most of the research on wave propagation had occurred in the context of seismology. The study of elastic wave propagation in multilayered media was introduced by Thomson [81] and Haskell [82] in which they used the matrix transfer method. The matrix method systematizes the analysis by directly relating

the stresses and displacements at the top of the individual layers to the bottom of the neighboring layer when the interface conditions are satisfied. However such a method suffered from numerical instability when the product of frequency and thickness, was large. An alternative to the matrix method, called the direct method was proposed by Schmidt [83]. In the direct method, the matrix solution of each layer is re-assembled as a single matrix once all interfacial conditions are satisfied. Many improvements and permutations of the direct method as well as the matrix method have been proposed in literature, however the solutions are problem dependent and vary in degree of computational complexity as well as assumptions on material geometry.

However, these modelling efforts were not able to account for all possible wave propagation scenarios, and in particular, were insufficient for anisotropic materials. Composite materials for example, consist of multiple layers to form a laminate which is both anisotropic and inhomogeneous. The material properties in the anisotropic case are dependent on the direction of the composite material. Moreover, when modelling interaction of UGW with anisotropic material, the elastic properties of each constituent material and layer should be known apriori. The properties vary, depending on individual components of the lamina. Efforts to develop approximate models to predict effective properties of composite material have been undertaken [84]. Other numerical techniques to model wave propagation in complex material have been proposed such as using the finite element method [85, 86], local interaction simulation approach (LISA) [87] and more recently a detailed physics based wave propagation model [88]. Despite these efforts, no closed form analytical solution has been developed for dispersion characterization of UGW in complex materials because of the difficulty in accurately modelling highly dispersive wave modes.

Since robust modelling of wave propagation through dispersive material is not

possible for many complex material systems, efforts have been made to analyze the experimental signals directly in the time domain. Time domain analysis methods primarily rely on identifying the time of flight (TOF) information associated with individual modes to identify and localize damage. TOF is the time it takes the sensor to receive the wave mode from the actuator or a reflected wave from interfaces and damage. For a known propagation distance, the time of flight can be calculated only if the wave velocity is known. However dispersive waves have frequency dependent wave velocities and multiple propagating modes. Due to the uncertainty in determining the frequency wave velocity, the TOF cannot be accurately predicted without special methods. One such method is dispersion compensation, which allows the frequency dependent velocity to be taken into account by using apriori knowledge of the dispersion curve [24]. While dispersion compensation can limit the effects of dispersion in simple scenarios such as isotropic single layered medium, for most non-isotropic or multilayered cases the dispersion curves cannot be calculated in advance. Similarly, use of narrow band excitation such as tone burst has been proposed with the aim of minimizing the affects of dispersive propagation [48]. However these techniques cannot completely eliminate dispersion, as such tone bursts will disperse as they propagate through the material. Time reversal techniques are also proposed which calculates TOF information from forward and backward propagating waveforms [89, 90]. Although simple, this technique is only shown to be effective for simple situations and single mode propagation as the technique does not account for dispersion.

In summary, for multimode dispersive propagation, time domain methods are less accurate The first reason for this phenomenon is dispersion. TOF estimation is complicated because time domain techniques do not take dispersion into account. Use of narrow band excitation and dispersion compensation techniques have been

proposed that aim to minimize the affects of dispersive propagation, however these techniques cannot completely eliminate dispersion. Moreover the techniques rely on apriori knowledge of materials hence limiting their applications. Secondly, the detection of peaks is an important part of the analysis. TOF determination in the time domain is a very challenging task in multimodal systems since various peaks may overlap. Moreover attenuation and noise may also affect determination of the mode peaks.

The complexity of modeling the dispersive UGW wave propagation depends on the material and cannot always be derived analytically. However, knowledge of the inherent dispersive properties for different material is critical in investigating structural failure modes. For UGW propagation modeling, we require a TFR that is highly localized along the signal's GD in addition to being able to reconstruct individual modes. In other words, we require analysis tools that can both separate guided wave dispersion curves that are closely spaced as well as extract highly localized information. The Synchrosqueezing technique with time reassignment, addresses the main requirements for UGW propagation analysis: high GD localization, substantial separation, and reconstruction of individual signal component modes. We thus propose a new SST TFR that is aimed to better match signals with nonlinear GD function.

The use of UGW propagation in SHM requires methods to analyze and extract the multiple dispersive modes. One such method involves highly-localized TFRs due to the multiple frequencies present in the signal at any given time [91]. The Wigner distribution (WD) is a highly localized TFR but suffers from interference terms for multicomponent signals and signals with nonlinear TF characteristics. Another widely used TFR is the short-time Fourier transform (STFT) given by

$$S_x(t, f; H) = \int X(f - \nu)\, H(\nu)\, e^{-j2\pi t\nu}\, d\nu\,, \tag{4.1}$$

Matched Phase	Estimator	Approach
$\phi(t) \propto t$	IF	FRO with $\frac{\partial}{\partial t}$ of STFT phase [94, 3]
$\phi(t) \propto t$	GD	TRO [6]
$\phi(t) \propto t^2$	IF	enhanced FRO with $\frac{\partial^2}{\partial t^2}$ of STFT phase [4]
$\phi(t) \propto t^2$	IF	UBE with $\frac{\partial}{\partial t}$ and $\frac{\partial^n}{\partial t^n}$ or $\frac{\partial}{\partial t}$ and $\frac{\partial^n}{\partial f^n}$ of STFT [5]
$\phi(t) \propto t^2$	GD	enhanced TRO [6]
$\phi(t) \propto t^3$	IF	$\frac{\partial^3}{\partial t^3}$ of STFT [95]
$\phi(t) \propto t^n$	IF	estimator with $\frac{\partial}{\partial t}$ of STFT, and $n-1$ iter. of $\frac{\partial}{\partial f}$ [96]
$\phi(t) \propto f^2$	GD	estimator with $\frac{\partial^2}{\partial f^2}$ of STFT [39]
$\phi(t) \propto f^3$	GD	estimator with $\frac{\partial}{\partial f}$, $\frac{\partial^2}{\partial f^2}$ and $\frac{\partial}{\partial t}\frac{\partial}{\partial f}$ of STFT [7]

Table 4.1: Summary of Synchrosqueezed STFT TFRs Providing High TF Localization for Signals with Time Domain Phase Function $\phi(t)$ and Signals with Frequency Domain Phase Function $\Phi(f)$.

where $X(f)$ and $H(f)$ are the Fourier transforms of the analysis signal $x(t)$ and real and even window $h(t)$. Although simple to implement and does not exhibit interference terms, the STFT, and its squared magnitude, the spectrogram, face a window-dependent trade off between time and frequency localization. The reassigned spectrogram resolves the localization issue by mapping TF points to regions of high signal concentration using a time reassignment operator (TRO) and frequency reassignment operator (FRO) [92, 17, 93]. It is a highly localized TFR for multicomponent signals and it is specifically matched to signals with quadratic phase function [17]. However, it cannot be used to reconstruct individual signal components.

The synchrosqueezing transform (SST) applied to the STFT exploits the high localization offered by the reassignment operators while allowing for signal mode reconstruction [97, 94, 3, 31]. The SST TFR is given by [94, 3]

$$\mathrm{SST}_x(t,f) = \int S_x(t,\nu;h)\,\delta(f-\zeta_x(t;\nu))\,e^{j2\pi tf}\,d\nu\,, \tag{4.2}$$

where $\zeta_x(t;f) = f + \text{Im}\{S_x(t,f;h_d)/S_x(t,f;h)\}$ is the FRO in [17], $\text{Im}\{z\}$ denotes the imaginary part of z, and $h(t)$ and $h_d(t) = \frac{d}{dt}h(t)$ are STFT windows in time. The TFR was shown to provide high localization for weakly-modulated signals also provide perfect localization for signals with linear phase in time (constant IF). Different synchrosqueezed STFT TFRs have been proposed in the literature (see Table 4.1) that differ in the domain of reassignment as well as the signal they match. Frequency SSTs (FSSTs or vertical SSTs) reassign in frequency using a local IF estimator $\hat{f}_x(t,f)$, thus moving a STFT TF point (t,f) to a new TF point $(t,\hat{f}_x(t,f))$ along the IF. On the other hand, time SSTs (TSSTs or horizontal SSTs) reassign in time using a local GD estimator; a STFT TF point (t,f) is thus moved to a new TF point $(\hat{t}_x(t,f),f)$ along the IF. As the FRO can be obtained from the first-order time derivative of the STFT phase, the TFR in (4.2) is considered a first-order FSST. A second-order FSST TFR was proposed in [4, 98] using second-order time derivatives of the STFT phase; it is matched to signals with quadratic phase in time (linear IF). Another second-order FSST was proposed in [5] based on multiple unbiased IF estimators obtained by solving a system of two linear equations. One equation is formed using the first-order time derivative of the STFT whereas multiple choices for the second equation result from the second or higher order time or frequency derivatives of the STFT. The higher-order FSST in [96] was developed to match signals with nth order polynomial phase function in time and thus provide high localization for stronger modulated signals. The frequency reassignment for this TFR is performed by first obtaining a local IF estimate using the first-order time derivative of the STFT, followed by $n-1$ iterations of the first-order frequency derivative of the IF estimate. This TFR was used to analyze seismic signals, fault bearing features, voice jitter and radar signals [99, 100, 101, 102]. Recently, a third-order FSST was obtained using third-order time-derivatives of the STFT for signals with third-order

polynomial phase in time [95]. TSST TFRs of first and second order were proposed in [6] using the TRO and an enhanced TRO for estimating GD. These TFRs were shown to provide high localization for impulsive signals. Note that a similar approach to [96] for vertical SST was presented for horizontal SSTs in [103].

4.2 Proposed Group Delay Estimation Approach

For matched analysis, we consider the generalized time-modulated (GTM) signal $x(t)$ with FT:

$$X(f) = A(f)\, e^{-j2\pi\Phi(f/f_r)}$$

where $\Phi(f/f_r)$ is the nonlinear phase function, $f_r = 1$ is a normalization frequency unit, and $\tau(f) = \frac{d}{df}\Phi(f)$ is the signal's GD. Note that the amplitude modulation allows for orthogonality if selected as $A(f) = \sqrt{|\tau(f)|}$ assuming the phase is an invertible and differentiable function [104]. For UGW propagation, the GTM phase matches that of the ℓth dispersive mode

$$\Phi(f) = r_\ell\, k_\ell(f)$$

GTM examples include hyperbolic time-modulated (HTM) signals with time-modulation rate (TMR) c and logarithmic phase $\Phi(f) \propto \ln(f),\ f > 0$, and power time-modulated (PTM) signals with real power parameter κ and power-law phase $\Phi(f) \propto f^\kappa$. Whereas HTM signals have similar TF characteristics as the echolocation signals of bats and dolphins [105, 106], PTM signals have similar TF structure as the echo returns from acoustic transmissions along a steel beam [107].

A matched TFR for the GTM signal can be obtained using the synchrosqueezing approach as

$$\mathrm{DSST}_x(t, f; H) = \int S_x(\eta, f; H)\, \delta(t - \hat{\tau}_x(f; \eta))\, e^{-j2\pi\eta f}\, d\eta\,, \tag{4.3}$$

STFT	Analysis Window
$S \equiv S_x(t,f;H)$ in (4.1)	$H(f)$
$S_{\mathcal{D}} \equiv S_x(t,f;\mathcal{D}H)$	$(\mathcal{D}H)(f) = \frac{d}{df}H(f)$
$S_{\mathcal{M}} \equiv S_x(t,f;\mathcal{M}H)$	$(\mathcal{M}H)(f) = f\,H(f)$
$S_{\mathcal{D}^2} \equiv S_x(t,f;\mathcal{D}^2H)$	$(\mathcal{D}\mathcal{D}H)(f) = \frac{d}{df^2}H(f)$
$S_{\mathcal{M}^2} \equiv S_x(t,f;\mathcal{M}^2H)$	$(\mathcal{M}^2H)(f) = f^2\,H(f)$
$S_{\mathcal{M}\mathcal{D}} \equiv S_x(t,f;\mathcal{M}\mathcal{D}H)$	$(\mathcal{M}\mathcal{D}H)(f) = f\,\frac{d}{df}H(f)$
$S_{\mathcal{M}^2\mathcal{D}} \equiv S_x(t,f;\mathcal{M}^2\mathcal{D}H)$	$(\mathcal{M}^2\mathcal{D}H)(f) = f^2\,\frac{d}{df}H(f)$
$S_{\mathcal{M}^3} \equiv S_x(t,f;\mathcal{M}^3H)$	$(\mathcal{M}^3H)(f) = f^3\,H(f)$

Table 4.2: Notation of STFTs Based on Choice of Window. Operators $\mathcal{D}$ and $\mathcal{M}$ Denote Differentiation and Multiplication, Respectively. The Operator Precedence Follows, for Example, $(\mathcal{M}^2\mathcal{D}H)(f) = (\mathcal{M}(\mathcal{M}(\mathcal{D}H)))\,(f)$.

provided $\hat{\tau}_x(f;t)$ is a matched estimator of the signal's GD. In order to find such an estimator, we assume a class of signals with power-law GD characteristics. Following [96], we can also assume an arbitrary nonlinear phase function that can be approximated by a polynomial using a Taylor's series expansion. In particular, we assume cubic polynomial phase function ,

$$\Phi(f) = \Phi_0 + t_x\,f + (b_x/2)\,f^2 + (c_x/3)\,f^3$$

resulting in the quadratic GD function

$$\tau(f) = t_x + b_x\,f + c_x\,f^2$$

Thus, $\hat{\tau}_x(f;t)$ in (4.3) is obtained by estimating the time constant t_x, the linear term b_x and the quadratic TMR parameter c_x.

Following the general approach in [4, 5], we formulate and solve a system of three linear equations that are derived by taking derivative of the STFTs. This derivation of the system of equations is provided in Appendix A In matrix form, the system of equations is given by

$$\begin{bmatrix} S_{\mathcal{D}} \\ S_{\mathcal{D}\mathcal{D}} \\ S_{\mathcal{M}\mathcal{D}} + S \end{bmatrix} = \begin{bmatrix} S_{\mathcal{M}^2} & S_{\mathcal{M}} & S \\ S_{\mathcal{M}^2\mathcal{D}} & S_{\mathcal{M}\mathcal{D}} & S_{\mathcal{D}} \\ S_{\mathcal{D}^3} & S_{\mathcal{M}^2} & S_{\mathcal{M}} \end{bmatrix} \begin{bmatrix} R_x \\ Q_x(f) \\ P_x(f) + j2\pi t \end{bmatrix} \tag{4.4}$$

where

$$\Upsilon_x(f) = -j2\pi(t_x + b_x\, f + c_x\, f^2)$$

$$L(f) = j2\pi(b_x + 2\, c_x\, f)$$

$$C_x = -j2\pi c_x$$

the STFTs with varying windows are defined in Table 4.2. The system in (4.4) was solved using Cramer's rule and validated numerically to obtain

$$\hat{C}_x = \frac{S_{\mathcal{D}\mathcal{D}} S_{\mathcal{M}}^2 - 2\, S_{\mathcal{M}} S_{\mathcal{M}\mathcal{D}} S_{\mathcal{D}} - S\, S_{\mathcal{M}} S_{\mathcal{D}} + S\, S_{\mathcal{M}\mathcal{D}}^2 + S^2\, S_{\mathcal{M}\mathcal{D}} - S\, S_{\mathcal{M}^2} S_{\mathcal{D}\mathcal{D}} + S_{\mathcal{M}^2} S_{\mathcal{D}}^2}{S_{\mathcal{D}} S_{\mathcal{M}^2}^2 - S\, S_{\mathcal{M}\mathcal{D}} S_{\mathcal{M}^2\mathcal{D}} S_{\mathcal{M}^2} - S_{\mathcal{M}^3} S_{\mathcal{D}} S_{\mathcal{M}} + S\, S_{\mathcal{M}^3} S_{\mathcal{M}\mathcal{D}}} \tag{4.5}$$

$$\hat{L}_x(f) = \frac{S^2 S_{\mathcal{M}^2\mathcal{D}} + S_{\mathcal{M}^3} S_{\mathcal{D}}^2 + S\, S_{\mathcal{M}^2\mathcal{D}} S_{\mathcal{M}\mathcal{D}} - S_{\mathcal{M}^2\mathcal{D}} S_{\mathcal{M}} S_{\mathcal{D}} + S_{\mathcal{M}^2} S_{\mathcal{M}} S_{\mathcal{D}\mathcal{D}} - S_{\mathcal{M}^2} S_{\mathcal{M}\mathcal{D}} S_{\mathcal{D}} - S\, S_{\mathcal{M}^2} S_{\mathcal{D}} - S_{\mathcal{M}^3} S_{\mathcal{D}\mathcal{D}}}{S_{\mathcal{D}} S_{\mathcal{M}^2}^2 - S_{\mathcal{M}\mathcal{D}} S_{\mathcal{M}^2} S_{\mathcal{M}} - S\, S_{\mathcal{M}^2\mathcal{D}} S_{\mathcal{M}^2} + S_{\mathcal{M}^2\mathcal{D}} S_{\mathcal{M}^2} - S_{\mathcal{M}^3} S_{\mathcal{D}} S_{\mathcal{M}} + S\, S_{\mathcal{M}^3} S_{\mathcal{M}\mathcal{D}}} \tag{4.6}$$

and $\hat{\Upsilon}_x(f) + j2\pi t = \Gamma(t, f)/\Lambda(t, f)$, where

$$\Gamma(t, f) = -S_{\mathcal{M}^2} S_{\mathcal{M}\mathcal{D}}^2 + S_{\mathcal{M}^2}^2 S_{\mathcal{D}\mathcal{D}} + S_{\mathcal{M}^2\mathcal{D}} S_{\mathcal{M}} S_{\mathcal{M}\mathcal{D}} - S_{\mathcal{M}^2} S_{\mathcal{M}^2\mathcal{D}} S_{\mathcal{D}} + S\, S_{\mathcal{M}^2\mathcal{D}} S_{\mathcal{M}} - S\, S_{\mathcal{M}^2} S_{\mathcal{M}\mathcal{D}}$$

$$- S_{\mathcal{M}^3} S_{\mathcal{M}} S_{\mathcal{D}\mathcal{D}} + S_{\mathcal{M}^3} S_{\mathcal{M}\mathcal{D}} S_{\mathcal{D}}$$

$$\Lambda(t, f) = S_{\mathcal{D}} S_{\mathcal{M}^2}^2 - S_{\mathcal{M}\mathcal{D}} S_{\mathcal{M}^2} S_{\mathcal{M}} - S\, S_{\mathcal{M}^2\mathcal{D}} S_{\mathcal{M}^2} + S_{\mathcal{M}^2\mathcal{D}} S_{\mathcal{M}}^2 - S_{\mathcal{M}^3} S_{\mathcal{D}} S_{\mathcal{M}} + S\, S_{\mathcal{M}^3} S_{\mathcal{D}}\,.$$

To obtain the GD estimate, we need to solve for $\tau(f) = t_x + b_x\, f + c_x\, f^2$. Since $j2\pi(t_x + b_x\, f + c_x\, f^2) = j2\pi t - \Gamma(t, f)/\Lambda(t, f)$, taking the imaginary part of both sides results in

$$\hat{\tau}(f; t) = (\hat{t}_x + \hat{b}_x\, f + \hat{c}_x\, f^2) = t - \frac{1}{2\pi} \operatorname{Im}\Big\{\Gamma(t, f)/\Lambda(t, f)\Big\}\,. \tag{4.7}$$

Using the estimated GD $\hat{\tau}(f;t)$ in Equation (4.3), we obtain the new dispersive SST (DSST) TFR. In addition to the GD estimate in (4.7), the solution of (4.4) provides an estimate of the quadratic TMR parameter $\hat{c}_x = -\frac{1}{2\pi}\,\mathrm{Im}\{\hat{C}_x\}$ using Equation (4.5). This is an important parameter that provides information on the rate of nonlinear change in group delay. The detailed mathematical derivation is provided in Appendix A.

4.3 Analysis of Parabolic Frequency Modulated Signal

To illustrate the performance of the new NSST, we consider a parabolic frequency modulation (PFM) signal modelled in the frequency domain. The reason to use this type of signal is to simulate high level of nonlinearity. PFM signals are a special case of frequency modulated signals and are frequently used in a variety of communication such as radar communication. PFM signals can suffer from non-linear distortion, which can lead to unwanted harmonic distortion and can be more sensitive to noise and interference than other types of signals.

The cubic coefficients and the maximum bandwidth of the PFM signal is selected to simulate a highly non-linear signal. The frequency modulated signal is generated with the phase function in the frequency domain such that

$$\Phi(f) = \frac{c_3}{3}f^3 + \frac{c_2}{2}f^2 + c_3 f + c_1$$

where $c_3 = 0.001$, $c_2 = 0.00000001$, $c_1 = 1.9$ and $c_4 = 0.001$. A maximum frequency bandwidth from $-\frac{f_{max}}{2}$ to $\frac{f_{max}}{2}$ is set such that $f_{max} = 402$. The signal does not suffer from aliasing, as the number of points is calculated to be $N = (GD_{max} - GD_{min}) * f_{max}$ which leads to a large value of N= 16241. Figure 4.1 compares the TFRs: STFT, FR-SST [3], FR-SST2 [4, 5], TR-SST2[6] and NSST[7]. Note that in the simulation, in the regions of high modulations such as slope changes, NSST provides a more concentrated representation.

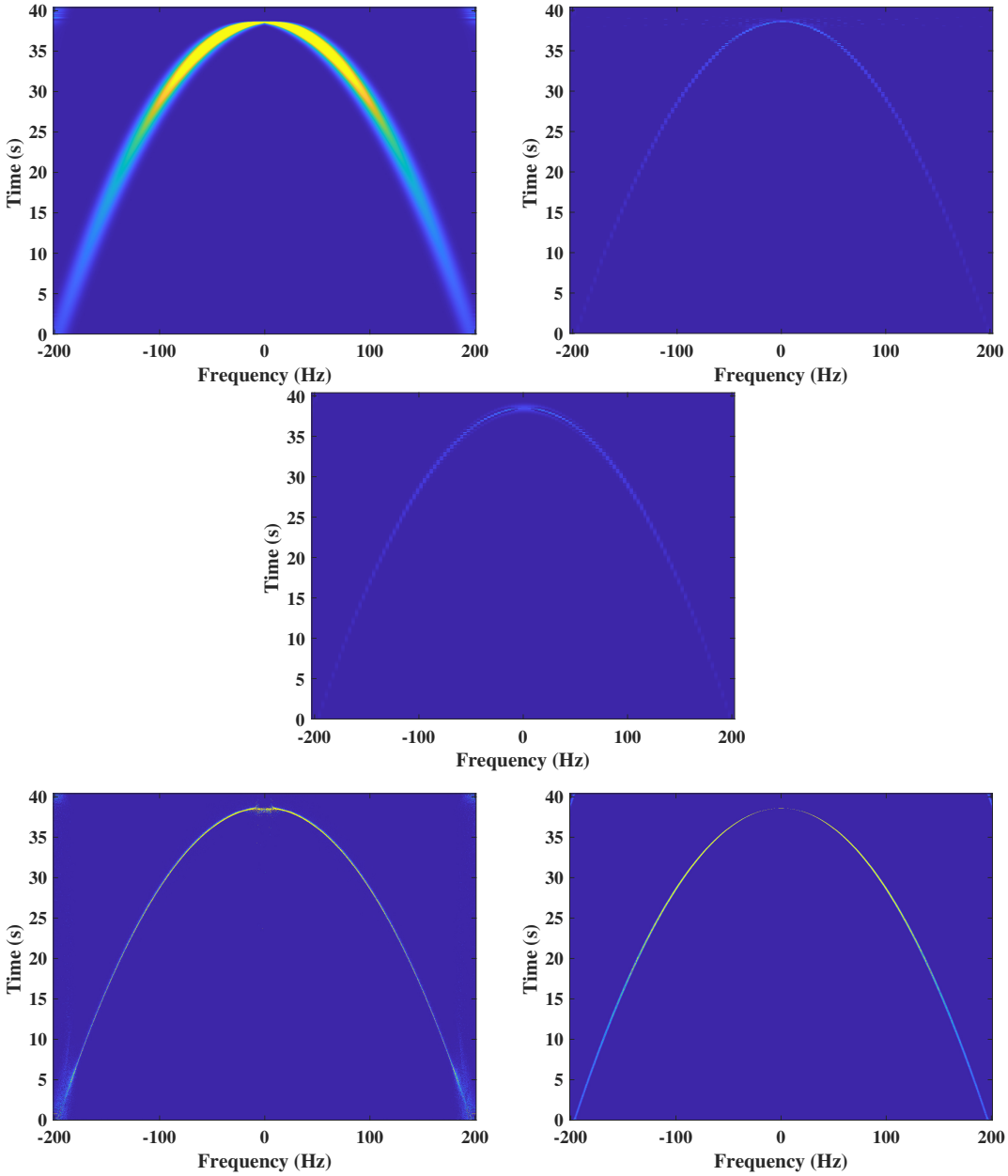

Figure 4.1: Time Frequency Representations: STFT, FR-SST [3], FR-SST2 [4, 5], TR-SST2[6] and NSST[7]

4.4 Quantitative Comparison

4.4.1 Normalized Energy

A qualitative comparison of the TFR can be obtained by illustrating the normalized energy as first proposed in [4]. In this technique, the normalized energy associated with the first N coefficients and the growth of energy towards 1 is computed. A faster growth towards 1 represents a sharper TFR. The analysis method is implemented by first sorting the absolute values of the TFR coefficients in descending order. The cumulative sum of the sorted coefficients is then calculated by the formula $\left(\frac{Cumsum(T^2)}{Sum(T^2)}\right)$. The abscissae are calculated by computing the number of coefficients over the size N of the signal which can be interpretted as the average number of coefficients for each column of the TF plane.

Figure 4.2 displays the normalized energies of the TFRs: STFT, FR-SST, FR-SST2, TR-SST2 and NSST. The energy of the NSST exhibits the fastest increase in energy to 1. Within just one coefficient, 99 percent of the energy of the NSST is retrieved. The explanation for the high energy localization is the optimal reassignment of TFR coefficients in the TF plane. In comparison, 95 percent of the FR-SST2 signal energy is retrieved within one coefficient, while the TR-SST2 requires 3 coefficients to reach maximum energy. SST and STFT stagnate at 20 percent, which implies that the signal is not retrieved within a reasonable number of coefficients.

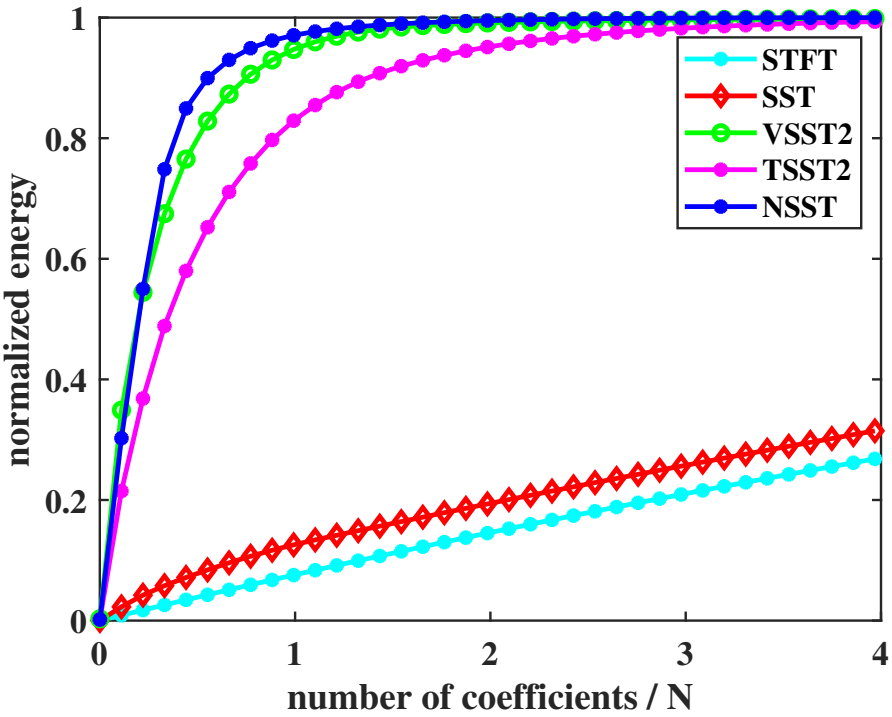

Figure 4.2: Normalized Energy as a Function of the Number of Coefficients. Faster Growth of Energy Towards 1 Represents Sharper Representation.

4.4.2 Signal Reconstruction

Synchrosqueezing techniques offer a significant benefit over traditional reassignment techniques due to the ability of the TF transform to be inverted back to the Time domain. The reconstruction formula used to reconstruct the mode in the time domain is:

$$f_k(t) = \int DSST_x(t, f; H)df \tag{4.8}$$

The signal reconstruction superimposed on the original signal shown in figure 4.3 demonstrates perfect reconstruction of the signal. A statistical analysis of reconstruction quality in the presence of noise is carried out in the next section.

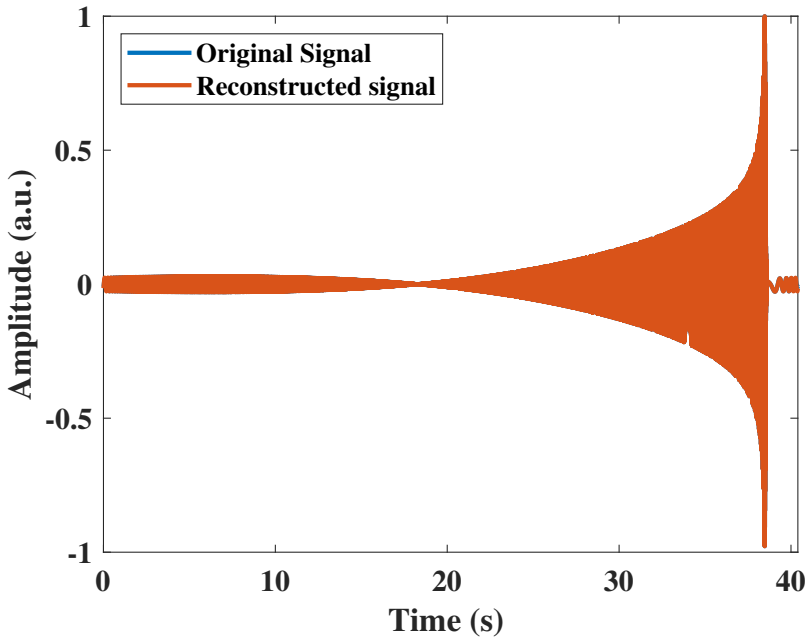

Figure 4.3: Signal Reconstructed from TF Domain to Time Domain

4.4.3 Reconstruction Quality Factor

In order to illustrate the influence of noise, we contaminate a PFM signal which has coefficients $c_3 = 0.0001$, $c_2 = 0.0001$, $c_1 = 0.1$ and $c_4 = 1$ with white Gaussian noise ranging from 10dB to 50dB. The reconstruction quality factory (RQF) is given by

$$RQF = 10log_{10}\left(\frac{\Sigma|x[n]|^2}{\Sigma|x[n] - \hat{x}[n]|^2}\right)$$

The equation is used to quantitatively assess the signal reconstruction capability of TFRs with noise. The RQF comparison is made between the NSST and the state of the art GD estimator TR-SST2 [6] in the presence of noise. Note that the other estimators proposed in literature are IF estimators [5, 3, 4, 18] and not GD estimators. Figure 4.4 demonstrates that the NSST obtains significantly higher RQF than the TR-SST2 [6]. The advantages of considering frequency modulation for representation and reconstruction purposes were demonstrated through numerical experiments. Notably, the new transformation displayed remarkable noise robustness.

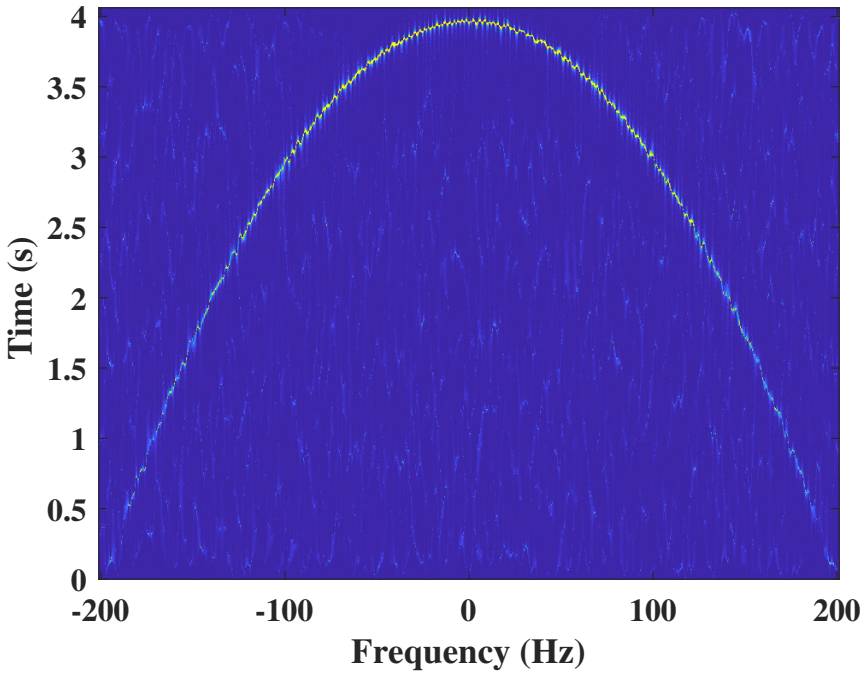

(a) NSST of Signal with 10dB White Gaussian Noise

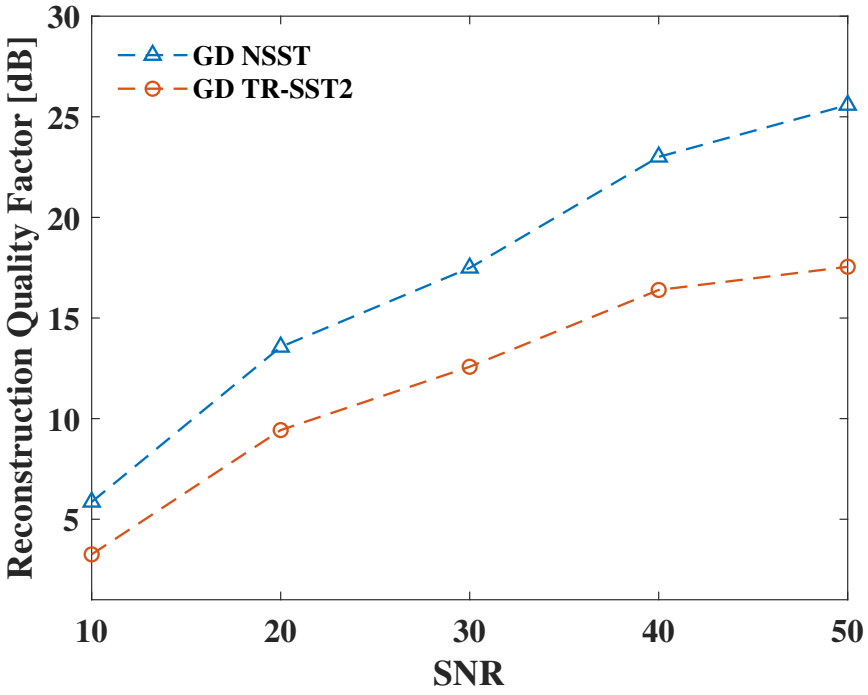

(b) Reconstruction Quality Factor in Presence of Noise

Figure 4.4: Analysis of Performance in Noise Using Reconstruction Quality Factor. Higher Value of RQF Represents Better Reconstruction Performance

4.5 Hyperbolic Frequency Modulated Signals

Hyperbolic Frequency Modulated (HFM) signals are a subclass of continuous-wave radar signals [108]. Unlike the linear frequency modulated signals, where the frequency increases or decreases linearly with time, in HFM signals the rate of frequency change varies hyperbolically over the pulse duration. Mathematically, the instantaneous frequency of an HFM signal can be expressed as:

$$f(t) = f_0 + B \cdot \ln(C \cdot t + 1)$$

where f_0 is the starting frequency, B is the bandwidth, C is a modulation constant, and t is the time. One of the primary advantages of using HFM signals in radar systems is their potential to improve range and velocity ambiguity resolution. Moreover, these signals are inherently resistant to certain types of electronic countermeasures, making them valuable in defense and electronic warfare applications.

The performance of the NSST is demonstarted by analyzing an HFM frequency-domain signal defined as $X(f) = A(f) \exp(-j2\pi c \ln(f + f_r))$. The HFM has hyperbolic GD $\tau(f) = c/(f + f_r)$, where c is the frequency modulation (FM) rate and f_r is a small frequency. For a modulation rate set at c=40, figure 4.5 shows the comparison of the MATLAB STFT implementation compared to the NSST. For visual verification, we compare the localization of the signal at Frequency at 200Hz using the line function. The TFR depict the perfect localization achieved by the NSST for this signal.

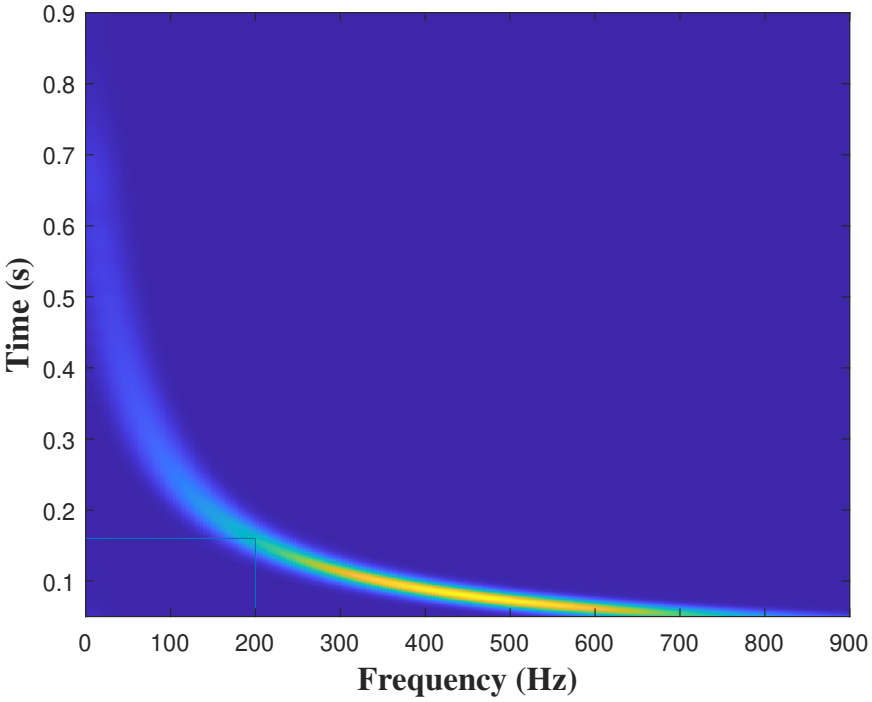

(a) STFT of HFM Signal

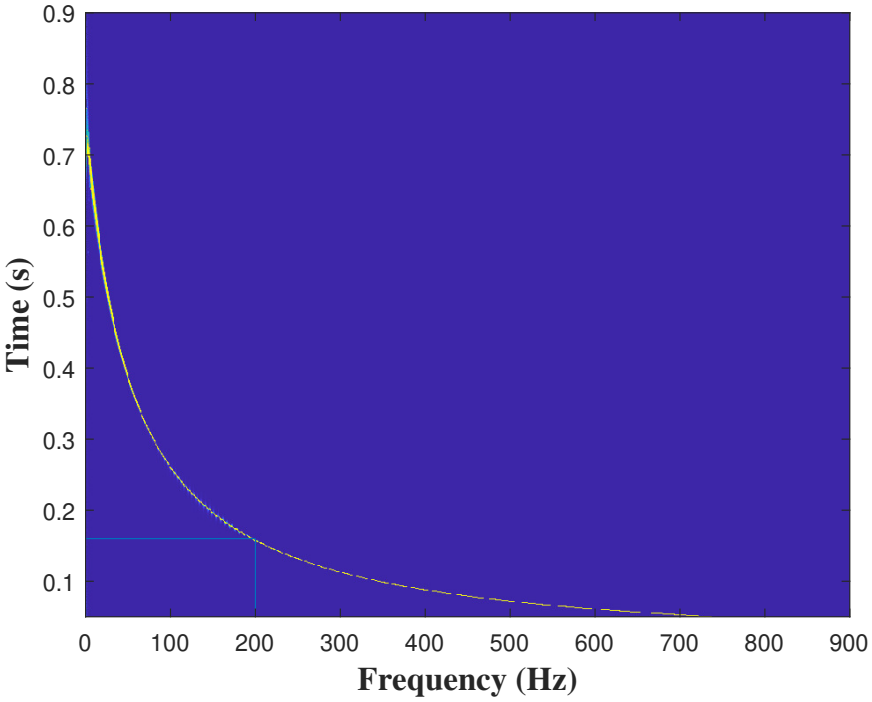

(b) NSST of HFM Signal

Figure 4.5: Perfect Localization in TF Plane for Nonlinear HFM Signal

Chapter 5

UNSUPERVISED MODE EXTRACTION

5.1 Previous Methods of Mode Extraction

In signal processing, the extraction of oscillatory modes from complex signals is a crucial task for various applications, including biomedical signal analysis, mechanical vibration monitoring, and financial data processing. Traditional methods, such as the Short-Time Fourier Transform (STFT) and the Wavelet Transform (WT), provide time-frequency representations of signals but often suffer from either poor temporal or poor frequency resolution due to the uncertainty principle. To address this limitation, the *synchrosqueezing* technique was introduced as an enhancement to the continuous wavelet transform (CWT)[18]. The core idea of synchrosqueezing is to refine the time-frequency representation by reassigning the energy of the wavelet transform to the true instantaneous frequencies, leading to an improved clarity and concentration in the time-frequency plane. As a result, this method enables sharper mode extraction, especially for signals with closely spaced oscillatory components. By using synchrosqueezing, one can achieve more precise identification and separation of oscillatory modes, enhancing the analysis and understanding of intricate signal behaviors [109]. However, it's essential to select an appropriate mother wavelet and ensure careful implementation to maximize the benefits of the synchrosqueezing technique.

Mode separation for multicomponent signals has been classically implemented using the ridge detection method proposed by Carmona et al [110]. The procedure uses a Markov Chain Monte Carlo (MCMC) approach called the Crazy climbers algorithm. The algorithm initializes random points on the TF grid, which then evolve based on the local magnitudes of the TFR. However the algorithm assumes a slow varying and smooth ridge function and hence is not suitable for analysis of dispersive signals. Another commonly used mode

separation technique was introduced by Thakur and Brevdo [76] for noisy and non uniformly sampled time series. In this method, an approximated energy curve for modes is found to be:

$$E_s(c) = \int log|T_s(c(t), t)|dt$$

and $J(c) = \int |c'(t)|^2 dt$ being the measure of irregularity. $c(t)$ represent the IF curve and T_s is the TFR. The ridges are then extracted by minimizing

$$E(c) = J(c) - \lambda E_s(c)$$

However, λ is a heuristic parameter that has to be set a priori. This method also approximates the curve c, based on the smooth and slowly varying function assumption. Improvements to the ridge extraction method were proposed by mathematical computation of local minima of the energy function [32]. However the proposed extraction procedure contained heuristic optimization control parameters λ and β. Moreover, the number of modes to be extracted are assumed to be known.

5.2 Unsupervised Mode Extraction

Various methods have been considered for detecting and identifying TF regions of high energy localization in the TF domain due to multiple components in the analysis signal [110, 76, 32]. Most of these methods assume a known number of components with slow-varying TF characteristics. Considering the received UGW signal spectrum with multiple signal modes,

$$Y(f) = \sum_{\ell=1}^{L} X(f)\, e^{-j2\pi r_\ell k_\ell(f)}\,,$$

the resulting GD functions $\tau_\ell(f) = r_\ell \frac{d}{df} k_\ell(f)$ can be highly dispersive. Also, the number of modes L is unknown as new modes can be generated every time the wave encounters a boundary. We thus consider an unsupervised mode segmentation method to cluster TF points to their corresponding modes without prior knowledge on the number of modes. The method uses a graph-based segmentation algorithm adopted from image processing [111].

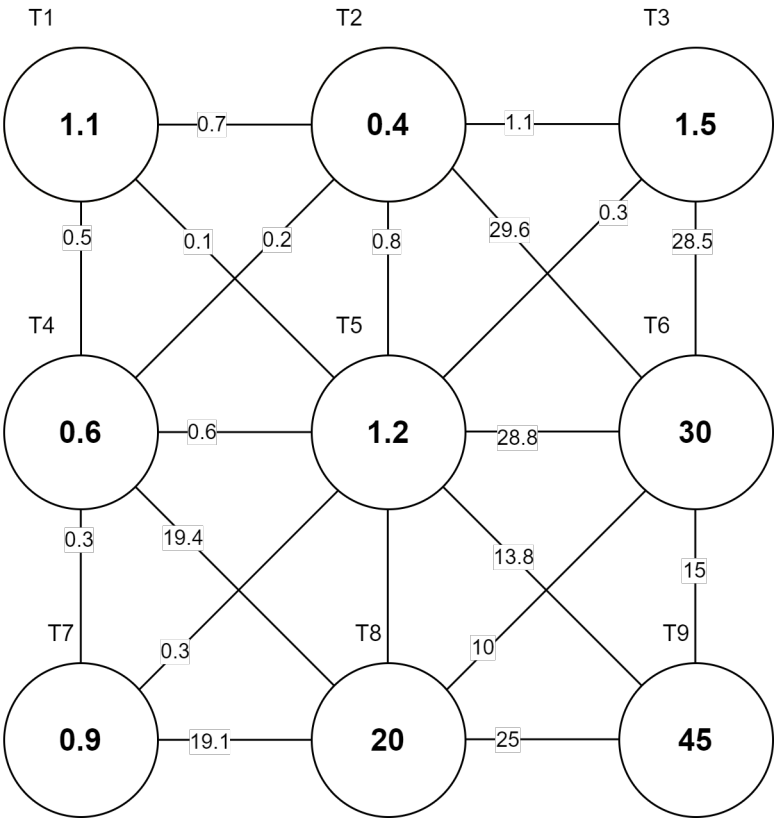

Figure 5.1: UMS Algorithm Example, Nine Time Frequency Vertices with Edge Weights

Similar to a graph-based representation of an image, we regard the DSST TFR as an edge-weighted undirected graph. Specifically, assuming N DSST TF points, the ith TF point (t_i, f_i) is the ith graph vertex, and the ith and jth neighboring TF points correspond to the ijth graph edge with edge weight $(T_i - T_j)$, where $T_i = |\mathrm{DSST}_x(t_i, f_i; h)|$ in (4.3), $i = 1, \ldots, N$. The clustering of the TF points uses the TFR-based minimum spanning tree (MST) which is formed as an acyclic subgraph of all DSST TF points with minimum total edge weight. Although different methods have been considered for MST-based clustering, we adopt the unsupervised mode separation (UMS) algorithm that follows the efficient image segmentation in [111]. The UMS algorithm uses two clustering metrics to adaptively separate all TF points based on the local characteristics of the DSST TFR. These metrics are used to decide whether two TF point clusters should be merged into one cluster; if they are merged, then all TF points are associated with the same mode.

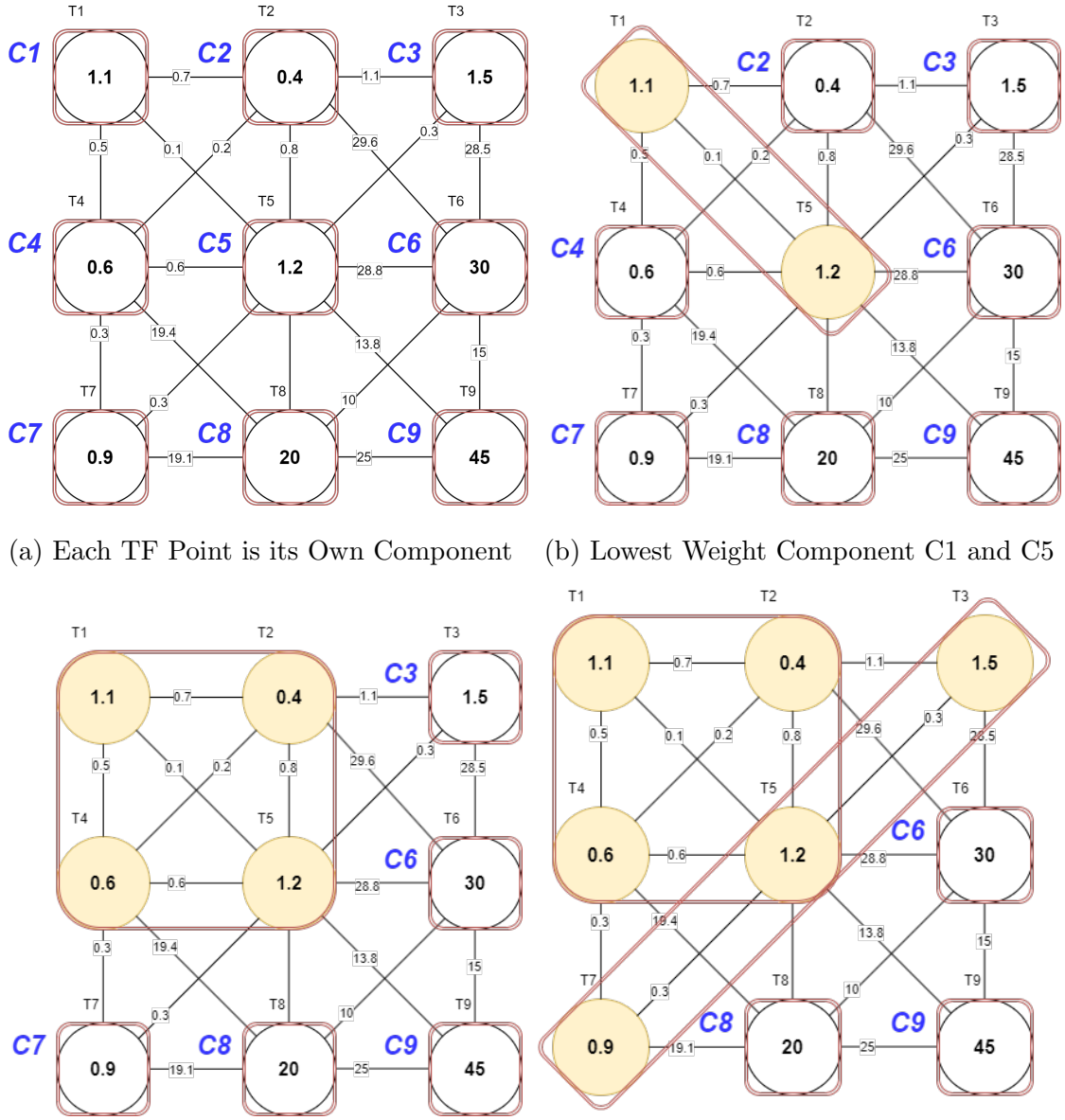

(a) Each TF Point is its Own Component

(b) Lowest Weight Component C1 and C5

(c) Merge Components C2 and C4

(d) Merge C3 and C7

Figure 5.2: Step by Step Implementation of UMS Algorithm Starting with Lowest Edge Weight to Largest for Component 1

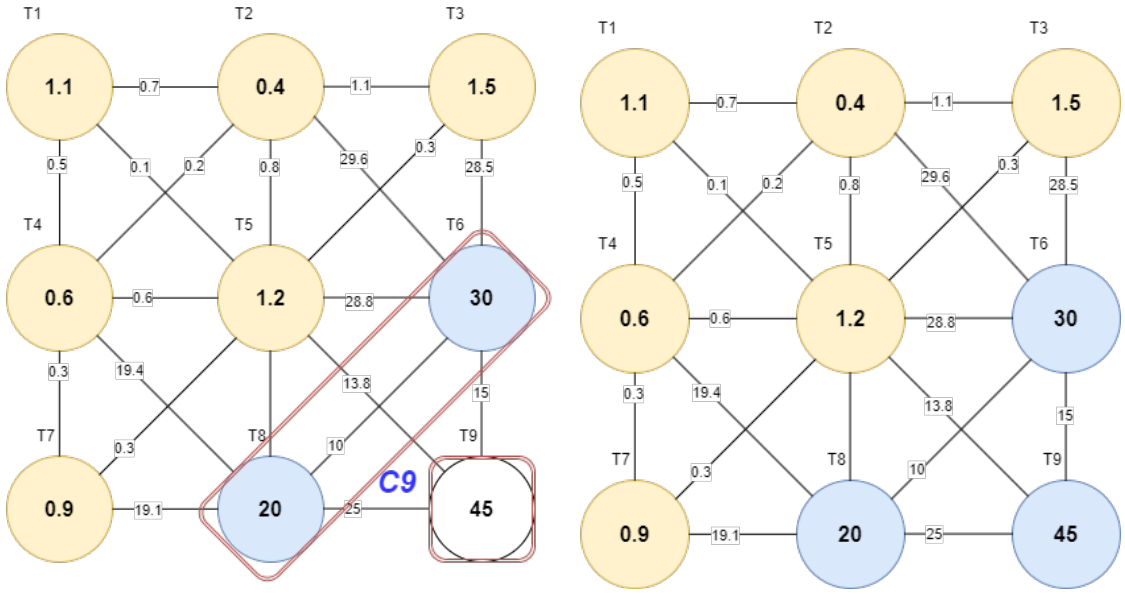

(a) Merge Component C6 and C8 (b) Merge Component C9

Figure 5.3: Step by Step Implementation of UMS Algorithm Starting with Lowest Edge Weight to Largest for Component 2

The UMS algorithm for separating TF modes is outlined in Algorithm 1. The algorithm initially orders the $M=(N-1)$ edge weights of the MST graph in ascending order $\varpi_1 \leq \varpi_2 \leq \ldots \leq \varpi_M$ and then assigns the ith cluster $C_i^{(0)}$ to the ith TF point, $i=1,\ldots,N$. The clustering process undergoes M iterations. At the mth iteration, the two TF points connecting the edge with weight ϖ_m are labeled $P_i=(t_i,f_i)$ and $P_j=(t_j,f_j)$. The clustering of these two points was determined at the $(m-1)$th iteration. Specifically, P_k is a TF point in Cluster $C_k^{(m-1)}$, which includes L_k edges with weights $w_\ell^{(k)}$, $\ell=1,\ldots,L_k$, for $k=i,j$. If the number of TF points in the cluster is $|C_k^{(m-1)}|=1$, then $L_k=0$ and $w_\ell^{(k)}=0$. Metric $E_{ij}^{(m)}$ is obtained as the minimum edge weight between the TF points connecting the two clusters. Metric

$$I_{ij}^{(m)} = \min\left(\max_{\ell=1,\ldots,L_i} (w_\ell^{(i)}+\gamma), \quad \max_{\ell=1,\ldots,L_j} (w_\ell^{(j)}+\gamma) \right), \tag{5.1}$$

finds the minimum value between the maximum edge weight in each cluster. Note that if the number of TF points in any one of the two clusters is $|C_k^{(m-1)}|=1$, $k=i,j$, then $L_k=0$, $w_\ell^{(k)}=0$ and $I_{ij}^{(m)}=\gamma$. If $E_{ij}^{(m)} < I_{ij}^{(m)}$, all TF points from clusters $C_i^{(m-1)}$ and $C_j^{(m-1)}$ are

merged into the new cluster $C_i^{(m)}$; otherwise the two clusters remain separated. Note that the threshold parameter γ in (5.1) is heuristically selected to control boundaries between clusters. For example, a large threshold γ results in more clusters merging, thus ensuring that low intensity noise terms do not form a new mode.

To illustrate the procedure, figure 5.1 shows nine time-frequency points in the TF plane connected together. The vertices are labelled as T_n. The weight between each vertex is indicated on the edge. Figure 5.2 shows the step by step implementaiton of the algorithm. The algorithm starts with initializing each vertex as its own component and cinsidering the smallest edge weight which is 0.1 between component 1 and component 2. Comparing the internal difference I_{ij}^m with component difference E_{ij}^m, we arrive at the conclusion to merge the components C1 and C2. The next smallest edge weight is considered as 0.2 between C2 and C4 and using a similar approach, the components are merged. Finally components C3 and C7 are also merged within the mode using the same predicate calculation.

However when the next smallest edge weight is considered, component C8 has the minimum weight of 18.8 as shown in figure 5.3. Hence the component cannot be merged with the large newly constructed mode. Next the vertex C8 and C6 are considered and merged based on the predicate calculations. Finally the component C9 is merged. This leads to a clear differentiation of the two modes shown in figure 5.3 (b).

The UMS algorithm for separating TF modes is outlined in Algorithm 1. We demonstrate the effectiveness of the UMS algorithm in separating TF modes using two examples. In the first example, we consider a signal consisting of the sum of two PTM signals that were generated using 20 Hz sampling frequency and 1 s duration. The UMS algorithm was implemented using python's scikit-image library [112] and $\gamma = 10$ was selected as the threshold value in (5.1).

5.3 Simulations

5.3.1 Parabolic Frequency Modulation

Parabolic frequency modulation (PFM) is an advanced modulation technique in which the instantaneous frequency of a signal changes according to a parabolic function over time [113]. In signal processing, PFM can offer a compromise between linear frequency modulation (LFM) and hyperbolic frequency modulation (HFM) in terms of time-bandwidth properties and autocorrelation characteristics [114]. In particular, the PFM waveform possesses some desirable properties for specific applications, such as radar imaging and sonar, where the target's Doppler shifts are unknown and can vary considerably. This modulation technique can achieve better range resolution than LFM while maintaining a relatively simple matched filter structure. Moreover, PFM provides an inherent capability to counter the Doppler effects due to its quadratic phase term. This quadratic phase compensates for the Doppler shift introduced by a target's movement, thus making PFM an attractive choice in scenarios where target motion is unpredictable [115]. As research progresses, advancements in the PFM domain, coupled with computational techniques, promise enhanced resolution and improved target detection capabilities in various signal processing applications.

5.3.2 Multiple PFM Signals with No Overlap

In order to demonstrate mode separation for two parabolas we find the parameters of PFM that best fit the two parabolas. The frequency modulated signal is generated with the phase function in the frequency domain such that $\Phi_(f) = \frac{c_3}{3}f^3 + \frac{c_2}{2}f^2 + c_3 f + c_1$, where $c_3 = 0.6$, $c_2 = 0.001$, $c_1 = 25$ and $c_4 = 1$ are the coefficients of the first parabola and $c_3 = 1$, $c_2 = -0.5$, $c_1 = 150$ and $c_4 = 1$ are the coefficients of the second parabola. A maximum frequency bandwidth from $-\frac{f_{max}}{2}$ to $\frac{f_{max}}{2}$ is set such that $f_{max} = 20$. The two parabolas do not overlap in the TF domain and shown in figure Figure 5.4 (a). The modes are separated using the mode extraction algorithm, and each separated mode is shown in figure Figure 5.4 (b) and (c).

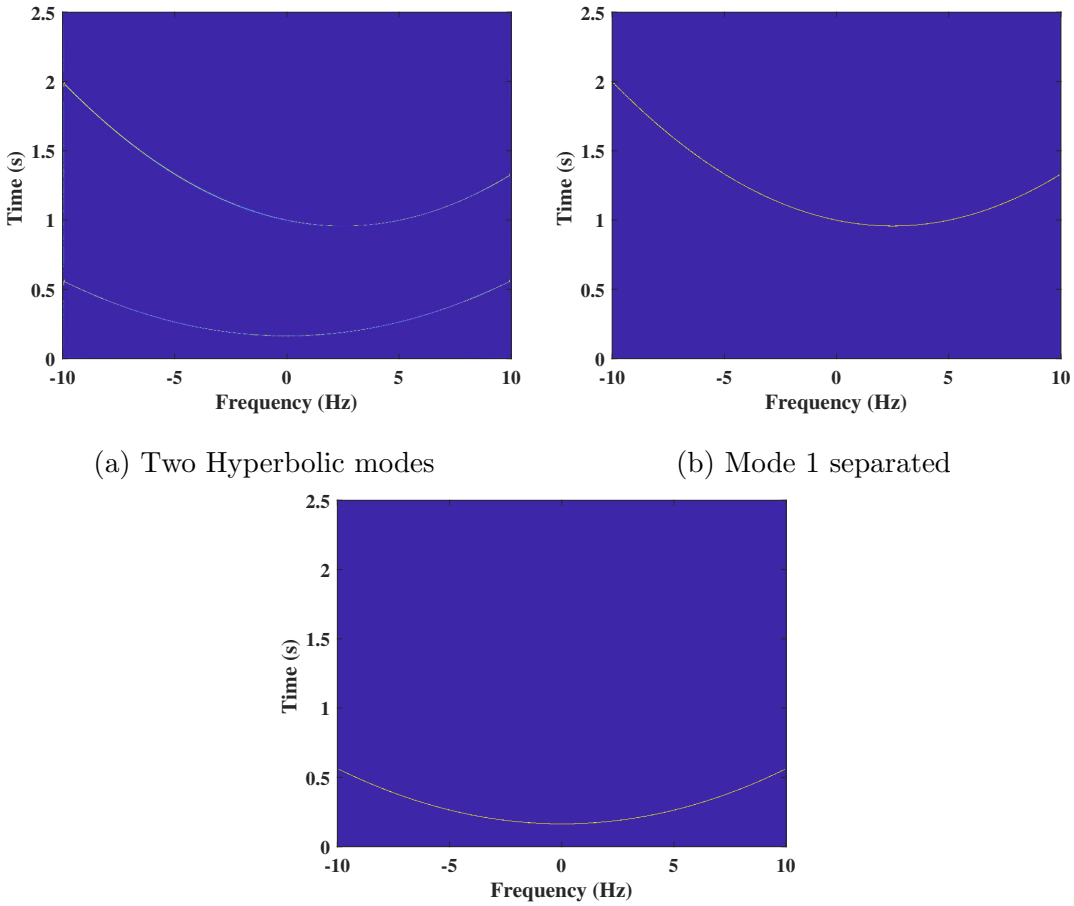

(a) Two Hyperbolic modes

(b) Mode 1 separated

(c) Mode 2 separated

Figure 5.4: Two PFM Matched to Dual Hyperbolas

5.4 Isotropic UGW Analysis

UGW dispersion curves can be obtained using NSST extracted GD and their relation to dispersive group velocity in $X_r(f) = X(f)\, e^{j2\pi r k_n(f)}$ We used the Waveform Revealer (WFR) tool to simulate the multimode UGW behavior in isotropic material [40]. In particular, we used the WFR to obtain UGW waveforms propagating in Aluminum 6061 plate with 2mm thickness and 2700 kg/m^3 material density. The input signal is a tone burst with center frequency ranging from 100 to 1500 kHz, in 1 kHz intervals. This input signal results in exciting both symmetric and antisymmetric Lamb waves through the plate. Measurements are provided using two sensors placed in a pitch-catch configuration. The first

sensor is collocated with the actuator to measure the excitation wave; the second sensor is placed 500 mm away from the source. The NSST in Figure 5.5 shows the dispersive TF characteristics of the modes in a highly localized representation. The mode group velocities can be calculated from these dispersive modes. Note that, in [39], we proposed an approach to separate modes using unsupervised clustering and graph-based image segmentation.

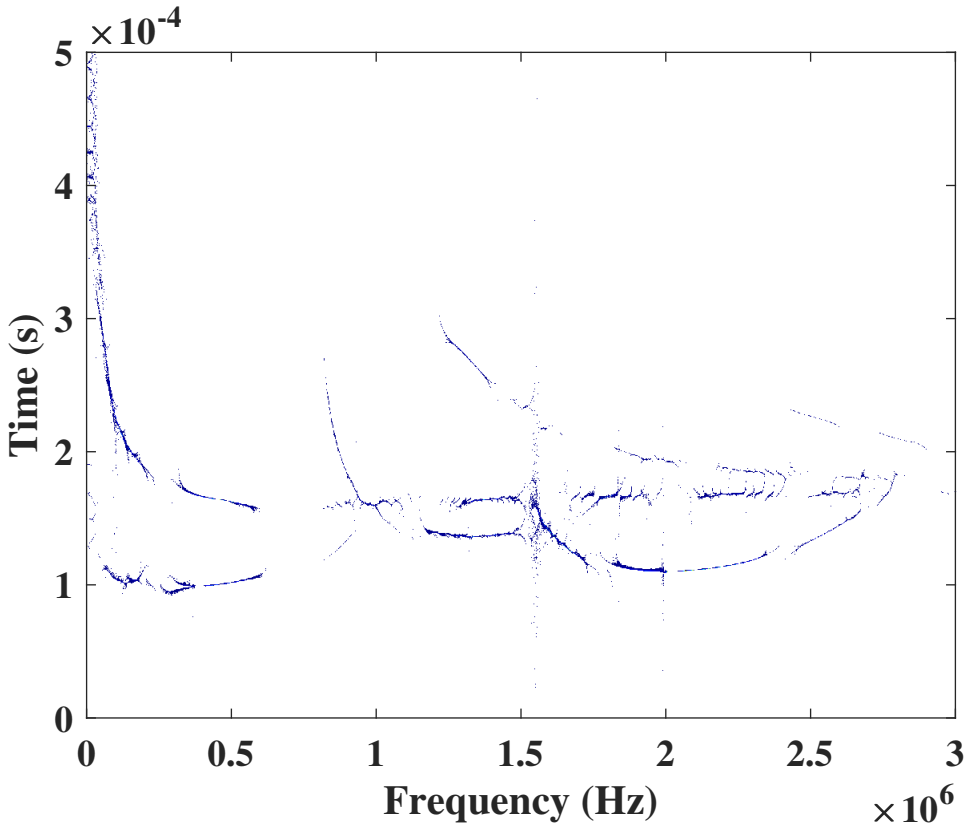

Figure 5.5: NSST GD Estimation in Isotropic Material.

Figure 5.6 plots the group velocity vs damage sensitivity parameter fd, the product of frequency and thickness. Strong agreement between the estimated group velocity and theoretical values of group velocity is observed by comparing the A0, S0, A1 and S1 modes with theoretical values.

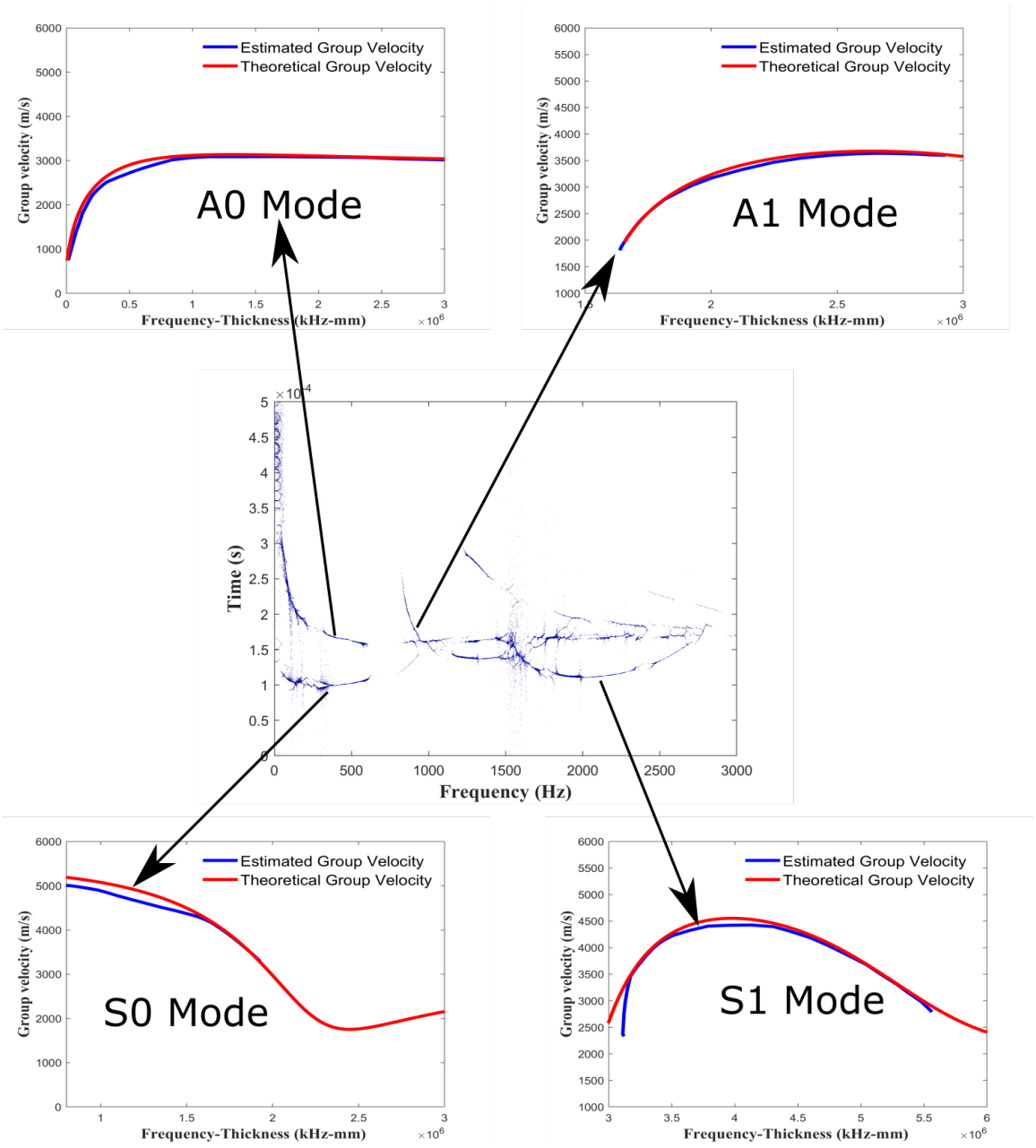

Figure 5.6: Group Velocity Estimation and Comparison of Dispersion curves

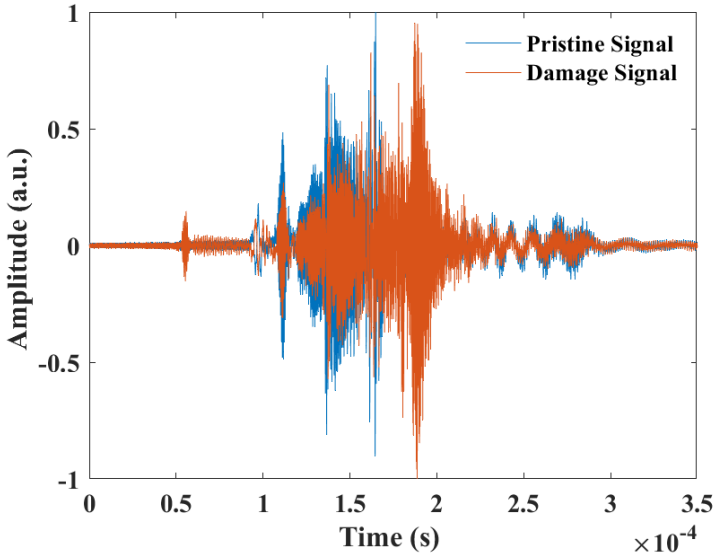

Figure 5.7: Time Domain Signal of Healthy and Damage CFRP

5.5 Defect Detection in Isotropic Media

The waveform of Lamb wave interaction with damage can be obtained by defining damage location and nonlinear parameters such as phase change, mode conversions and higher harmonics. Figure 5.7 shows the time domain signals of Lamb wave propagation through a pristine and damaged Aluminum plates. Clearly, the identification of peak intensity of the UGW modes in TD is a challenging task because the intensity and phase information is superimposed. Figure 5.8 (a) shows the NSST of wave propagation through the pristine Aluminum plate. It can be seen that unlike the TD signal, the A0, A1, S0 and S1 modes are clearly separated in the TF domain. Figure 5.8 (b) shows the NSST of Lamb wave propagation through an Aluminum plate with damage at location 200mm. We observe occurrence of new modes due to reflection and mode conversions due to damage. The intensity of A0, S0 and A1 modes is dissipated due to presence of damage.

5.6 Analysis of Real Data

The performance evaluation for damage detection with real experimental data can be performed using open source dataset comprising of UGW propagating through composite

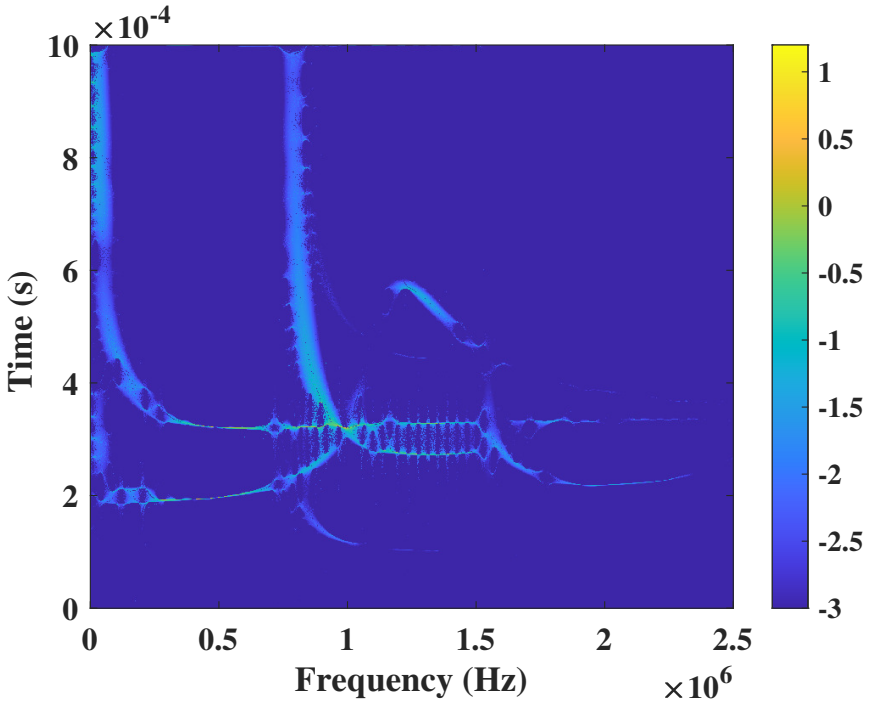

(a) NSST Healthy

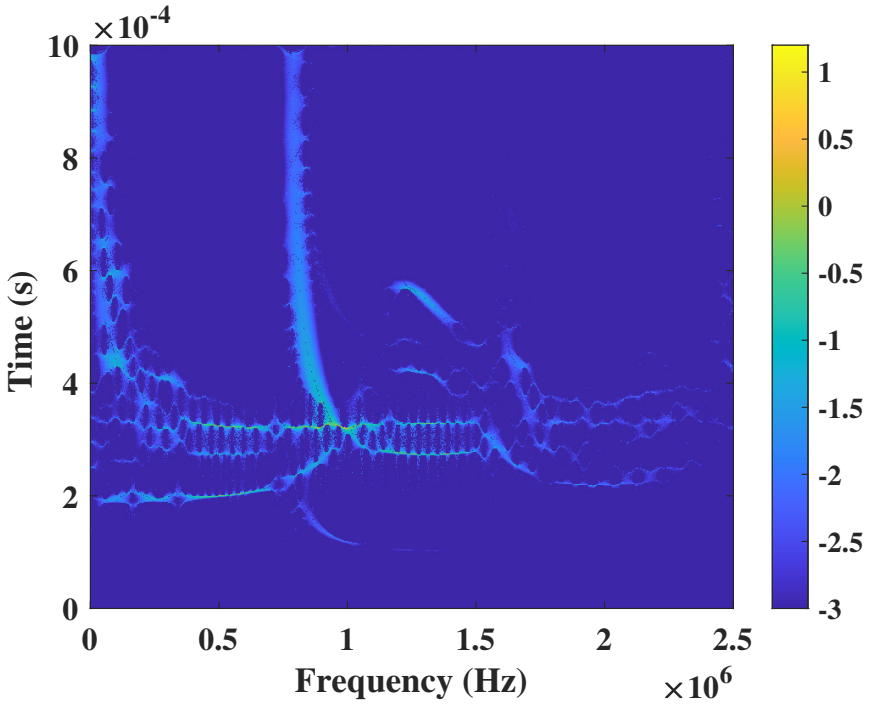

(b) NSST Damaged

Figure 5.8: NSST Isotropic UGW Simulated Signal with Damage

plate [41]. The carbon fiber-reinforced polymer (CFRP) test plate is quasi-isotropic in nature and the dimensions are 500 mm x 500 mm x 2 mm thick. The quasi-isotropic laminate layup is $[45/0/-45/90/-45/0/45/90]_s$. Twelve piezoelectric transducers (PZT) (DuraAct, 0.2 mm thick, 5 mm in diameter) were embedded on the plate in pitch catch configuration. The excitation signal is a 0.125 ms broadband linear chirp from 20 to 500 kHz. The guided wave response is recorded by a 14-bit A/D converter connected to a PD200 (PiezoDrive) amplifier. Noise reduction was accomplished by taking five baseline measurements and maintaining a consistent temperature within a climate-controlled chamber. The resulting data was then averaged. To simulate damage, an omega stringer feature (1.5 mm nominal thickness and 0.125 mm ply thickness) was bonded to the plate surface. The time domain response of UGW propagating through the CFRP in healthy and damage state are represented in the figure 5.9a. The DSST of each of the signals is taken and shown in figures 5.9b and 5.9c. Significant difference in the higher order modes of the damage and undamaged DSST is observed.

Damage features were added to cause stiffness asymmetry leading to decrease in amplitude, change in time of flight (TOF) and mode conversions. Figure 5.10 (a) and (b) show Mode 2 and 3 superimposed. It is clearly seen that the damage modes exhibit intensity reduction. The mode reconstruction is shown in figures 5.10 (c) and (d) which demonstrates the difference between healthy and damage modes.

Algorithm 1 Unsupervised Mode Separation Algorithm

– Input $\{t_i, f_i, T_i\}$, $i = 1, \ldots, N$, for the ith TF point (t_i, f_i) and corresponding DSST magnitude $T_i = |\mathrm{DSST}_x(t_i, f_i; h)|$

– Input threshold γ

1. Compute weight $(T_i - T_j)$, $i \neq j$, $i, j = 1, \ldots, N$, for the edge between the ith and jth neighboring TF points

2. Construct minimum spanning tree (MST) as acyclic subgraph of all DSST TF points with minimum total edge weight

3. Order MST edge weights ϖ in ascending order $\varpi_1 \leq \varpi_2 \leq \ldots \leq \varpi_{N-1}$

4. Set iteration index $m = 0$ and number of clusters $L = N$

5. Cluster the ith TF point (t_i, f_i) to the ith cluster, $C_i^{(0)}$, $i = 1, \ldots, L$

6. Set iteration number $m = m + 1$

7. Observe the two TF points of the edge weight ϖ_m, $P_i = (t_i, f_i)$ from Cluster $C_i^{(m-1)}$ and $P_j = (t_j, f_j)$ from $C_j^{(m-1)}$

8. Observe all TF points and L_k edges with weights $w_\ell^{(k)}$, $\ell = 1, \ldots, L_k$, in Cluster $C_k^{(m-1)}$, $k = i, j$

9. Obtain $E_{ij}^{(m)}$ as the minimum edge weight between the TF points connecting clusters $C_i^{(m-1)}$ and $C_j^{(m-1)}$

10. Compute $I_{ij}^{(m)}$ using γ and Equation (5.1)

if $E_{ij}^{(m)} < I_{ij}^{(m)}$ **then**

Merge all TF points from Clusters $C_i^{(m-1)}$ and $C_j^{(m-1)}$ into Cluster $C_i^{(m)}$

Update number of clusters $L = L - 1$

else

$C_i^{(m)} = C_i^{(m-1)}$ and $C_j^{(m)} = C_j^{(m-1)}$

end if

if $m \leq N-1$ **then**

Return to 6

end if

– Output L clusters; TF points in ℓth cluster form the ℓ mode, $\ell = 1, \ldots, L$

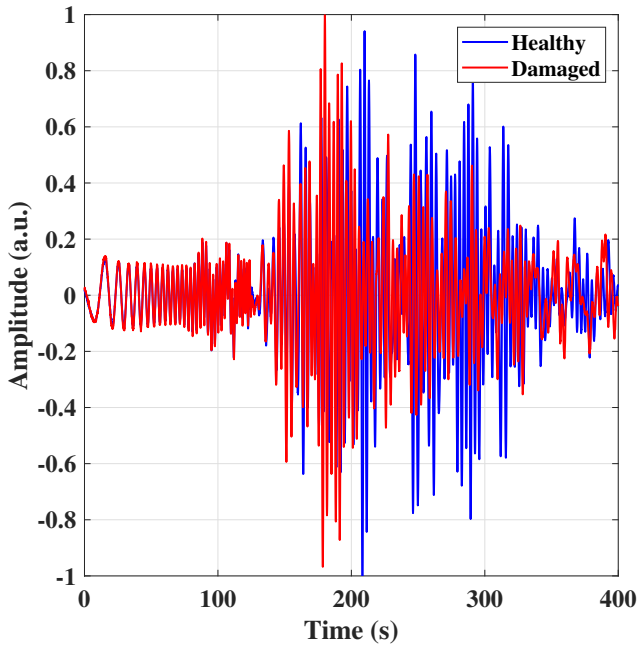

(a) Time Domain Signal

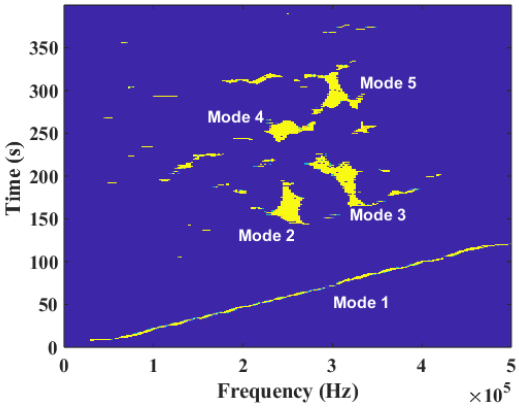

(b) Healthy CFRP Plate

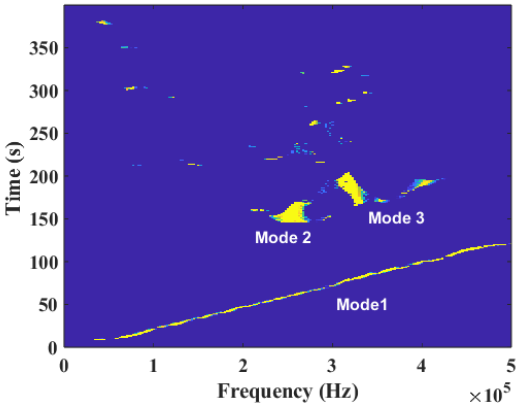

(c) CFRP Plate with Damage

Figure 5.9: NSST of UGW Propagating in Quasi-Isotropic Media

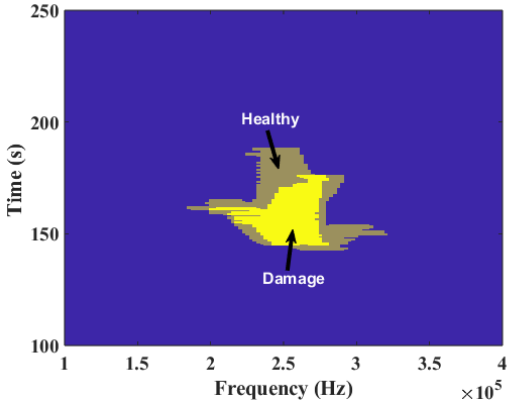

(a) Mode 2 in TF Domain

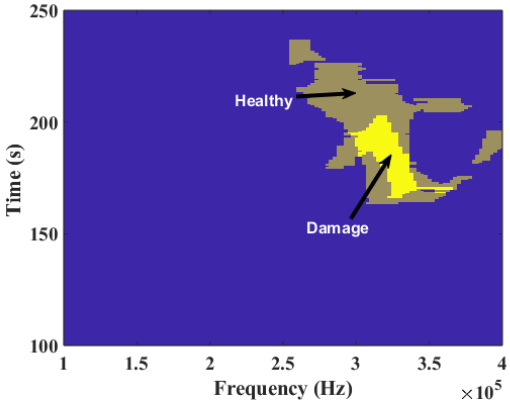

(b) Mode 3 in TF Domain

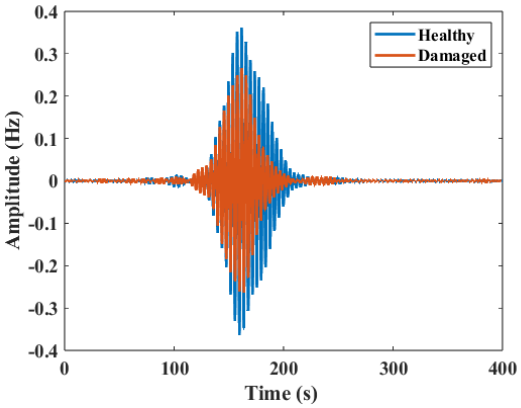

(c) Mode 2 in Time Domain

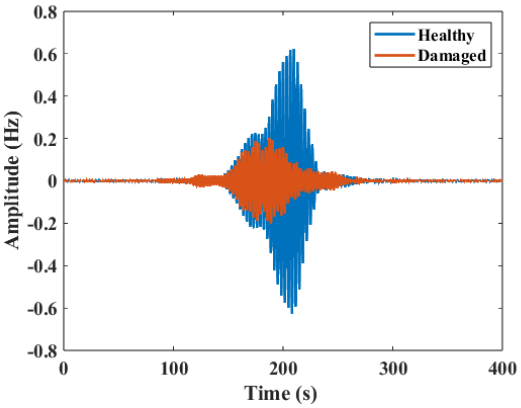

(d) Mode 3 in Time Domain

Figure 5.10: Damage Detection in CFRP Using DSST with Unsupervised Mode Separation

Chapter 6

BAYESIAN GROUP DELAY MODE MERGING

6.1 Extracting Signals Overlapping in Time-frequency

A very challenging problem when processing time-varying signals is how to separate multiple signal components from their joint time-frequency representation (TFR) when the signals time-frequency (TF) signatures overlap in both time and frequency. When two or more signal components with varying group delays overlap in the TF domain, their individual group delays in the TFR can become indistinguishable. As multiple TF points are shared by multiple components, his complicates the use of the TFRs for component separation, feature extraction, and accurate interpretation of the signal's behavior. For TFRs based on the reassignment method, the processing becomes problematic when modes intersect in TF [26]. In these overlapping TF regions, the reassignment method tends to favor the mode with the highest energy concentration, treating these regions as the main focus. This results in obtaining information only on the strongest mode. However, this causes lesser modes to appear fragmented or separated where they intersect with the dominant mode. Recent approaches to address the problem of intersecting modes include the direction of arrival method [116, 117]. The suggested method initially divides sources using a multi-sensor instantaneous frequency (IF) estimation technique followed by utilizing the algorithm to estimate the location of the sources. However, the methods exhibit poor performance in estimating nonlinear signals with overlap in the TF domain. Thus, signal extraction when overlapping in TF necessitates advanced signal processing techniques to separate and accurately represent the signal's individual components.

This challenging problem is particularly important when using our proposed nonlinear synchrosqueezed transform (NSST) in Chapter 4 to separate multiple modes from ultrasonic

guided wave (UGW) testing. Our unsupervised mode extraction method in Chapter 5 was successful in extracting individual signal components from their joint NSST provided the signals overlapped only in time or only in frequency. However, when using this method to extract signal components that overlap in both time and frequency, the number of clusters extracted exceeds the number of signal terms in the NSST. For example, Figure 6.1 shows the NSST of two parabolic frequency-modulated (PFM) signals that overlap in both time and frequency. After unsupervised mode extraction clustering, however, instead of two clusters, we obtained the 6 NSST clusters depicted in Figure 6.2. Note that the intersection TF points in Figure 6.1 are not clustered in Figure 6.2. This is because we first use the Hessian filter [118] to identify interrupted edges and their corresponding TF points; the we use morphological operators to remove these TF points and thus avoid clusters of very small size.

In this chapter, we propose a new method to extract overlapping signal terms that uses the multiple clusters of the unsupervised mode extraction approach. The method exploits Bayesian inference [119], as described in the following sections, to adaptively merge clusters that belong to a mode whose group delay signature is continuous over a span of TF points. An illustration of the framework is shown in figure 6.3

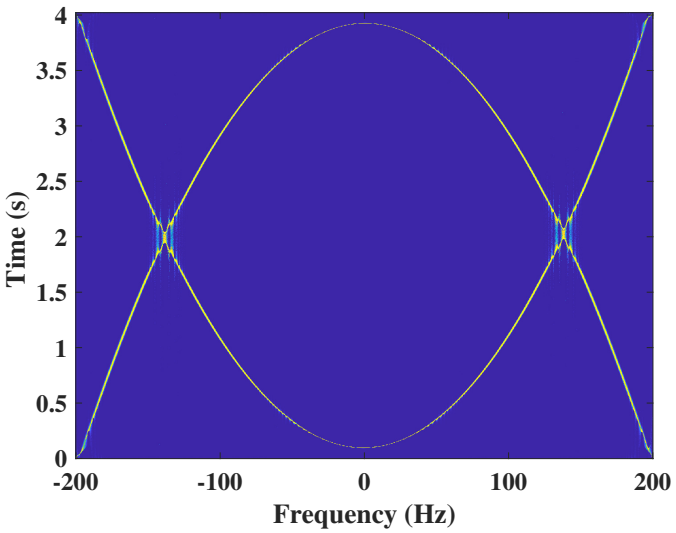

Figure 6.1: NSST of Two Overlapping PFM Signals in the TF Domain.

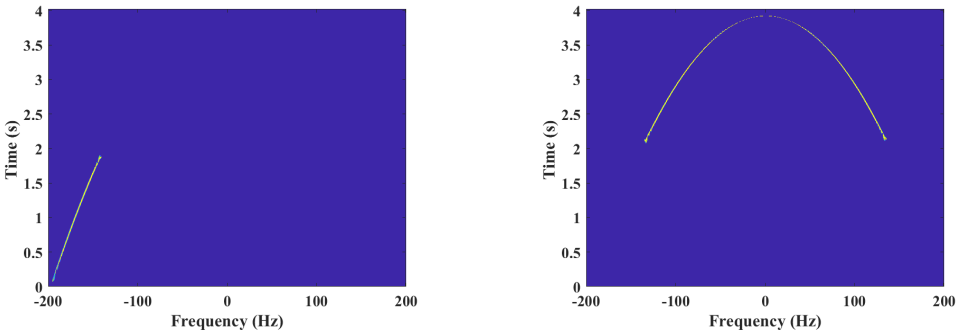

(a) Cluster c_1 (b) Cluster c_2

(c) Cluster c_3 (d) Cluster c_4

(e) Cluster c_5 (f) Cluster c_6

Figure 6.2: Cluster Components After Unsupervised Mode Extraction of the NSST in Figure 6.1.

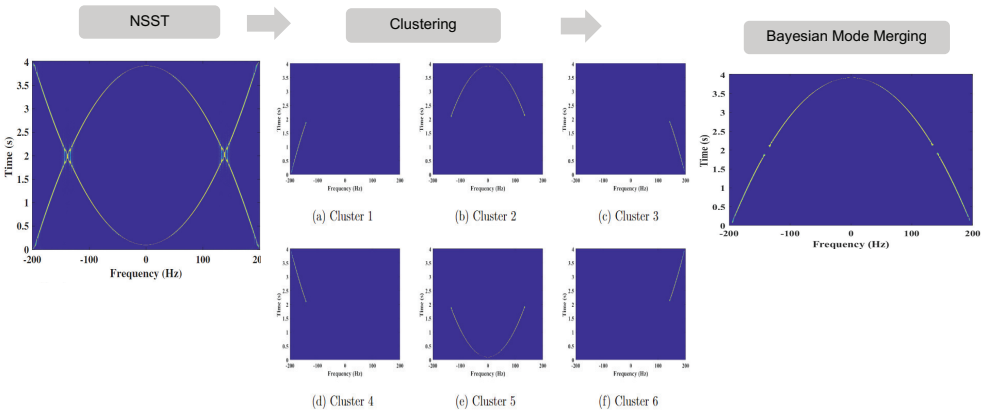

Figure 6.3: Mode Merging Framework

6.2 Summary on Bayesian Inference Methods

6.2.1 Bayesian Filtering

Bayesian inference or Bayesian filtering is a statistical approach based on Bayes' theorem that can be used to estimate an unknown state parameter by updating its prior distribution given a new measurement [119, 120]. The approach depends on a prior probability model to relate the unknown parameter to its previous estimated value and a likelihood model to relate the measurement to the unknown parameter [119]. Assuming an unknown time-varying parameter x_t at time t and a measurement z_t, Bayesian inference estimates the posterior distribution $p(x_t \mid y_t)$ using the prior transition model $p(x_t \mid x_{t-1})$ and the likelihood distribution $p(y_t \mid x_t)$. Specifically, the posterior can be obtained using

$$p(x_t \mid z_t) \;\propto\; p(z_t \mid x_t) \int p(x_t \mid x_{t-1})\, p(x_{t-1} \mid z_{t-1}) dx_{t-1}$$

where $p(x_{t-1} \mid z_{t-1})$ is the likelihood at the previous time. The estimation model depends on the Markovian assumption that the current state x_t is conditionally independent of all earlier states $x_0, \ldots, x_{t-2}$ given the previous state x_{t-1}, and also that the current measurement z_t is conditionally independent of past measurements $z_1, \ldots, z_{t-1}$ given the current state x_t. Written in terms of a state space formulation, the Bayesian filtering problem can be

described by the state transition equation

$$x_t = g(x_{t-1}) + u_{t-1} \tag{6.1}$$

where $g(\cdot)$ is the transition function and u_{t-1} is a modeling error process, and the measurement equation given by

$$z_t = h(x_t) + w_t \tag{6.2}$$

where $h(\cdot)$ is a function that relates the state to the measurement and w_t is measurement noise. If the two functions in Equations (6.1) and (6.2) are linear and the the two processes are Gaussian, then the unknown state can be obtained sequentially using the Kalman filter [121]. For nonlinear functions and/or non-Gaussian processes, the particle filter (PF), a sequential Monte Carlo method, is used [122, 120, 123, 124, 125].

6.2.2 Monte Carlo Methods

Monte Carlo methods are numerical techniques for solving problems through random sampling [126]. In Bayesian filtering, Monte Carlo methods can be used to approximate the posterior distribution by drawing samples from it. Particle filtering is one such Monte Carlo method used for recursive Bayesian estimation. Monte Carlo methods encompass a broad class of computational algorithms that rely on random sampling to estimate numerical results. These methods have been successfully applied to various problems in signal processing where analytical solutions are difficult or impossible to obtain. At their core, Monte Carlo methods generate a large number of random samples from a known distribution, process the samples samples according to some stochastic model, and aggregate the the results to obtain an estimate of the desired distribution.

Monte Carlo methods can be used to estimate parameters of a system when the analytical relationship between parameters and observations is known but intractable. Monte Carlo techniques, especially particle filtering, are employed to estimate the states of nonlinear and non-Gaussian systems over time using noisy observations. In scenarios where a

system's model is unknown, Monte Carlo methods can be applied to identify or approximate the system's behavior based on measurements.

6.2.3 Particle Filter Algorithm

The fundamental idea behind particle filtering is to represent the posterior distribution using a set of weighted samples or "particles" [120, 123, 124, 125]. Each particle corresponds to a possible state of the system, and its weight represents the likelihood of that state given the measurements. The particle filtering algorithm is first initialized by sampling N_s particles from some uniform or Gaussian distribution $p(x_0)$. During the prediction stage at time t, the particles from time $t-1$ are propagated to time t using the transition function in Equation (6.1); specifically,

$$x_t^{(i)} \;\propto\; p(x_t^{(i)} \mid x_{t-1}^{(i)}), \quad i = 1, \ldots, N_s \,.$$

During the update stage, weights for each particle are computed based on the likelihood of the measurements given the state particle in Equation (6.2). The weight of the ith particle at time t is given by

$$\omega_t^{(i)} \propto \omega_{t-1}^{(i)}\; p(z_t|x_t^{(i)}), \quad i = 1, \ldots, N_s.$$

Note that, at each time t, the particles are resampled so that only particles with large weights are kept to avoid degeneration where all the particles collapse around a single state [123]. The predict and update stages are depicted in Figure 6.4, where the particles are illustrated as circles and the circles with higher radius indicate higher weights. The resulting posterior distribution is estimated as

$$p(x_t|z_t) = \sum_{i=1}^{N_s} \omega_t^{(i)}\; \delta(x_t - x_t^{(i)})$$

and the estimated unknown state at time t is given by

$$\hat{x}_t = \sum_{i=1}^{N_s} \omega_t^{(i)}\; x_t^{(i)}$$

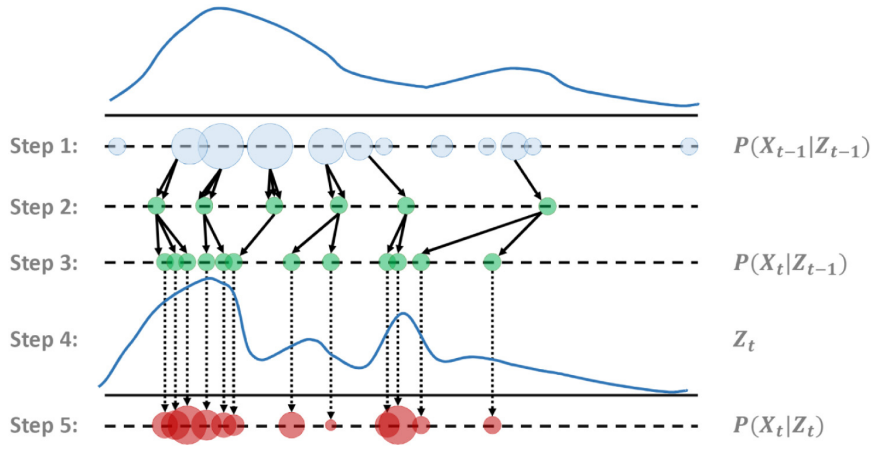

Figure 6.4: Steps of Particle Filter Algorithm (Taken From [8]).

The PF has been used in many signal processing applications due to its versatility in handling non-linear and non-Gaussian problems. In particular, it has been used in tracking applications to estimate the position and velocity of a moving target; in such applications, the system functions can be highly non-linear due to different types of motion models and complex environmental models. PFs have also been used in robotics to determine the position of the robot within an environment and simultaneous perform mapping tasks [127, 128]. Another application of PFs is in speech and audio processing for source separation, denoising, and acoustic echo cancellation [129, 130].

6.3 Bayesian Mode Merging

We propose a new method that uses the output of the unsupervised mode extraction algorithm from Chapter 5 to merge matched NSST clusters. By matched clusters, we mean all NSST clusters that belong to the same signal component as a result of overlapping, and possibly nonlinear, signatures in the TF plane. We consider a signal $x(t)$ with M_x individual signal components given by

$$x(t) = \sum_{l=1}^{M_x} x_l(t)\,.$$

We first compute the NSST $\mathrm{NSST}_x(t,f)$ of $x(t)$, as in Chapter 4, resulting in N TF points (t_i, f_j), $i,j = 1,\ldots,N$. The N NSST TF points are used as input to the unsupervised mode

extraction algorithm to obtain $L \geq M_x$ clusters with unique TF points. We denote by $\mathcal{P}_\ell$ the set of unique TF points belonging to the ℓth cluster, $\ell = 1, \ldots, L$. Using these TF points, we form the following $N \times N$ binary mask for the ℓ cluster

$$\mathcal{M}_\ell(t, f) = \begin{cases} 1, & \text{if } (t_i, f_j) \in P_\ell, \quad i, j = 1, \ldots, N \\ 0, & \text{otherwise} \end{cases}$$

Using the binary mask, we compute the NSST corresponding to the ℓ cluster as

$$\mathrm{MS}_\ell(t, f) = \mathrm{NSST}_x(t, f)\, \mathcal{M}_\ell(t, f)\,. \tag{6.3}$$

An example of the process thus far was demonstrated using Figure 6.1, for the NSST TFR of the sum $M_x = 2$ signal components and Figure 6.2 that shows $\mathrm{MS}_\ell(t, f)$, $\ell = 1, \ldots, L$, for the resulting $L = 6$ clusters. For each of the L masked TFRs in Equation (6.3), we extract the time-domain signal $s_\ell(t)$ as (see Equation (4.8))

$$s_\ell(t) = \int_{f \in P_\ell} \mathrm{MS}_\ell(t, f) df$$

with corresponding Fourier transform $S_\ell(f)$.

The new method uses a Bayesian sequential approach to approximate the highly-localized $\mathrm{MS}_\ell(t, f)$ as a linear combination of Q non-overlapping linear group delay (GD) representations [131]. Specifically, we express the ℓth cluster NSST as

$$\mathrm{MS}_\ell(t, f) = \sum_{q=1}^{Q} (\tau_{\ell,q} + c_{\ell,q}\, f)\, p_q(f)\, r_q(t) \tag{6.4}$$

where $p_q(f)$ is the frequency spread of each linear GD representation with corresponding time spread $r_q(t)$. Here, we assume that within the support of $p_q(f)$ and $r_q(t)$, the slope $c_{\ell,q}$ of the qth TF segment does not change with time. Note that we assume that $\tau_{\ell,q}$ and the slope $c_{\ell,q}$ of the qth linear segment of the ℓth cluster remain constant within the segment. We then estimate the unknown parameters using Bayesian inference by formulating the estimation problem within a state space model framework in the frequency domain. Note that this is different from the PF formulation with time-dependent state x_t in Section 6.2.

Specifically, we denote the unknown state as $X_{\ell,q,f} = X_{\ell,q} = \{\tau_{\ell,q}, c_{\ell,q}\}$, resulting in

$$X_{\ell,q,f} = X_{\ell,q,f-1} + U_{f-1} = X_{\ell,q} + U_{f-1}$$
$$Z_{\ell,q,f} = e^{j2\pi(\tau_{\ell,q}\, f + (c_{\ell,q}/2)\, f^2)} + W_f$$

As the state parameters $X_{\ell,q,f}$ are constant with respect to frequency, the transition equation includes a modeling error process U_f that is assumed zero-mean white Gaussian with very low variance. The measurement equation assumes that the signal model belongs to a linear frequency-modulated signal. Note that, our actual input to the PF, is the actual measurements with measurement noise process assumed zero-mean white Gaussian with known variance.

6.4 Bayesian Mode Merging Simulations

6.4.1 Merging of Two Overlapping Parabolic Frequency-Modulated Signals

We demonstrate the Bayesian mode merging algorithm using the example in Figure 6.1. In particular, we consider four of the 6 clusters in Figure 6.2 and set $Q = 1$ to demonstrate the merging of 4 segments into two modes. The four segments are shown in Figure 6.5. The resulting slope estimates using the PF are shown in Figure 6.6. The merging was decided based on grouping segment slopes similar in value, resulting in two modes. The merged Mode 1 NSST is shown in Figure 6.8. Figure 6.9(a) shows the reconstruction of the mode 1 signal into the time domain, superimposed with the actual PFM signal. The root mean-squared error (RME) between the actual and estimated signals is shown in Figure 6.9(b). Note that, as TF points from the intersection were not included in the clusters, and are not used in the reconstruction, the RMSE shows a large RMSE at time $t = 2$ s. This can be overcome by performing a region search at the intersection locations and including smaller segments in the vicinity of the intersection point for reconstruction.

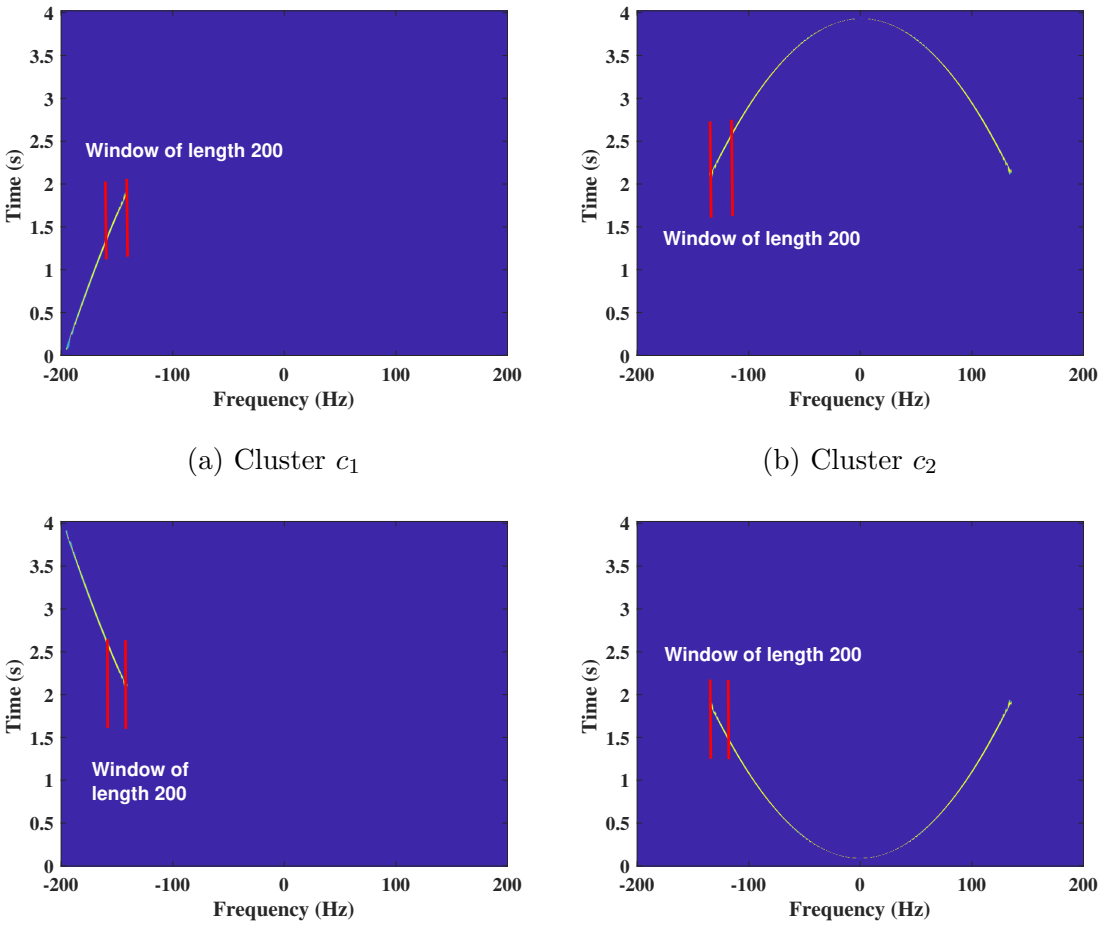

(a) Cluster c_1

(b) Cluster c_2

(c) Cluster c_3

(d) Cluster c_4

Figure 6.5: Segments of 200 Sample Length for 4 Out of the 6 Clusters c_1, c_2, c_3, And c_4 of the Sum of Two PFM Signals in Figure 6.2.

6.4.2 Merging of UGW Modes

The intersecting modes of UGW can be merged by Bayesian mode merging. Figure 6.10 shows the region of intersection of three modes, namely A_0, A_1 and S_0. The Bayesian GD mode merge algorithm is applied by selecting parameter vectors $X = [c, A_0; c, S_0; c, A_1]$. Due to intersection, the clustering algorithm provides two segments of A0, two segments of A1 and a one segment of S0 mode. In order to identify which clusters to merge together, the sequential Bayesian approach is applied. Figure 6.11 depicts the slopes of the segments in the vicinity of the intersection location. It can be seen that the modes can be merged

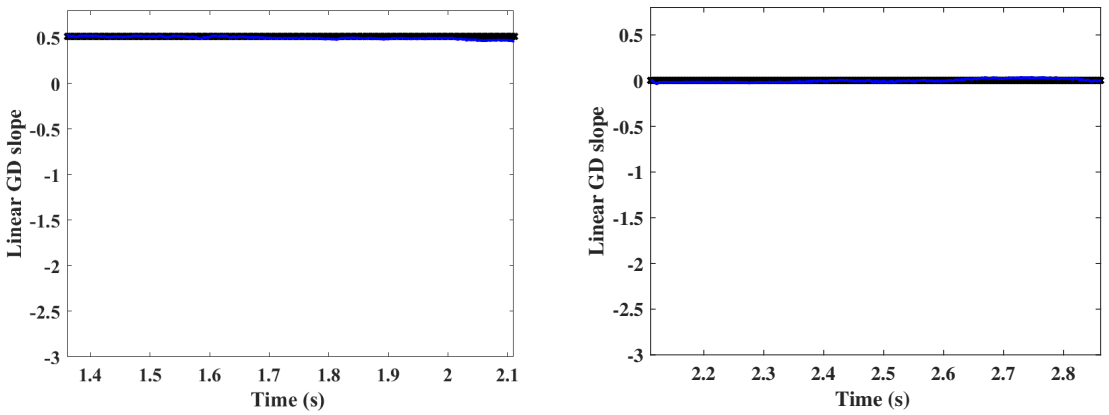

(a) Segment 1

(b) Segment 2

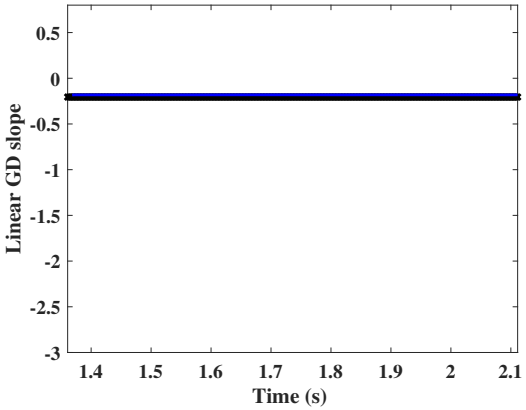

(c) Segment 3

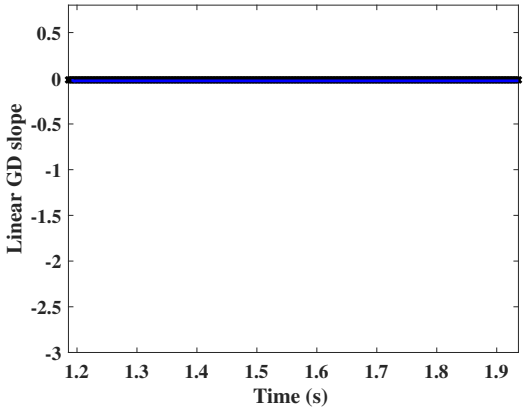

(d) Segment 4

Figure 6.6: Particle Filter Estimation of the Slopes of the Indicated Segments in Figure 6.5.

by joining the appropriate linear GD slope. The RMSE is plotted in figure 6.12 shows the RMSE values of each of the cluster.

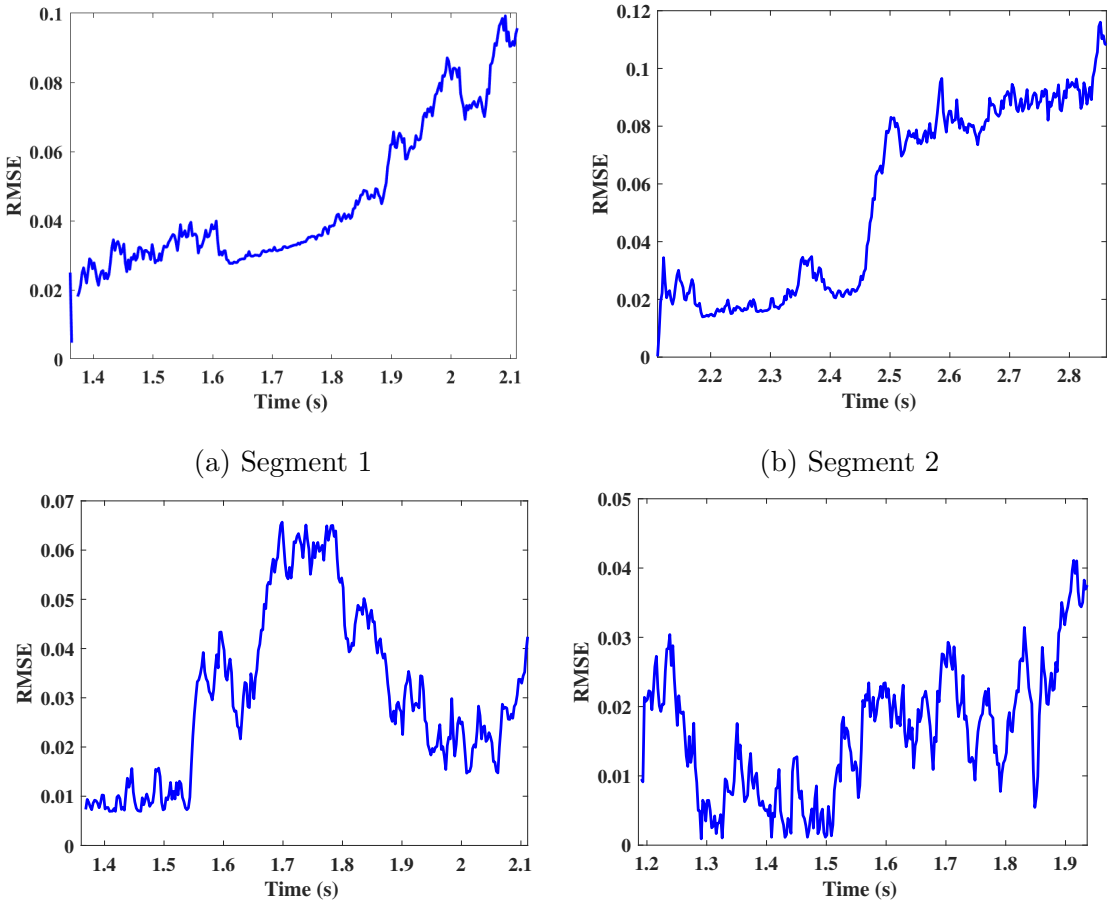

(a) Segment 1

(b) Segment 2

(c) Segment 3

(d) Segment 4

Figure 6.7: Particle Filter Estimation of Slopes

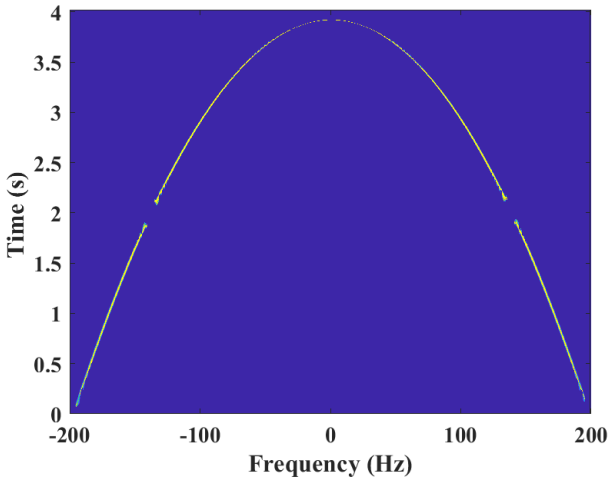

Figure 6.8: Bayesian Mode Merging for Mode 1

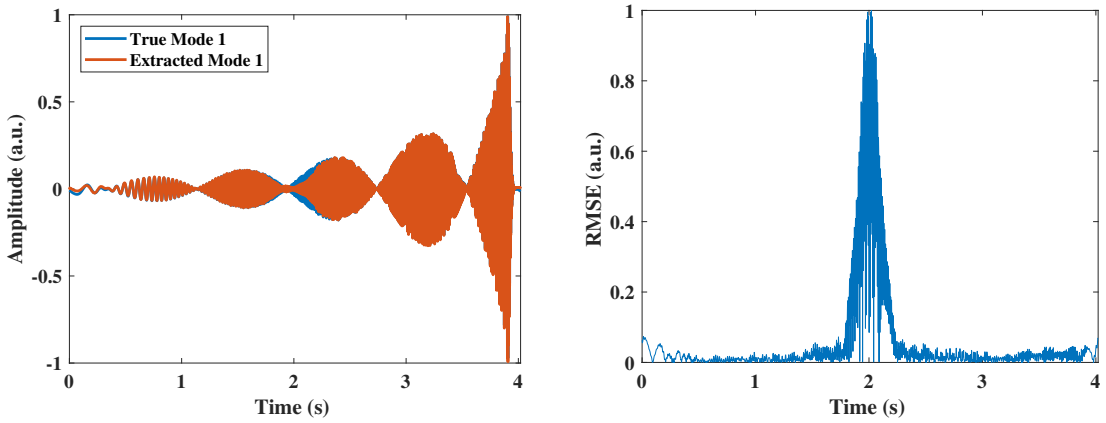

(a) Reconstructed Signals (b) Root Mean-Squared Error

Figure 6.9: Time Domain Signal Reconstruction of Mode 1. Note That the Large Error Around $t = 2$ s is Due to the Missing Data at Intersection points.

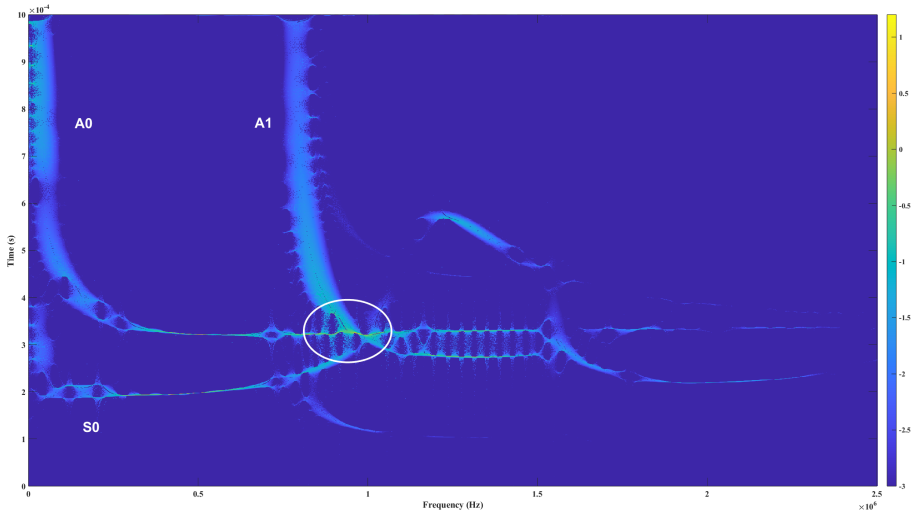

Figure 6.10: Region of Interest for Bayesian Mode Merging.

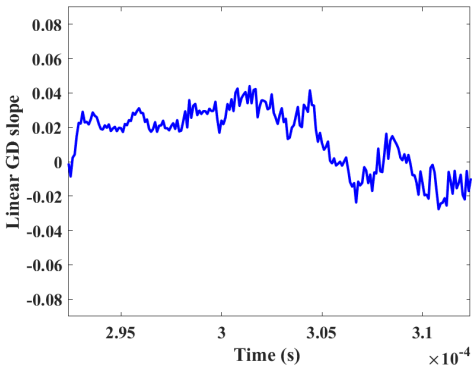

(a) A0 Segment 1

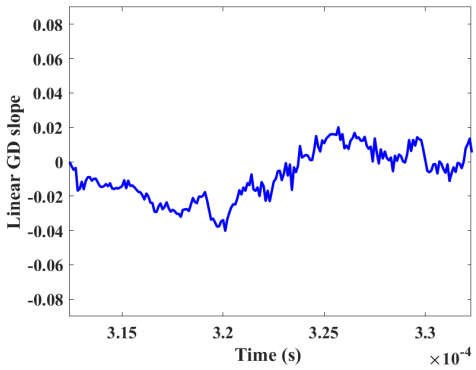

(b) A0 Segment 2

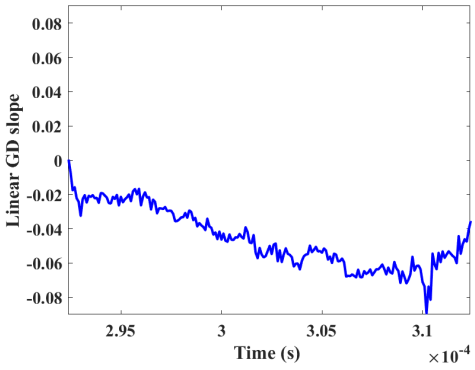

(c) A1 Segment 1

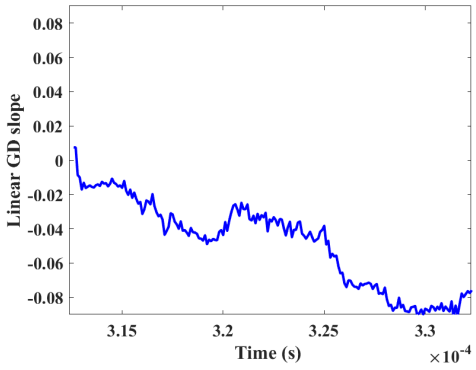

(d) A1 Segment 2

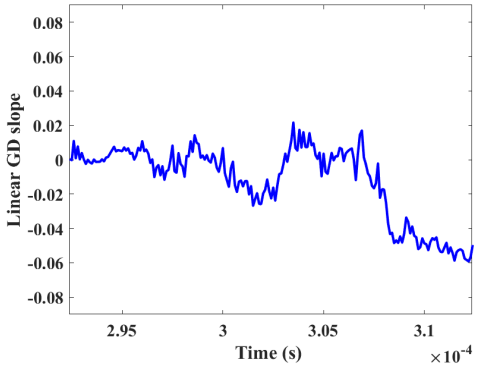

(e) S0 Segment 1

Figure 6.11: Particle Filter Estimation of Slopes of the Indicated Segments of UGW

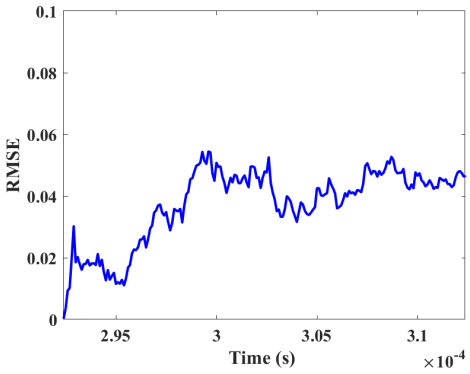

(a) A0 Segment 1

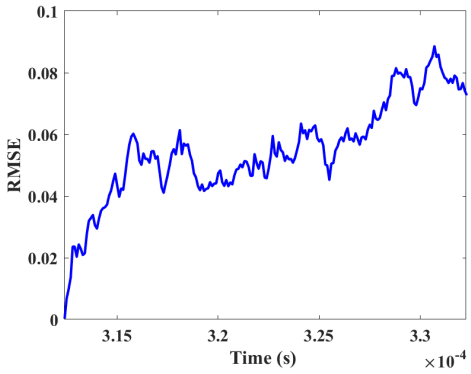

(b) A0 Segment 2

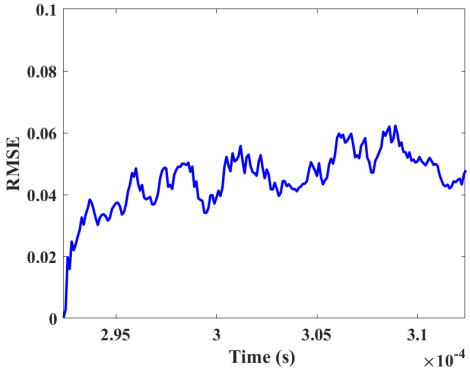

(c) A1 Segment 1

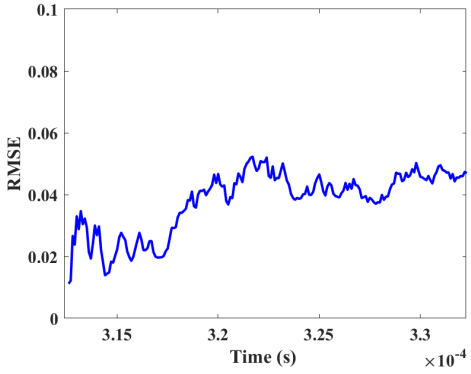

(d) A1 Segment 2

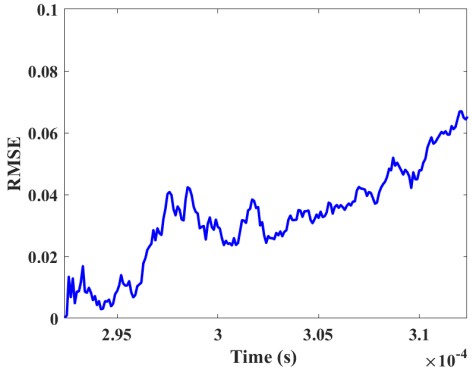

(e) S0 Segment 1

Figure 6.12: RMSE of Segments in UGW

Chapter 7

CONCLUSIONS AND FUTURE WORK

7.1 Conclusions

In this disseration, we proposed new methodologies for processing highly dispersive signals in the time-frequency domain. We developed a novel time-reassigned synchrosqueezing time-frequency representation (TFR), which provides high-localization in the time-frequency plane for signals with nonlinear group delay signatures. This transform is well-matched to analyze the ultrasonic guided wave dispersive propagation in complex materials and can be used to identify damage features in structural health monitoring applications.

Our first contribution was the use of the first order synchrosqueezing transform and the matching pursuit decomposition to inspect integrated circuit (IC) packages using ultrasonic guided waves. The synchrosqueezing transform added the benefit of the reconstruction of different signal components. We considered both healthy and damage states; the damage can occur at the integrated interface between the heat spreader and the substrate as a result of loading conditions or manufacturing defects. Preliminary IC package health inspection results from experimental data demonstrated the potential usefulness of this approach for health inspections.

Our second contribution was the mathematical derivation for the nonlinear synchrosqueezing transform (NSST) that was specifically designed to match signals with dispersive time-frequency characteristics. The transform was obtained by modeling the phase function of the analysis signal spectrum as a third order polynomial and solving a system of linear equations to obtain an estimator of the signal's group delay function. This estimator was then used in the first order synchrosqueezing transform formulation by reassigning time-frequency points to the estimated group delay. We demonstrated the effectiveness of the

NSST by analyzing ultrasonic guided waves propagating in isotropic Aluminum plates. The NSST provided the expected group velocity of the propagating waves through the isotropic plate. We also investigated the NSST's performance for signals in white Gaussian noise using the reconstruction quality factor for comparison. We demonstrated that the NSST provided the best reconstruction performance, when compared to other synchrosqueezing transforms, for signals with quadratic group delay function.

Our third contribution was an unsupervised mode extraction method that separates and the different signal components using graph-based segmention. When compared to other ridge extraction methods, the proposed approach does not require knowledge of the number of signal modes. This is important for UGW propagation as new modes can be generated based on interactions of the wave with different boundaries in the material. The new method considers the time-frequeny points of the NSST as vertices on a graph with connecting edges; the edge weight is the difference in intensity between neighboring time-frequency points.

Our fourth contribution was the separation of modes that have overlapping time-frequency characteristics. Using the graph-based segmentation method with the NSST can result in more clusters than the actual number of components. To avoid this clustering issue, we proposed a Bayesian mode merging method that uses Bayesian inference to identify cluster regions that are continuous over a span of time-frequency points.

7.2 Future Work

The new NSST time-frequency representation, together with the unsupervised mode separation of both non-overlapping and overlapping modes, is very promising for use to detect damage in structures. Although this was successfully demonstrated with a few examples, additional processing and evaluation is required to formalize the method as an effective structural health monitoring tool for localization, quantification and prognosis of damage. The extracted time-frequency modes can also be used as features in machine

learning algorithms for modeling or clustering

The Bayesian group delay model merging algorithm can be further improved to in extracting individual modes. In particular, the clustering algorithm can be modified to allow for different size clusters; having clusters with a small number of time-frequency points will increase the extraction of modes at the points of overlap. The performance of the merging algorithm can be further improved by using the Kullback-Leibler distance metric to improve the estimation of the constant slope of the linear group delay by the particle filter [131].

REFERENCES

[1] M. S. Harb and F.-G. Yuan, "Damage imaging using non-contact air-coupled transducer/laser doppler vibrometer system," *Structural Health Monitoring*, 2016.

[2] A. Papandreou-Suppappola and S. B. Suppappola, "Adaptive time-frequency representations for multiple structures," in *Proceedings of the Tenth IEEE Workshop on Statistical Signal and Array Processing (Cat. No. 00TH8496)*, IEEE, 2000.

[3] T. Oberlin, S. Meignen, and V. Perrier, "The Fourier-based synchrosqueezing transform," in *IEEE Int. Conf. Acoustics, Speech and Signal Processing*, pp. 315–319, 2014.

[4] T. Oberlin, S. Meignen, and V. Perrier, "Second-order synchrosqueezing transform or invertible reassignment? towards ideal time-frequency representations," *IEEE Transactions on Signal Processing*, vol. 63, pp. 1335–1344, 2015.

[5] D. Fourer, F. Auger, K. Czarnecki, S. Meignen, and P. Flandrin, "Chirp rate and instantaneous frequency estimation: Application to recursive vertical synchrosqueezing," *IEEE Signal Processing Letters*, vol. 24, pp. 1724–1728, 2017.

[6] D. Fourer and F. Auger, "Second-order time-reassigned synchrosqueezing transform: Application to Draupner wave analysis," in *European Signal Processing Conference*, pp. 1–5, 2019.

[7] J. Ikram, A. Chattopadhyay, and A. Papandreou-Suppappola, "Synchrosqueezing transform matched to nonlinear group delay for mode estimation of ultrasonic guided waves," in *Asilomar Conf. Signals, Systems and Computers*, pp. 558–562, 2021.

[8] J. Wan, C. Xu, W. Chen, R. Wang, and X. Zhang, "Abrupt moving target tracking based on quantum enhanced particle filter," *ISA Transactions*, vol. 138, pp. 254–261, 2023.

[9] J. L. Rose, "Ultrasonic Guided Waves in Structural Health Monitoring," *Key Engineering Materials*, vol. 270-273, pp. 14–21, 2004.

[10] L. Cohen, *Time-Frequency Analysis*, vol. 778. Prentice Hall New Jersey, 1995.

[11] D. Alleyne and P. Cawley, "A two-dimensional fourier transform method for the measurement of propagating multimode signals," *The Journal of the Acoustical Society of America*, vol. 89, no. 3, pp. 1159–1168, 1991.

[12] S. Mitra, Mira Gopalakrishnan, "Wave propagation analysis in anisotropic plate using wavelet spectral element approach," *Journal of Applied Mechanics*, 2008.

[13] W. H. Prosser, M. D. Seale, and B. T. Smith, "Time-frequency analysis of the dispersion of Lamb modes," *J. Acoustical Soc. Am.*, vol. 105, pp. 2669–2676, 1999.

[14] S. Das, I. Kyriakides, A. Chattopadhyay, and A. Papandreou-Suppappola, "Monte Carlo matching pursuit decomposition method for damage quantification in composite structures," *Journal of Intelligent Material Systems and Structures*, 2009.

[15] N. E. Huang and Z. Wu, "A review on Hilbert-Huang transform: Method and its applications to geophysical studies," *Reviews of geophysics*, 2008.

[16] K. Kodera, C. De Villedary, and R. Gendrin, "A new method for the numerical analysis of non-stationary signals," *Physics of the Earth and Planetary Interiors*, vol. 12, pp. 142–150, 1976.

[17] F. Auger and P. Flandrin, "Improving the readability of time-frequency and time-scale representations by the reassignment method," *IEEE Transactions on Signal Processing*, vol. 43, pp. 1068–1089, 1995.

[18] I. Daubechies, J. Lu, and H.-T. Wu, "Synchrosqueezed wavelet transforms: An empirical mode decomposition-like tool," *Applied and Computational Harmonic Analysis*, 2011.

[19] L. Yu, J. Bao, and V. Giurgiutiu, "Signal processing techniques for damage detection with piezoelectric wafer active sensors and embedded ultrasonic structural radar," in *Smart Structures and Materials 2004: Sensors and Smart Structures Technologies for Civil, Mechanical, and Aerospace Systems*, vol. 5391, pp. 492–503, SPIE, 2004.

[20] S. Kim and H. Sohn, "Application of time-reversal guided waves to field bridge testing for baseline-free damage diagnosis," in *Health Monitoring and Smart Nondestructive Evaluation of Structural and Biological Systems V*, vol. 6177, pp. 50–59, SPIE, 2006.

[21] D. N. Alleyne and P. Cawley, "Optimization of lamb wave inspection techniques," *Ndt & E International*, vol. 25, no. 1, pp. 11–22, 1992.

[22] R. P. Dalton, P. Cawley, and M. J. Lowe, "The potential of guided waves for monitoring large areas of metallic aircraft fuselage structure," *Journal of Nondestructive Evaluation*, vol. 20, no. 1, pp. 29–46, 2001.

[23] P. Wilcox, M. Lowe, and P. Cawley, "The effect of dispersion on long-range inspection using ultrasonic guided waves," *NDT & E International*, vol. 34, pp. 1–9, 2001.

[24] P. D. Wilcox, "A rapid signal processing technique to remove the effect of dispersion from guided wave signals," *IEEE Transactions on Ultrasonics, Ferroelectrics, and Frequency Control*, vol. 50, no. 4, pp. 419–427, 2003.

[25] H. Sohn, H. W. Park, K. H. Law, and C. R. Farrar, "Instantaneous damage diagnosis without prior baseline data," *Journal of Intelligent Material Systems and Structures*, 2005.

[26] M. Niethammer, L. J. Jacobs, J. Qu, and J. Jarzynski, "Time-frequency representation of Lamb waves using the reassigned spectrogram," *J. Acoustical Soc. Am.*, vol. 107, pp. 19–24, 2000.

[27] M. Niethammer, L. Jacobs, J. Qu, and J. Jarrzynski, "Time-frequency representations of Lamb waves," *J. Acoustical Soc. America*, vol. 109, p. 1841–1847, 2001.

[28] L. De Marchi, A. Marzani, S. Caporale, and N. Speciale, "Ultrasonic guided-waves characterization with warped frequency transforms," *IEEE Trans. Ultrasonics, Ferroelectrics, and Frequency Control*, vol. 56, pp. 2232–2240, 2009.

[29] M. Zhao, L. Zeng, J. Lin, and W. Wu, "Mode identification and extraction of broadband ultrasonic guided waves," *Measurement Science and Technology*, vol. 25, 2014.

[30] J. Ikram, A. Papandreou-Suppappola, G. Li, and A. Chattopadhyay, "Guided wave based inspection of integrated circuit packages using the time-frequency synchrosqueezing transform," in *Smart Structures and NDE for Energy Systems and Industry*, vol. 10973, p. 109730A, 2019.

[31] F. Auger, P. Flandrin, Y.-T. Lin, S. McLaughlin, S. Meignen, T. Oberlin, and H.-T. Wu, "Time-frequency reassignment and synchrosqueezing: An overview," *IEEE Signal Processing Magazine*, vol. 30, pp. 32–41, 2013.

[32] S. Meignen, D.-H. Pham, and S. McLaughlin, "On demodulation, ridge detection, and synchrosqueezing for multicomponent signals," *IEEE Transactions on Signal Processing*, vol. 65, pp. 2093–2103, 2017.

[33] V. Giurgiutiu, *Structural health monitoring of aerospace composites*. Academic Press, 2015.

[34] G. Song, C. Wang, and B. Wang, "Structural health monitoring (SHM) of civil structures," *Applied Sciences*, vol. 7, no. 8, p. 789, 2017.

[35] D. Montalvao, N. M. M. Maia, and A. M. R. Ribeiro, "A review of vibration-based structural health monitoring with special emphasis on composite materials," *Shock and Vibration Digest*, vol. 38, no. 4, pp. 295–324, 2006.

[36] J. L. Rose, *Ultrasonic Guided Waves in Solid Media*. Cambridge University Press, 2014.

[37] G. Li, R. K. Neerukatti, and A. Chattopadhyay, "Ultrasonic guided wave propagation in composites including damage using high fidelity local interaction simulation," *J. Intelligent Material Systems Structures*, vol. 29, pp. 969–985, 2018.

[38] J. Ikram, A. Papandreou-Suppappola, G. Li, and A. Chattopadhyay, "Guided wave based inspection of integrated circuit packages using the time-frequency synchrosqueezing transform," in *Smart Structures and NDE for Energy Systems and Industry 4.0*, SPIE, 2019.

[39] J. Ikram, A. Chattopadhyay, and A. Papandreou-Suppappola, "Unsupervised mode extraction and group velocity estimation for ultrasonic guided waves propagating in dispersive material," in *Asilomar Conf. Signals, Systems, and Computers*, pp. 343–347, 2020.

[40] Y. Shen and V. Giurgiutiu, "Predictive modeling of nonlinear wave propagation for structural health monitoring with piezoelectric wafer active sensors," *Journal of Intelligent Material Systems and Structures*, vol. 25, pp. 506–520, 2014.

[41] J. Moll, R. Schulte, B. Hartmann, C. Fritzen, and O. Nelles, "Multi-site damage localization in anisotropic plate-like structures using an active guided wave structural health monitoring system," *Smart Materials and Structures*, 2010.

[42] C. Hodges, J. Power, and J. Woodhouse, "The use of the sonogram in structural acoustics and an application to the vibrations of cylindrical shells," *Journal of Sound and Vibration*, vol. 101, 1985.

[43] K. H. Sun, J.-C. Hong, and Y. Y. Kim, "Dispersion-based continuous wavelet transform for the analysis of elastic waves," *Journal of Mechanical Science and Technology*, vol. 20, pp. 2147–2158, 2006.

[44] K. Kishimoto, H. Inoue, M. Hamada, and T. Shibuya, "Time frequency analysis of dispersive waves by means of wavelet transform," *Journal of Applied Mechanics*, 1995.

[45] Y. Jiang and A. Papandreou-Suppappola, "Discrete time-frequency characterizations of dispersive linear time-varying systems," *IEEE Transactions on Signal Processing*, 2007.

[46] C. Ioana, A. Jarrot, C. Gervaise, Y. Stéphan, and A. Quinquis, "Localization in underwater dispersive channels using the time-frequency-phase continuity of signals," *IEEE Transactions on Signal Processing*, 2010.

[47] Y. Liu, M. Y. Fard, A. Chattopadhyay, and D. Doyle, "Damage assessment of cfrp composites using a time–frequency approach," *Journal of Intelligent Material Systems and Structures*, 2012.

[48] W. Sachse and Y.-H. Pao, "On the determination of phase and group velocities of dispersive waves in solids," *Journal of Applied Physics*, vol. 49, no. 8, pp. 4320–4327, 1978.

[49] A. H. Nayfeh, *Wave Propagation in Layered Anisotropic Media: With Application to Composites*. Elsevier, 1995.

[50] X. Yu, M. Ratassepp, P. Rajagopal, and Z. Fan, "Anisotropic effects on ultrasonic guided waves propagation in composite bends," *Ultrasonics*, vol. 72, 2016.

[51] O. Putkis, R. P. Dalton, and A. J. Croxford, "The anisotropic propagation of ultrasonic guided waves in composite materials and implications for practical applications," *Ultrasonics*, vol. 65, 2016.

[52] P. B. Nagy, F. Simonetti, and G. Instanes, "Corrosion and erosion monitoring in plates and pipes using constant group velocity lamb wave inspection," *Ultrasonics*, vol. 54, no. 7, 2014.

[53] P. Wilcox, M. Lowe, and P. Cawley, "The effect of dispersion on long-range inspection using ultrasonic guided waves," *Ndt & E International*, vol. 34, 2001.

[54] P. D. Wilcox, "A rapid signal processing technique to remove the effect of dispersion from guided wave signals," *IEEE transactions on ultrasonics, ferroelectrics, and frequency control*, vol. 50, 2003.

[55] A. Papandreou-Suppappola, "Time-frequency processing: Tutorial on principles and practice," *Applications in Time-Frequency Signal Processing*, 2002.

[56] H. G. Feichtinger and T. Strohmer, *Gabor Analysis and Algorithms: Theory and Applications*. Springer Science & Business Media, 2012.

[57] P. Tua, S. Quek, and Q. Wang, "Detection of cracks in plates using piezo-actuated lamb waves," *Smart Materials and Structures*, 2004.

[58] M. F. Gunther, A. Wang, B. R. Fogg, S. E. Starr, K. A. Murphy, and R. O. Claus, "Fiber optic impact detection and location system embedded in a composite material," in *Fiber optic smart structures and skins V*, SPIE.

[59] R. Seydel and F.-K. Chang, "Impact identification of stiffened composite panels: I. system development," *Smart materials and structures*, 2001.

[60] G. Li and A. Chattopadhyay, "Multi-dimensional signal processing and mode tracking approach for guided wave based damage localization in x-cor sandwich composite," *Mechanical Systems and Signal Processing*, 2018.

[61] H. Sohn, G. Park, J. R. Wait, N. P. Limback, and C. R. Farrar, "Wavelet-based active sensing for delamination detection in composite structures," *Smart Materials and structures*, 2003.

[62] H. Kuttig, M. Niethammer, S. Hurlebaus, and L. J. Jacobs, "Model-based analysis of dispersion curves using chirplets," *The Journal of the Acoustical Society of America*, 2006.

[63] S. G. Mallat, "A theory for multiresolution signal decomposition: the wavelet representation," *IEEE Transactions on Pattern Analysis and Machine Intelligence*, vol. 11, no. 7, 1989.

[64] I. Daubechies, "The wavelet transform, time-frequency localization and signal analysis," *IEEE Transactions on Information Theory*, vol. 36, no. 5, 1990.

[65] E. Wigner, "On the quantum correction for thermodynamic equilibrium," *Physical review*, vol. 40, no. 5, 1932.

[66] J. Ville, "Theorie et application de la notion de signal analytic, cables et transmissions, 2a (1), 61-74, paris, france, 1948," *Translation by I. Selin, Theory and applications of the notion of complex signal, Report T-92, RAND Corporation, Santa Monica, CA*, 1948.

[67] F. Hlawatsch and G. F. Boudreaux-Bartels, "Linear and quadratic time-frequency signal representations," *IEEE signal processing magazine*, vol. 9, no. 2, pp. 21–67, 1992.

[68] S. G. Mallat and Z. Zhang, "Matching pursuits with time-frequency dictionaries," *IEEE Transactions on Signal Processing*, vol. 41, no. 12, pp. 3397–3415, 1993.

[69] S. Qian and D. Chen, "Decomposition of the wigner-ville distribution and time-frequency distribution series," *IEEE Transactions on Signal Processing*, vol. 42, no. 10, pp. 2836–2842, 1994.

[70] J. A. Tropp and A. C. Gilbert, "Signal recovery from random measurements via orthogonal matching pursuit," *IEEE Transactions on information theory*, vol. 53, no. 12, 2007.

[71] S. S. Chen, D. L. Donoho, and M. A. Saunders, "Atomic decomposition by basis pursuit," *SIAM review*, vol. 43, no. 1, pp. 129–159, 2001.

[72] P. Flandrin, *Time-Frequency/Time-Scale Analysis*. Academic Press, 1998.

[73] J. Ikram, G. Li, R. K. Neerukatti, and A. Chattopadhyay, "Ultrasonic guided wave inspection and characterization of integrated circuit packages with delamination," in *11th International Workshop on Structural Health Monitoring 2017: Real-Time Material State Awareness and Data-Driven Safety Assurance, IWSHM 2017*, pp. 2320–2326, DEStech Publications, 2017.

[74] G.-M. Zhang, D. M. Harvey, and D. R. Braden, "Resolution improvement of acoustic microimaging by continuous wavelet transform for semiconductor inspection," *Microelectronics Reliability*, 2006.

[75] J. Yang, "Non-destructive identification of defects in integrated circuit packages by scanning acoustic microscopy," *Microelectronics reliability*, 1996.

[76] G. Thakur, E. Brevdo, N. S. Fučkar, and H.-T. Wu, "The synchrosqueezing algorithm for time-varying spectral analysis: Robustness properties and new paleoclimate applications," *Signal Processing*, vol. 93, pp. 1079–1094, 2013.

[77] D. He, H. Cao, S. Wang, and X. Chen, "Time-reassigned synchrosqueezing transform: The algorithm and its applications in mechanical signal processing," *Mechanical Systems and Signal Processing*, vol. 117, pp. 255–279, 2019.

[78] L. Rayleigh, "On waves propagated along the plane surface of an elastic solid," *Proceedings of the London mathematical Society*, vol. 1, no. 1, pp. 4–11, 1885.

[79] A. E. H. Love, *Some Problems of Geodynamics: Being an Essay to which the Adams Prize in the University of Cambridge was Adjudged in 1911*. CUP Archive, 1911.

[80] H. Lamb, "On waves in an elastic plate," *Proceedings of the Royal Society of London. Series A, Containing papers of a mathematical and physical character*, vol. 93, no. 648, pp. 114–128, 1917.

[81] W. T. Thomson, "Transmission of elastic waves through a stratified solid medium," *Journal of applied Physics*, vol. 21, no. 2, pp. 89–93, 1950.

[82] N. A. Haskell, "Crustal reflection of plane p and sv waves," *Journal of Geophysical Research*, vol. 67, no. 12, pp. 4751–4768, 1962.

[83] H. Schmidt and F. B. Jensen, "Efficient numerical solution technique for wave propagation in horizontally stratified environments," *Computers & Mathematics with Applications*, vol. 11, no. 7-8, pp. 699–715, 1985.

[84] Z. Hashin, "Analysis of composite materials—a survey," 1983.

[85] O. C. Zienkiewicz, R. L. Taylor, P. Nithiarasu, and J. Zhu, *The finite element method*, vol. 3. McGraw-hill London, 1977.

[86] Y. Tsuji and M. Koshiba, "Finite element method using port truncation by perfectly matched layer boundary conditions for optical waveguide discontinuity problems," *Journal of lightwave technology*, vol. 20, no. 3, pp. 463–468, 2002.

[87] M. Scalerandi, V. Agostini, P. P. Delsanto, K. Van Den Abeele, and P. A. Johnson, "Local interaction simulation approach to modelling nonclassical, nonlinear elastic behavior in solids," *J. Acoustical Soc. Am.*, vol. 113, pp. 3049–3059, 2003.

[88] L. Borkowski, K. Liu, and A. Chattopadhyay, "Fully coupled electromechanical elastodynamic model for guided wave propagation analysis," *Journal of intelligent material systems and structures*, vol. 24, no. 13, pp. 1647–1663, 2013.

[89] B. Xu and V. Giurgiutiu, "Single mode tuning effects on lamb wave time reversal with piezoelectric wafer active sensors for structural health monitoring," *Journal of Nondestructive Evaluation*, vol. 26, no. 2, pp. 123–134, 2007.

[90] S. Kim, H. Sohn, D. Greve, and I. Oppenheim, "Application of a time reversal process for baseline-free monitoring of a bridge steel girder," in *International Workshop on Structural Health Monitoring, Stanford, CA*, pp. 15–17, 2005.

[91] A. Papandreou-Suppappola, ed., *Applications in Time-Frequency Signal Processing*. CRC Press, 2002.

[92] K. Kodera, R. Gendrin, and C. De Villedary, "Analysis of time-varying signals with small BT values," *IEEE Transactions on Acoustic, Speech and Signal Processing*, vol. 26, pp. 64–76, 1978.

[93] P. Flandrin, F. Auger, and E. Chassande-Mottin, "Time-frequency reassignment: From principles to algorithms," in *Applications in Time-Frequency Signal Processing* (A. Papandreou-Suppappola, ed.), ch. 10, pp. 179–204, CRC Press, 2002.

[94] S. Meignen, T. Oberlin, and S. Mclaughlin, "A new algorithm for multicomponent signal analysis based on synchrosqueezing: With an application to signal sampling and denoising," *IEEE Transactions on Signal Processing*, vol. 60, p. 5787–5798, 2012.

[95] K. Abratkiewicz, "On the instantaneous angular jerk estimation in the time-frequency domain," *IEEE Signal Processing Letters*, vol. 28, pp. 798–802, 2021.

[96] D.-H. Pham and S. Meignen, "High-order synchrosqueezing transform for multicomponent signals analysis-with an application to gravitational-wave signal," *IEEE Transactions on Signal Processing*, vol. 65, p. 3168–3178, 2017.

[97] I. Daubechies and S. Maes, "A nonlinear squeezing of the continuous wavelet transform based on auditory nerve models," in *Wavelets in Medicine and Biology* (A. Aldroubi and M. Unser, eds.), ch. 2, pp. 527–546, CRC, 1996.

[98] R. Behera, S. Meignen, and T. Oberlin, "Theoretical analysis of the second-order synchrosqueezing transform," *Applied and Computational Harmonic Analysis*, vol. 45, pp. 379–404, 2018.

[99] W. Liu, S. Cao, Z. Wang, K. Jiang, Q. Zhang, and Y. Chen, "A novel approach for seismic time-frequency analysis based on high-order synchrosqueezing transform," *IEEE Geoscience and Remote Sensing Letters*, vol. 15, pp. 1159–1163, 2018.

[100] W. Liu, W. Chen, and Z. Zhang, "A novel fault diagnosis approach for rolling bearing based on high-order synchrosqueezing transform and detrended fluctuation analysis," *IEEE Access*, vol. 8, pp. 12533–12541, 2020.

[101] J. M. Miramont, M. A. Colominas, and G. Schlotthauer, "Voice jitter estimation using high-order synchrosqueezing operators," *IEEE/ACM Transactions on Audio, Speech, and Language Processing*, vol. 29, pp. 527–536, 2021.

[102] K. Abratkiewicz and J. Gambrych, "Real-time variants of vertical synchrosqueezing: Application to radar remote sensing," *IEEE Journal of Selected Topics in Applied Earth Observations and Remote Sensing*, vol. 15, pp. 1760–1774, 2022.

[103] X. Tu, Q. Zhang, Z. He, Y. Hu, S. Abbas, and F. Li, "Generalized horizontal synchrosqueezing transform: Algorithm and applications," *IEEE Transactions on Industrial Electronics*, vol. 68, pp. 5293–5302, 2021.

[104] A. Papandreou-Suppappola, "Time-frequency processing: A tutorial on principles and practice," in *Applications in Time-Frequency Signal Processing*, ch. 1, CRC Press, 2002.

[105] A. Papandreou-Suppappola, F. Hlawatsch, and G. F. Boudreaux-Bartels, "The hyperbolic class of quadratic time-frequency representations part i: Constant-Q warping, the hyperbolic paradigm, properties, and members," *IEEE Transactions on Signal Processing*, vol. 41, p. 3425–3444, 1993.

[106] R. A. Altes and E. L. Titlebaum, "Bat signals as optimally Doppler tolerant waveforms," *Journal of the Acoustical Society of America*, vol. 48, pp. 1014–1020, 1970.

[107] F. Hlawatsch, A. Papandreou-Suppappola, and G. F. Boudreaux-Bartels, "The power classes—quadratic time-frequency representations with scale covariance and dispersive time-shift covariance," *IEEE Transactions on Signal Processing*, vol. 47, p. 3067–3083, 1999.

[108] F. Wang, S. Du, W. Sun, Q. Huang, and J. Su, "A method of velocity estimation using composite hyperbolic frequency-modulated signals in active sonar," *The Journal of the Acoustical Society of America*, vol. 141, no. 5, 2017.

[109] G. Thakur and H.-T. Wu, "Synchrosqueezing-based recovery of instantaneous frequency from nonuniform samples," *SIAM Journal on Mathematical Analysis*, vol. 43, p. 2078–2095, 2011.

[110] R. A. Carmona, W. L. Hwang, and B. Torrésani, "Multiridge detection and time-frequency reconstruction," *IEEE Transactions on Signal Processing*, vol. 47, pp. 480–492, 1999.

[111] P. F. Felzenszwalb and D. P. Huttenlocher, "Efficient graph-based image segmentation," *International Journal of Computer Vision*, vol. 59, pp. 167–181, 2004.

[112] S. Van der Walt, J. L. Schönberger, J. Nunez-Iglesias, F. Boulogne, J. D. Warner, N. Yager, E. Gouillart, and T. Yu, "scikit-image: image processing in python," *PeerJ*, 2014.

[113] S. Barbarossa and A. Farina, "Detection and imaging of moving objects with synthetic aperture radar. part 2: Joint time-frequency analysis by wigner-ville distribution," in *IEE Proceedings F (Radar and Signal Processing)*, vol. 139, IET, 1992.

[114] C. Cook, *Radar signals: An introduction to theory and application*. Elsevier, 2012.

[115] M. A. Richards, J. Scheer, W. A. Holm, and W. L. Melvin, "Principles of modern radar," 2010.

[116] N. A. Khan, S. Ali, and K. Choi, "An efficient direction of arrival estimation algorithm for sources with intersecting signature in the time–frequency domain," *Applied Sciences*, vol. 11, no. 4, 2021.

[117] N. A. Khan and S. Ali, "A robust and efficient instantaneous frequency estimator of multi-component signals with intersecting time-frequency signatures," *Signal Processing*, vol. 177, 2020.

[118] C.-C. Ng, M. H. Yap, N. Costen, and B. Li, "Automatic wrinkle detection using hybrid hessian filter," in *Computer Vision–ACCV 2014: 12th Asian Conference on Computer Vision, Singapore, Singapore, November 1-5, 2014, Revised Selected Papers, Part III 12*, pp. 609–622, 2015.

[119] A. Gelman, J. B. Carin, H. S. Stern, D. B. Dunson, A. Vehtari, and D. B. Rubin, *Bayesian Data Analysis*. Chapman and Hall/CRC, 3 ed., 2013.

[120] A. Doucet, N. D. Freitas, and N. Gordon, eds., *Sequential Monte Carlo Methods in Practice*. Springer-Verlag, 2001.

[121] R. E. Kalman, "A new approach to linear filtering and prediction problems," *Journal of Basic Engineering*, vol. 82, pp. 35–45, 1960.

[122] N. J. Gordon, D. J. Salmond, and A. F. Smith, "Novel approach to nonlinear/non-gaussian bayesian state estimation," in *IEE proceedings F (radar and signal processing)*, vol. 140, IET, 1993.

[123] M. S. Arulampalam, S. Maskell, N. Gordon, and T. Clapp, "A tutorial on particle filters for online nonlinear/non-gaussian bayesian tracking," *IEEE Transactions on signal processing*, vol. 50, no. 2, 2002.

[124] B. Ristic, S. Arulampalam, and N. Gordon, *Beyond the Kalman filter: Particle filters for tracking applications*. Artech house, 2003.

[125] A. Doucet, A. M. Johansen, *et al.*, "A tutorial on particle filtering and smoothing: Fifteen years later," *Handbook of nonlinear filtering*, vol. 12, p. 3, 2009.

[126] C. P. Robert and G. Casella, *Monte Carlo Statistical Methods*. Springer, 1999.

[127] S. Thrun, "Particle filters in robotics.," in *UAI*, vol. 2, Citeseer, 2002.

[128] A. Howard, "Multi-robot simultaneous localization and mapping using particle filters," *The International Journal of Robotics Research*, vol. 25, no. 12, 2006.

[129] D. N. Zotkin, R. Duraiswami, and L. S. Davis, "Joint audio-visual tracking using particle filters," *EURASIP Journal on Advances in Signal Processing*, vol. 2002, 2002.

[130] F. Mustiere, M. Bolic, and M. Bouchard, "Rao-blackwellised particle filters: examples of applications," in *2006 Canadian Conference on Electrical and Computer Engineering*, IEEE, 2006.

[131] Y. Li, A. Papandreou-Suppappola, and D. Morrell, "Instantaneous frequency estimation using sequential bayesian techniques," in *2006 Fortieth Asilomar Conference on Signals, Systems and Computers*, IEEE, 2006.

APPENDIX A

7.3 QUADRATIC GD FUNCTION ESTIMATION

We consider the GTM signal spectrum $X(f) = A(f)\, e^{-j2\pi\Phi(f)}$ with phase function $\Phi(f) = \Phi_0 + t_x\, f + b_x\, f^2 + c_x\, f^3$ and GD function $\tau(f) = t_x + b_x\, f + c_x\, f^2$. We assume signals with large bandwidth so $A(f)$ can be considered Gaussian with large spread or constant. To estimate the unknown GD parameters t_x, b_x and c_x, we follow the approach in [5] that was used to estimate the IF of chirp signals. The GD parameters are estimated by solving a system of three linear equations that are formed using derivatives of the STFT in Equation (4.1), which can also be expressed as

$$S_x(t, f; H) = e^{-j2\pi tf} \int X(\nu)\, H(f-\nu)\, e^{j2\pi t\nu}\, d\nu \tag{A-1}$$

We first take the partial derivative of the STFT in Equation (A-1) with respect to frequency to obtain

$$\frac{\partial}{\partial f} S_x(t, \frac{\partial}{\partial f}\Big(e^{-j2\pi tf} \int X(\nu)\, H(f-\nu)\, e^{j2\pi t\nu}\, d\nu\Big)$$

$$= (-j2\pi t)\, e^{-j2\pi tf} \int X(\nu)\, H(f-\nu)\, e^{j2\pi t\nu}\, d\nu + e^{-j2\pi tf} \int X(\nu)\, \Big(\frac{\partial}{\partial f} H(f-\nu)\Big)\, e^{j2\pi t\nu}\, d\nu$$

$$= -j2\pi t\, S_x(t, f; H) + S_x(t, f; \mathcal{D}H)\,. \tag{A-2}$$

where window $\mathcal{D}H(f)$ is defined in Table 4.2. Taking the same derivative but using Equation (4.1), we obtain

$$\frac{\partial}{\partial f} S_x(t, f; H) =$$

$$\int \Big(\frac{\partial}{\partial f} X(f-\nu)\Big)\, H(\nu)\, e^{j2\pi t\nu}\, d\nu = \int X(f-\nu)\, (-j2\pi)\, \Phi'(f-\nu)\, H(\nu)\, e^{j2\pi t\nu}$$

where we used the relation $\frac{d}{df} X(f) = X(f)\, \frac{d}{df} \ln(X(f)) = -j2\pi\, X(f)\, \Phi'(f)$. From (A-3),

$$\Phi'(f-\nu) = t_x + b_x\, (f-\nu) + c_x\, (f-\nu)^2 = (t_x + b_x\, f + c_x\, f^2) - (b_x + 2\, c_x\, f)\, \nu + c_x\, \nu^2\,.$$

If we define $\Upsilon_x(f) = -j2\pi(t_x + b_x\, f + c_x\, f^2)$, $L(f) = j2\pi(b_x + 2\, c_x\, f)$ and $C_x = -j2\pi c_x$, then Equation (A-3) simplifies to

$$\begin{aligned}\frac{\partial}{\partial f} S_x(t, f; H) &= \int X(f-\nu) \Big(C_x\, \nu^2 + L_x(f)\, \nu + \Upsilon_x(f) \Big)\, H(\nu)\, e^{j2\pi t\nu}\, d\nu \\ &= C_x \int X(f-\nu)\, \nu^2\, H(\nu)\, e^{j2\pi t\nu}\, d\nu + L_x(f) \int X(f-\nu)\, \nu\, H(\nu)\, e^{j2\pi t\nu}\, d\nu + \Upsilon_x(f) \\ &\qquad \int X(f-\nu) H(\nu)\, e^{j2\pi t\nu}\, d\nu \\ &= C_x\, S_x\Big(t, f; \mathcal{M}^2 H\Big) + L_x(f)\, S_x\Big(t, f; \mathcal{M} H\Big) + \Upsilon_x(f)\, S_x(t, f; H)\end{aligned} \tag{A-4}$$

Equating (A-2) and (A-4), and using the STFT notation in Table 4.2, We obtain the first linear system equation as

$$S_{\mathcal{D}} = C_x\, S_{\mathcal{M}^2} + L_x(f)\, S_{\mathcal{M}} + \big(\Upsilon_x(f) + j2\pi t\big)\, S \tag{A-5}$$

from (A-2) and (A-3) to $S_x(t, f; \mathcal{D}H)$ in (A-5) instead of $S_x(t, f; H)$. This results in

$$S_{\mathcal{D}\mathcal{D}} = C_x\, S_{\mathcal{M}^2\mathcal{D}} + L_x(f)\, S_{\mathcal{M}\mathcal{D}} + \big(\Upsilon_x(f) + j2\pi t\big)\, S_{\mathcal{D}}\,, \tag{A-6}$$

The third equation is obtained by taking the derivative of

$-j2\pi S_{\mathcal{M}\mathcal{D}} = -j2\pi C_x\, S_{\mathcal{M}^3} - j2\pi L_x(f)\, S_{\mathcal{M}^2} - j2\pi\big(\Upsilon_x(f) + j2\pi t\big)\, S_{\mathcal{M}} + j2\pi S$, which yields the third equation as

$$S_{\mathcal{M}\mathcal{D}} + S = C_x\, S_{\mathcal{M}^3} + L_x(f)\, S_{\mathcal{M}^2} + \big(\Upsilon_x(f) + j2\pi t\big)\, S_{\mathcal{M}} \tag{A-7}$$

In summary, the three linear system equations are given by (A-5), (A-6) and (A-7). Note that similar equations were mentioned, but not solved, in [5] for processing the IF of third-order polynomials in time.